VALIDATION OF A FELINE FEMORAL BONE SURROGATE WITH MECHANICAL AND CLINICAL EVALUATION OF FELINE ORTHOPEDIC IMPLANTS

By

Danielle Marie Marturello

A THESIS

Submitted to
Michigan State University
in partial fulfillment of the requirements
for the degree of

Comparative Medicine and Integrative Biology – Master of Science

2021

ABSTRACT

VALIDATION OF A FELINE FEMORAL BONE SURROGATE WITH MECHANICAL AND CLINICAL EVALUATION OF FELINE ORTHOPEDIC IMPLANTS

By

Danielle Marie Marturello

A bone surrogate was developed and subsequently used to evaluate the mechanical behavior of two novel feline interlocking nails against plate controls *in vitro,* in an attempt to evaluate their safety and efficacy. Following testing in both torsion and 4-point bending, the I-Loc nail was evaluated in 30 clinical feline trauma cases.

Fracture gap constructs were implanted with an I-Loc (3 or 4 mm), Targon (2.5 or 3.0 mm) or LCP (2.0 or 2.4 mm) and mechanically compared. Additionally, explanted surrogates with implant specific pilot holes were failed to assess the effect of implant removal on bone surrogate strength. Finally, a prospective clinical case series of 30 feline fractures were evaluated for time to clinical union, return to function and complications following repair using the I-Loc nail.

The I-Loc 3 and 4 mm nails overall were mechanically stronger than either the Targon nails or locking plates, including explanted specimens. All cats in the clinical study were weight bearing within 2 days of surgery and reached clinical union in a mean time of 7.2 weeks. All returned to full limb function. No major complications were encountered.

These studies suggest that the I-Loc may represent a safe and effective alternative to other available feline osteosynthesis options.

To my parents, Bill and Victoria. Your love and support over the years means more to me than you will ever know. I could not have pursued my dreams without you, and I hope that I have made you proud.

ACKNOWLEDGEMENTS

I owe the biggest thank you of all to **Dr. Loïc Déjardin**. Your continued guidance, mentorship, and friendship throughout my career as a surgeon has been truly invaluable. Your passion and precision for your craft is remarkable and I will be forever grateful to you for taking me under your wing and teaching me to fly. I hope that I have made you proud; know that I am incredibly honored to call myself your protégée.

To the members serving on my committee:

Dr. Karen Perry for your continued support, both professionally and personally since I began my time at Michigan State. We have shared many laughs over the years and I will always appreciate the things you have taught me. **Dr. Sun Young Kim** for your patience with teaching me how to use CAD software and become proficient at design. **Dr. Feng Wei** for your engineering expertise and assistance running the statistics for this project.

I also wish to thank **Dr. Dirsko von Pfeil** for his constant support, as well as his assistance with the Targon nail portion of this work.

Finally, I would like to thank **BioMedtrix**, **DePuy Synthes** and **Aesculap** for their very gracious implant and equipment donations.

This work was supported by the **Comparative Orthopedic Investigations Laboratory** at the College of Veterinary Medicine at Michigan State University. Additionally, by the **Michigan State University Endowed Research Fund** and the **ACVS Foundation Surgeon-In-Training grant.**

TABLE OF CONTENTS

LIST OF TABLES

LIST OF FIGURES

KEY TO ABBREVIATIONS

°/Nm	Degrees per Newton-Meter
3D	3 Dimensionally
ABS	Acrylonitrile Butadiene Styrene
AD	Angular Deformation
AMI	Area Moment of Inertia
ANOVA	Analysis of Variance
AS-ILN	Angle-Stable Interlocking Nail
BC	Bending Compliance
BU	Bony Union
CAD	Computer Aided Design
CC	Construct Compliance
CNC	Computer Numerical Control
CT	Computed Tomography
CU	Clinical Union
FBS	Feline Bone Surrogate
FEA	Finite Element Analysis
F_M	Failure Moment
F_T	Failure Torque
Hz	Hertz
ILN	Interlocking Nail
IM	Intramedullary
IMR	Intramedullary Rod

LCP	Locking Compression Plate
MC	Medullary Canal
MIPO	Minimally Invasive Plate Osteosynthesis
MINO	Minimally Invasive Nail Osteosynthesis
mm	Millimeters
Nm	Newton-Meter
NU	Non-union
ORIF	Open Reduction Internal Fixation
PBE	Plastic-Based Powder Dipped Epoxy
pcf	Pounds per Cubic Foot
PO	Post-operatively
PRC	Plate Rod Construct
PCV	Polyvinyl Chloride
SFE	Short Fiber Epoxy
SYN	Synbone
SD	Standard Deviation
TC	Torsional Compliance
VWP	VeroWhitePlus
WL	Working Length

STUDY 1:

CHARACTERIZATION OF THE STRUCTURAL PROPERTIES OF FELINE FEMURS AND SURROGATE BONE MODELS FOR MECHANICAL TESTING OF ORTHOPEDIC IMPLANTS

INTRODUCTION

Mechanical testing of orthopedic implants is a critical aspect of their design and development. Data generated by such evaluations may help assess and compare implant safety and efficacy, and thus may assist orthopedic surgeons in predicting clinical outcome following fracture repair. While cadaveric bones have historically been used in biomechanical studies, this testing methodology is fraught with shortcomings including difficulties in procurement, ethical considerations, biohazard concerns as well as vast biological variations inherent to bone shape and material properties.[1] These biological inconsistencies generate large standard deviations, frequently in excess of 100%.[1] This in turn often requires unrealistically large sample sizes to detect statistically significant differences between groups.[1,2,3] To circumvent these limitations, reduce inter-specimen variability and provide a more accurate implant evaluation, the use of bone surrogates has been advocated.[1,4] In veterinary orthopedics, however, such models have most often been designed and used as canine analogs.[3,5,6]

Traditionally, canine bone surrogates have been simple cylindrical models such as aluminum tubes[7] or PVC pipes[8] which were available “off-the-shelf”. While the use of these simple surrogates is cost effective and provides consistency among samples during

testing, wide variations in structural properties between models limits their clinical relevance and precludes meaningful comparisons between studies. Additionally, because of their simple cylindrical shape, the testing of anatomically contoured implants is not possible. In an effort to improve the clinical relevance of mechanical testing, our research group has relied on custom models that provide a more realistic profile with tapered extremities meant to mimic the metaphyseal and epiphyseal flare of long bones.[6] However, machining of these models from solid rods has been costly and resulted in substantial material waste.

Recent developments in 3D printing has presented an attractive alternative to conventional machining methods. Using this technology, creation of models can be simplified making them potentially more affordable. Additionally, large numbers can be produced more rapidly than their machined counterparts. Printed models also offer the advantage of including features, such as holes specific to an implant so that specimen preparation can be considerably simplified and more easily standardized. Although CT based 3D printed models are frequently used for surgical planning, to the authors' knowledge no study has assessed whether these materials could be used as a bone substitute for mechanical testing.

In an effort to validate a feline bone surrogate, the mechanical properties of feline bone were recently evaluated by testing small cortical sections of the femoral diaphysis in compression and bending.[2,9] However, torsion, which represents the primary *in vivo* mode of bone loading,[10,11] was not evaluated. Additionally, these validation studies failed to identify a test material that was similar to native feline femoral bone.[2,9] While the data generated by this type of analysis may be used to evaluate the behavior of the bone-

implant interface, it has limited value for the assessment of an entire bone or a bone-implant construct. Ideally, the evaluation of the biomechanical behavior of a bone, as well as the mechanical performance of an implant used to repair a fracture, requires that the structural properties of the bone be known. These structural properties are highly dependent on the entire bone geometry, including its shape, size and cortical thickness.[12]

To the authors' knowledge, while ample information is available for the canine species,[13,14] there is a paucity of data on the structural properties of native feline bone.[2] Furthermore, a bone model surrogate designed to replicate the structural properties of a feline bone has yet to be developed. As the femur is the most commonly fractured long bone,[15-18] we chose to replicate this bone as our model. Therefore, the purpose of this study was two-fold: 1) to characterize the structural properties of feline femora and 2) to design and validate a bone model substitute for the feline femur. The null hypothesis was that the structural properties of the proposed bone model would be statistically similar to those of the native feline femur for all outcome measures and materials tested.

MATERIALS AND METHODS

1.1 FEMORAL MEASUREMENTS

Thirty pairs of femurs were harvested from adult domestic shorthair cats euthanized for reasons unrelated to this study. The study was approved by the Institutional Animal Care and Use Committee. The cats' hind limbs were clipped and prepared as for a routine surgery. A standard lateral approach to the femur was performed using a #10 scalpel blade.[19] A lateral stifle arthrotomy was completed and the ligamentous attachments (intra and extra-articular) were severed. Proximally, the coxofemoral joint was disarticulated by severing the round ligament, and the muscular attachments were transected close to the femur. Once removed, femurs were dissected free of all soft tissues by gently scraping the surface with #10 blades until bones were completely devoid of cartilage and muscle. The femurs were then grossly evaluated for the presence of any anatomical abnormalities. If noted, these femoral pairs were discarded. Using a precision digital caliper (Mitutoyo 500-196-30, Mitutoyo America Corporation, Aurora, IL) various anatomical measurements were obtained. The femoral length was determined from the most proximal point on the greater trochanter to the most distal aspect of the lateral femoral condyle (**Figure 1.1A**). The lateral surface was chosen because it is what the surgeon would see intraoperatively and is most easily repeatable. The femoral width was measured in both mediolateral (**Figure 1.1A**) and craniocaudal directions (**Figure 1.1B**). Width measurements were taken at three locations as follows:

1) Lesser trochanter

2) Mid-diaphysis

3) Immediately proximal to the femoral trochlea

Dissected specimens were then wrapped in saline soaked towels, placed in two hermetically sealed plastic bags and frozen at -20º C until testing. Approximately 24 hours prior to testing, femurs were thawed at room temperature.

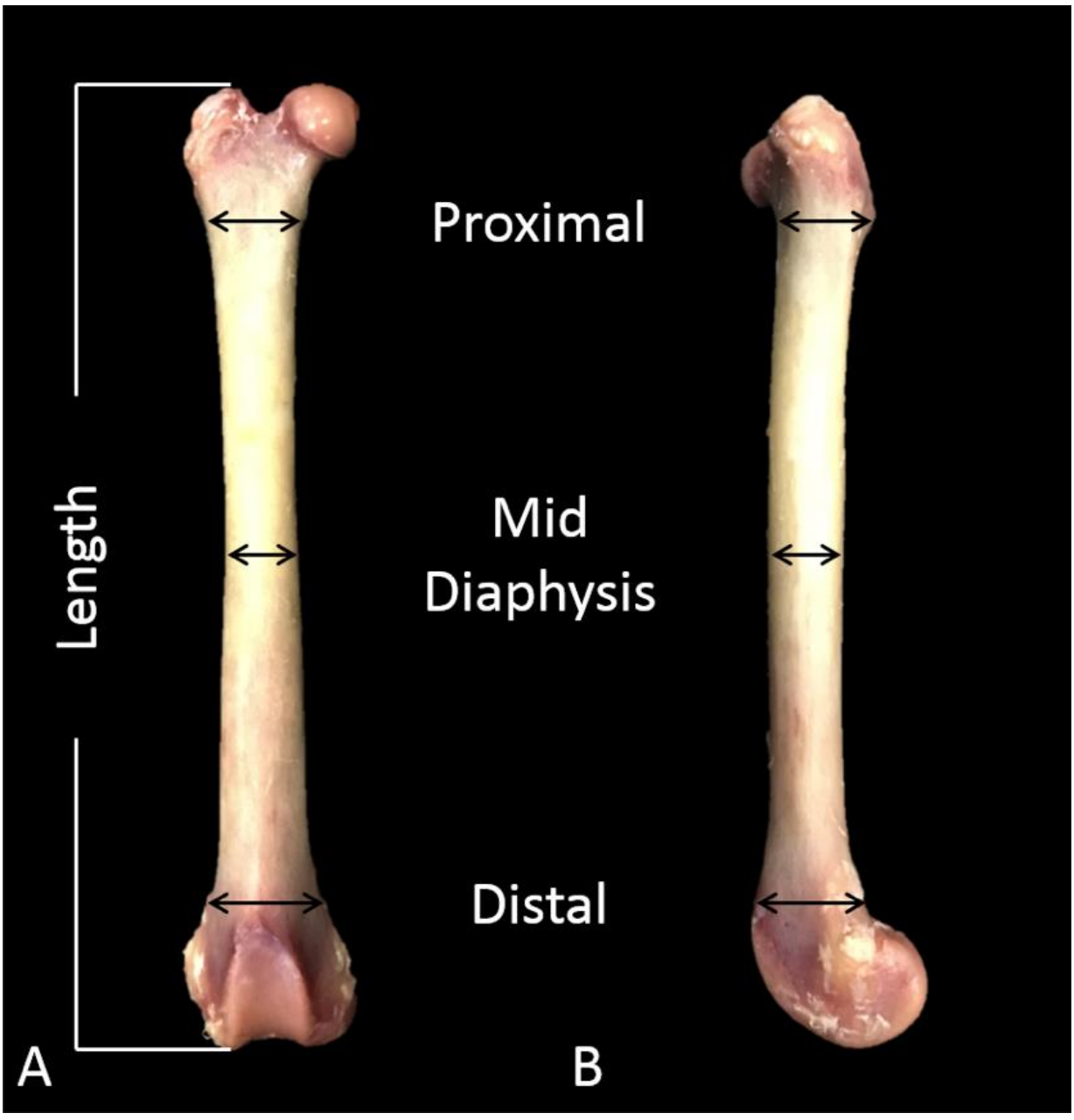

Figure 1.1: Morphometric measurements of cadaveric femurs
Cadaveric femurs with morphometric measurements that served as the basis for the design of the feline femoral bone model surrogate (A, length and mediolateral widths; B, craniocaudal widths).

1.2. BONE POTTING PROCEDURE

See **Figure 1.2** and **SOP S1**

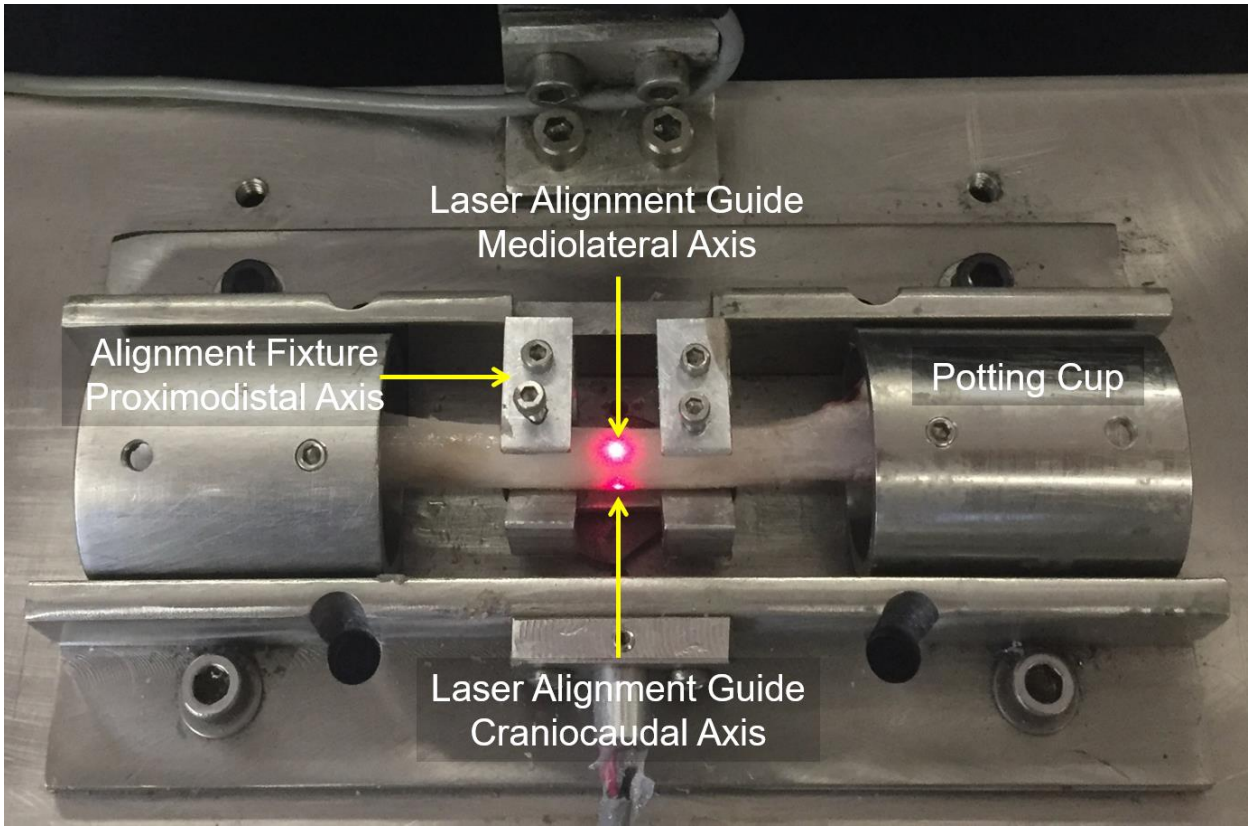

Figure 1.2: Custom designed potting fixture featuring laser alignment guides
Custom designed torsion potting fixture featuring laser alignment guides used to ensure centralization of the specimens in the x, y, and z directions.

1.3. MECHANICAL TESTING

1.3a. Cadaveric torsion tests: Potted specimens were mounted in a dedicated torsional fixture that converts the linear displacement of the actuator of a servo-hydraulic testing machine (Instron model 1331, Instron Corp., Canton, MA) into rotation via a rack and pinion assembly (**Figure 1.3**). Applied torque was recorded via a 22.6 Nm (200 in-lb) torque load cell (Model TRT-200, Transducer Technique LLC, Temecula, CA) whereas angular deformation was recorded via a rotary encoder (Baumer Electric, Southington, CT). Specimens were tested non-destructively at a torque level of ± 1 Nm under load control for 10 cycles. This represents ~15% of the ultimate torsional strength of feline femurs from a pilot study performed in our laboratory and are typical of intrinsic forces the femur sustained *in vivo*.[10,11] Data was recorded at a sampling rate of 250 Hz. Following cyclic testing, specimens were loaded to failure in internal torsion at a displacement rate of 1°/second in accordance with previous studies.[5,6,20,21]

Outcome measures consisted of torsional compliance (TC, °/Nm), maximum angular deformation (AD, °) and failure torque (F_T, Nm). Failure modes were recorded and reported as descriptive statistics. Torsional compliance was defined as the loading slope of the angle of twist versus torque curves between ± 0.5 and ± 1 Nm during positive and negative loading. Mean TC (between internal and external rotation) was computed, as opposed to torsional stiffness, since testing was conducted under load control. Total AD was calculated as the sum of the absolute value of the AD provided by the rotary encoder between the maximum applied torques (± 1 Nm). Failure torque (i.e. torsional strength) was defined as the maximum torque prior to either 1) a 10% drop in torque magnitude, 2) an angle of twist greater than 25º or 3) visible structural failure of the bone.

Following fracture, the cranial, caudal, lateral and medial cortical wall thicknesses were measured at the mid-diaphysis with the digital calipers and recorded. These measurements were later used for subsequent model design.

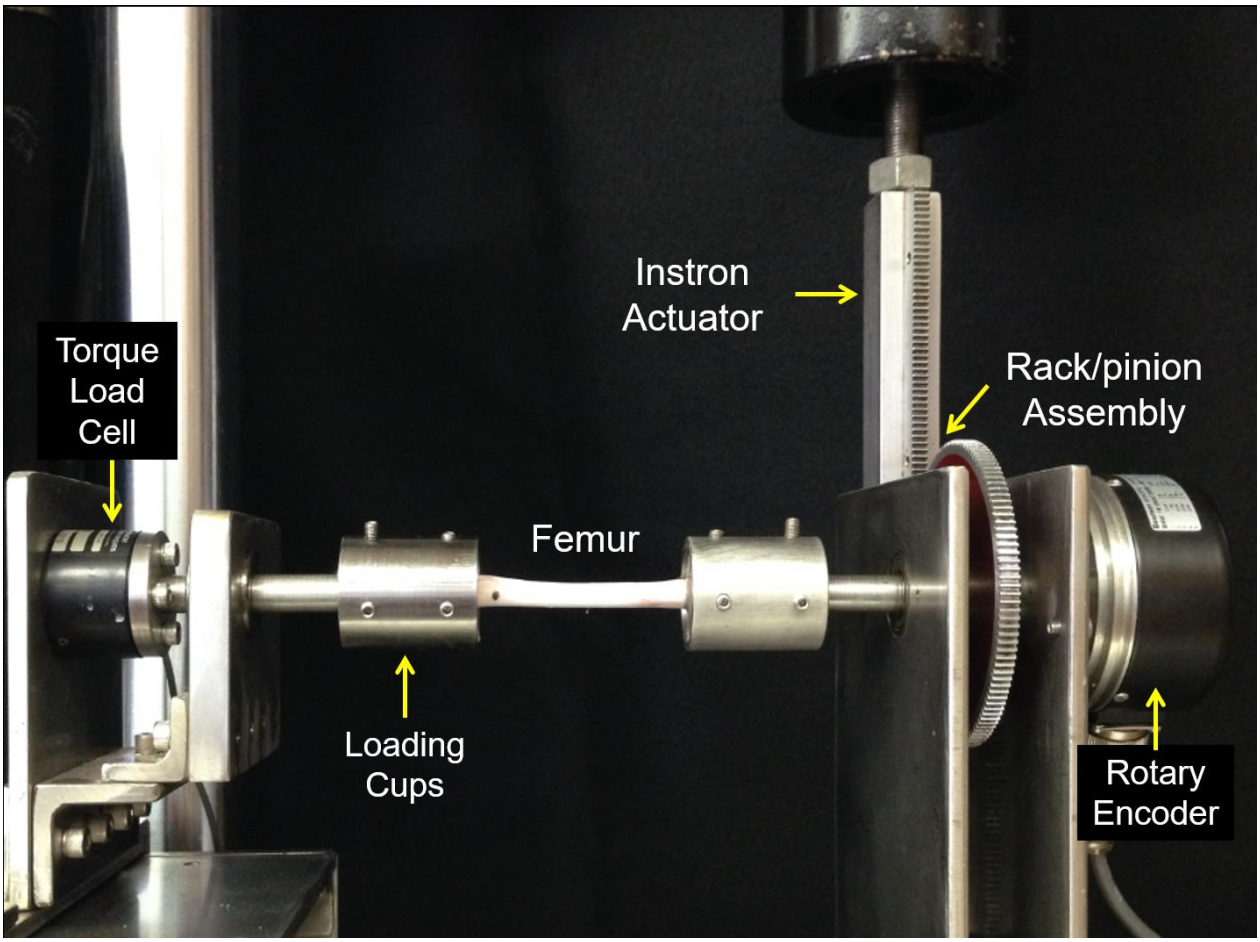

Figure 1.3: Photograph of the torsional testing setup
A femoral specimen is mounted in the servohydraulic testing machine instrumented with a torque load cell and a rotary encoder used to record torque and angular deformation of the specimens, respectively.

1.3b. Cadaveric bending tests: During potting, specimens were carefully oriented to ensure that the lateral diaphyseal surface was aligned directly with the loading surface of the cup. Using custom designed loading cups, all specimens were mounted into a dedicated 4-point bending fixture coupled to a servo-hydraulic testing machine via a 444.8 N load cell (Model 1500ASK-100, Interface Manufacturing Inc., Scottsdale, AZ, USA). The loading cups were instrumented with rotary encoders (Baumer Electric, Southington, CT, USA) to document angular deformation of the constructs. Rotary encoders were aligned to be co-axial with the loading cups. Both loading cups were mounted on an X-Y table (**Figure 1.4**) to allow freedom of movement of the specimens during testing. To mimic medial and lateral bending, non-destructive tests were conducted under load control in alternating positive and negative directions beginning from a neutral position,[20,22] using a bending moment of ± 0.7 Nm for 10 cycles. Following cyclic testing, a 2,228.8 N load cell (Model 1010AF-500, Interface Manufacturing Inc., Scottsdale, AZ, USA) was coupled to the Instron and specimens were loaded to failure at a displacement rate of 1 mm/sec in the mediolateral direction.

Outcome measures consisted of bending compliance (BC, °/Nm), maximum AD (°) and failure moment (F_M, Nm). Failure modes were recorded and reported as descriptive statistics. A deformation versus load curve was created for each specimen. Bending compliance was defined as the loading slope of the AD versus applied moment between ± 0.5 and ± 0.7 Nm during positive (medial) and negative (lateral) loading. Mean BC (between positive and negative loading) was calculated. Total AD was recorded as the sum of the absolute value of the AD provided by the rotary encoder between maximum applied moments (± 0.7 Nm). Failure moment (i.e. bending strength) was defined as the

maximum moment prior to either a 10% drop in moment magnitude or visible structural failure of the bone.

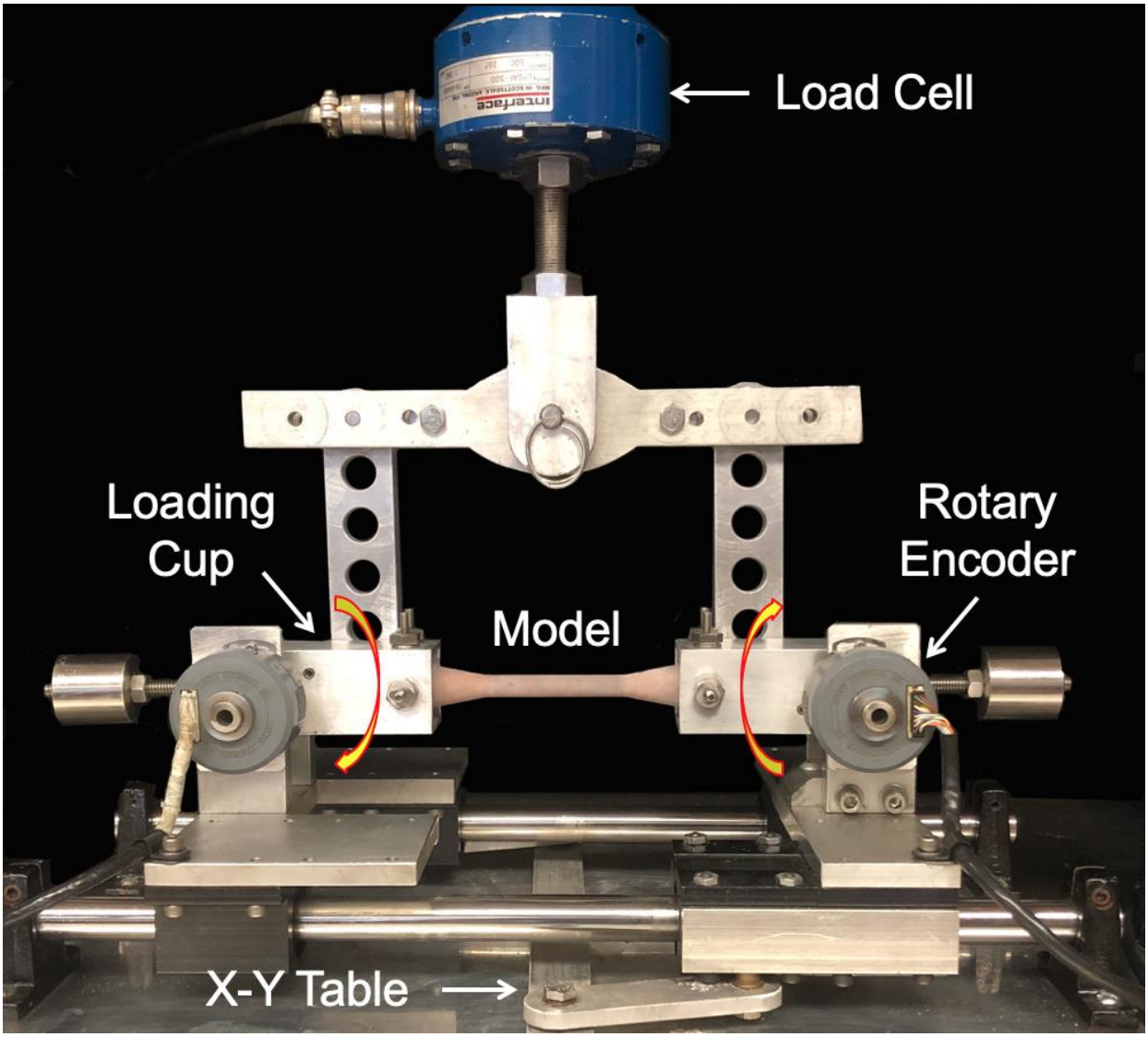

Figure 1.4: Photograph of the bending testing setup
A surrogate model is mounted in the servohydraulic testing machine instrumented with a load cell and a rotary encoder used to record moment and angular deformation of the specimens, respectively. The unique X-Y table allowed unconstrained deformation of the specimens.

1.4. BONE SURROGATE DESIGN AND POTTING

A generic femoral bone model was designed with 3D CAD software (Fusion 360™, Autodesk Incorporated, San Rafael, CA, USA) using the morphometric measurements of the native feline femurs obtained in the first phase of the study (See **SOP S1**).

The overall shape of this symmetrical model was similar to that of a canine bone model previously used in our laboratory.[6,20,22,23] The model was 115 mm long and featured a 20 mm outer diameter coupling segment (15 mm in length) at each extremity (**Figure 1.5**). Adjacent segments representing the epi-metaphyses had a gradual taper from 20 mm down to 10 mm (outer diameter) with an 11° slope. A 60 mm central segment mimicked the diaphysis. Cortical wall thickness was 1.5 mm throughout.

In order to reduce the number of trials necessary to design an appropriate bone model surrogate, available material data sheets and existing literature for potential 3D printed and composite materials were reviewed. Materials tested included: 4th generation short fiber epoxy (SFE – SawBones®), Solid foam (SYN – Synbone®), GPCL04 Resin (Formlabs©) ABS (Stratasys©), Acura 60 (3D Systems©), PA615-GS (Advanced Laser Materials©), VeroWhitePlus (VWP – Stratasys©) and plastic based powder dipped in epoxy (PBE – Markforged©). The SFE and SYN models were machined from solid bar stock using a CNC router (model Quick Turn Start 350m; Yamazaki Mazak, Binh Duong Province, Vietnam) while all the other models were 3D printed.

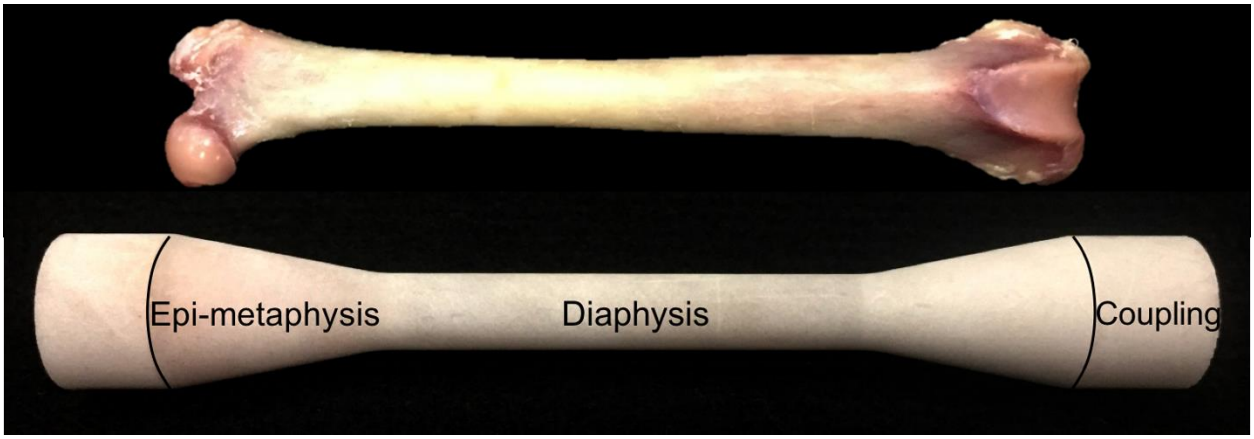

Figure 1.5: Surrogate model with dimensions based on morphometric measurements from 30 cat femurs
The model features a central diaphyseal portion and flared ends that mimic the epiphysis and metaphysis. The outermost segments are used for coupling the model to the testing machine.

1.4a. Bone model surrogate potting procedure:

See **SOP S1**

1.4b. Bone model surrogate mechanical testing: Torsional testing was completed first, for all eight of the above materials. The testing procedure was performed as outlined for cadaveric femurs. The rationale for completing the torsion portion of the study first was that torsion is the most common loading mode of long bones. As such, and to minimize waste, bending tests were performed only on materials that were not different from the cadaveric bones to complete the validation of the bone surrogate. Following statistical analysis and identification of a suitable surrogate material, bending tests were conducted as described above, using only those materials. Outcome measures included compliance (TC and BC, °/Nm), maximum AD (torsion and bending, °) and failure load (F_T and F_M, Nm).

1.5. STATISTICAL ANALYSIS

Outcome measures were compared using Student's t-test, with significance set at $P < 0.05$. Failure modes were recorded and reported as descriptive statistics.

The cadaveric bone sample size (n = 30) was based on 1) previous literature using biological samples in mechanical testing[2,24] and 2) the desire for a representative sample of the feline population. Bone surrogate sample size was chosen based on previous studies from our laboratory which consistently demonstrated that due to sample homogeneity, small standard deviations and significant differences were obtained with n = 4 samples / group.[6,20,21]

As a result of our deliberate choice to use groups with a large difference in sample size, the homogeneity of variance requirement to conduct parametric tests was not met. In such cases where the larger group also has the larger standard deviation, overestimation of the level of significance may occur.[25] Several options are then available for data analysis: 1) a less stringent non-parametric test could be[26] 2) data could be randomized and a smaller number of samples could be selected, following which, a parametric test could be performed[25] or 3) one could elect not to perform statistical analyses at all and rather simply state that the mean of the experimental group is within the standard deviation of the control group. Since parametric tests are considered more powerful, we elected to use the randomization method. Ten cat femurs for torsion and ten femurs for bending were selected at random for statistical comparison. Randomization was performed a total of three separate times for each outcome measure using Excel software (Microsoft, Redmond, WA, USA). Given that the P value for each randomization was not significant, we felt that appropriate sampling had been conducted and our results were therefore valid.

RESULTS

1.6. CADAVERIC BONE

There were 21 males and 9 females. Mean body weight was 4.35 kg. There was no statistical difference between right and left femora for any of the morphometric measurements, nor between mediolateral and craniocaudal cortical measurements (**Table 1.1**). Mean femoral dimensions (± SD) were 111.7 ± 4.4 mm (length), 9.3 ± 0.7 mm (mediolateral mid-diaphyseal diameter), 8.4 ± 0.6 mm (craniocaudal mid-diaphyseal diameter), and 1.6 ± 0.2 mm (mid-diaphyseal cortical thickness).

Morphometric Data		Left		Right	
All data in mm		**Mean ± SD**	**Range**	**Mean ± SD**	**Range**
Lateral length		111.7 ± 4.4	103.9 - 121.9	111.6 ± 4.3	106.4 - 123.4
ML Width	**Proximal**	13 ± 1	10.4 - 14.6	12.8 ± 1	11.4 - 14.7
	Diaphysis	9.3 ± 0.7	8.3 - 10.5	9.1 ± 0.7	8.1 - 10.3
	Distal	11.6 ± 1.1	10 - 14	11.8 ± 1.1	10 - 12.9
CC Width	**Proximal**	9.8 ± 0.8	8.3 - 11.5	9.4 ± 0.6	8.3 - 10.6
	Diaphysis	8.4 ± 0.6	7.5 - 9.4	8.3 ± 0.6	7.6 - 9.2
	Distal	10.5 ± 0.9	9 - 12.2	10.7 ± 0.9	9.8 - 13
Cortex Ø	**ML**	1.5 ± 0.1	1.3 - 1.7	1.5 ± 0.2	1.2 - 1.9
	CC	1.6 ± 0.2	1.2 - 1.9	1.5 ± 0.1	1.3 - 1.8

Table 1.1: Morphometric measurements feline femurs
Morphometric measurements (mm) of 30 feline femurs with mean, SD, and range values for both left and right paired femurs. There was no statistical difference between sides for any of the measurements.

1.7. TORSION TESTS

Mean TC (± SD) was not significantly different (P = 0.3) between native femurs (1.6 ± 0.3 °/Nm) and the SFE model (2.0 ± 0.1 °/Nm, **Figure 1.6**). Similarly, there was no significant difference (P = 0.13) in maximum AD between native bones and the SFE model (3.1 ± 0.6° and 3.8 ± 0.2°, respectively [**Figure 1.6**]). Finally, F_T for the native bone was 7.8 ± 1.2 Nm and 8.1 ± 1.3 Nm for the SFE model. That difference was not significant (P = 0.18). In contrast, the TC of printed materials ranged from 5.9 to 12.7 °/Nm, AD ranged from 5.2 to 48.3°, and torque to failure ranged from 2.8 to 6.7 Nm.

Failure mode for both feline bone and SFE surrogate was a spiral fracture through the diaphysis (**Figure 1.7A)**. Conversely, all but one printed model failed by plastic deformation without fracture (**Figure 1.8)**. The PBE model failed via a transverse fracture which occurred at 5° of torsion.

Of the eight materials tested, only the SFE was statistically similar to the native feline femur for all outcome measures. All other models had structural properties that were significantly different from those of the native bone (outcome measures greatly varied between materials, **Table 1.2**).

Material	TC (°/Nm)	AD (°)	F_T (Nm)	F_{Mode}
Bone	1.6 ± 0.3[a]	3.1 ± 0.6[b]	7.8 ± 1.2[c,d]	Fracture Spiral
SFE	2.0 ± 0.1[a]	3.8 ± 0.2[b]	8.1 ± 1.3[c]	Fracture Spiral
SYN	26.4 ± 1.3	48.3 ± 1.9	2.1 ± 0.5	Deformation
GPCL04	12.7 ± 1.7	22.8 ± 0.2	3.6 ± 0.2	Deformation
Acura 60	6.4 ± 0.7	12.1 ± 1.4	6.7 ± 0.2[d]	Deformation
PA615-GS	5.9 ± 0.6	10.6 ± 1.2	2.9 ± 0.1	Deformation
VWP	12.2 ± 0.8	19.5 ± 0.3	3.0 ± 0.2	Deformation
PBE	2.8 ± 0.2	5.2 ± 0.01	2.8 ± 0.3	Fracture Trans
ABS	9.1 ± 0.1	17.6 ± 0.7	4.1 ± 0.1	Deformation

Table 1.2: Torsional properties for cadaver bone and surrogate models
Torsional properties (mean ± SD) for cadaver bone and surrogate models. Tenth cycle outcome measures used for comparison of cadaveric bone to surrogate materials were torsional compliance (TC), angular deformation (AD) and failure torque. Failure mode was also recorded. Cadaver bone and SFE outcome measures were not statistically different. Conversely, outcome measures from all other groups were statistically different from both cadaver bone and SFE model. Identical letters indicate lack of statistical difference between groups.

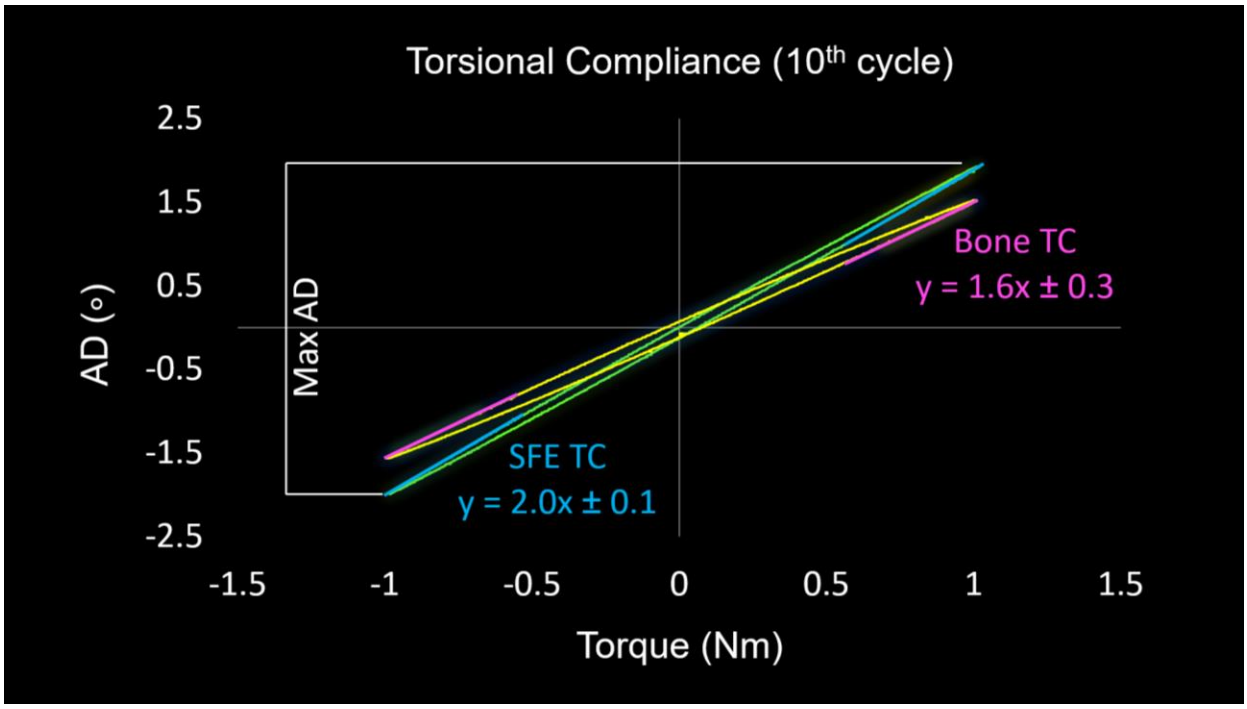

Figure 1.6: Representative mean torsional compliance curve (10th cycle) of the cadaveric bone and SFE model

Torsional compliance (TC, mean positive and negative slopes ± SD) for the sample populations was 1.6 ± 0.3 °/Nm (cadaver bone, yellow) and 2.0 ± 0.1 °/Nm (SFE model, green) while maximum angular deformation (AD, mean ± SD) was 3.1 ± 0.6° and 3.8 ± 0.2°, respectively.

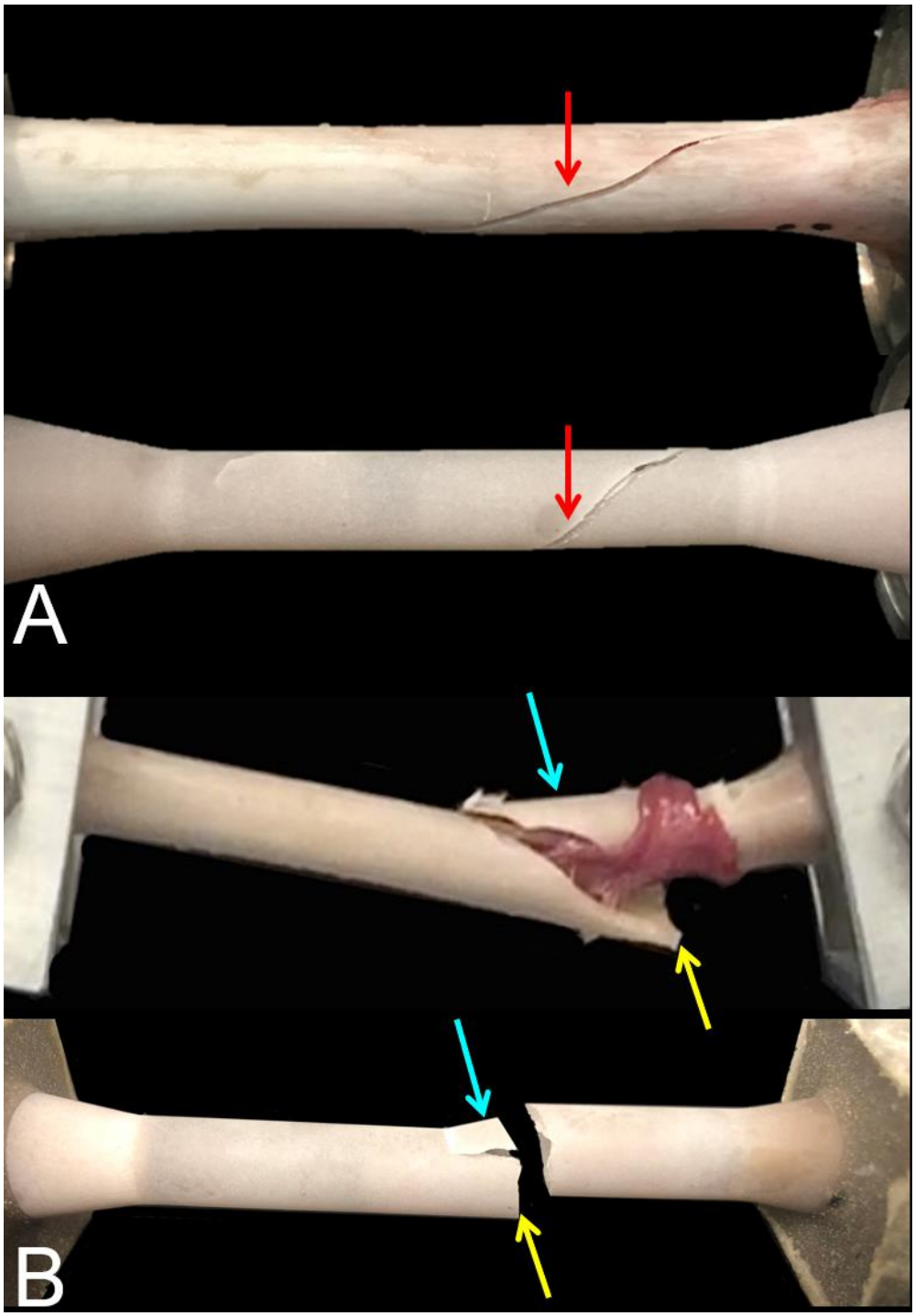

Figure 1.7: Failure mode for both cadaver specimens and SFE models
A, Both cadaver bone specimens (top) and SFE surrogate models (bottom) failed in torsion via spiral fractures in the diaphysis (red arrows). B, Both cadaver bone specimens (top) and SFE surrogates (bottom) failed via a diaphyseal transverse fracture initiating on the trans-cortex (yellow arrows) with a butterfly fragment on the cis-cortex (blue arrows).

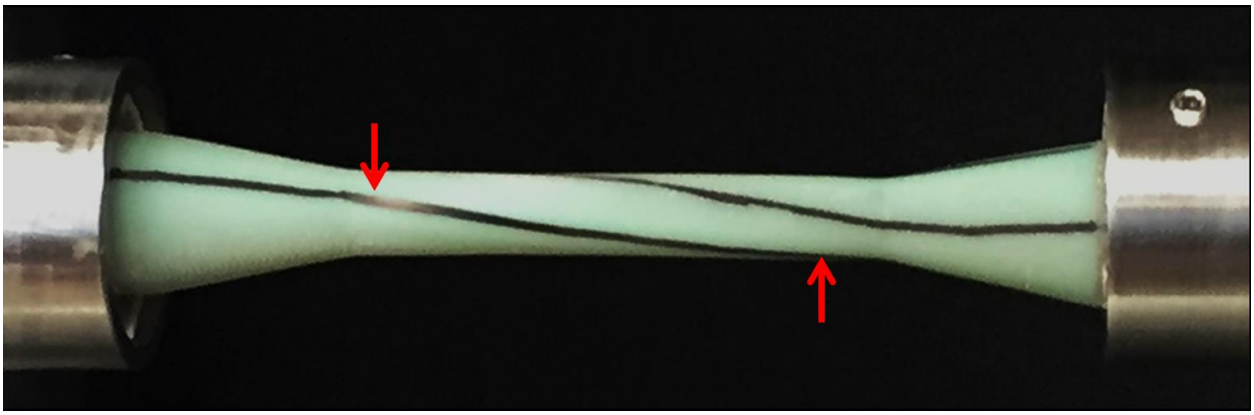

Figure 1.8: Plastic deformation of one of the 3D printed materials in torsion Representative sample of one of the 3D printed materials (ABS) that underwent extreme plastic deformation (> 240°) without fracture failure in torsion. Black lines on the model illustrate the ductility of the material (red arrows).

1.8. BENDING TESTS – SFE ONLY

Mean BC (± SD) was not significantly different (P = 0.24) between native femurs (0.9 ± 0.4 °/Nm) and the SFE model (1.2 ± 0.1 °/Nm, **Figure 1.9**). Similarly, there was no significant difference in maximum AD (**Figure 1.9**) between native bones and the SFE model (1.2 ± 0.5° and 1.6 ± 0.1°, respectively – [P = 0.13]). Finally, F_M for the native bone was 12.7 ± 3.2 Nm and 9.7 ± 0.1 Nm for the SFE model (P = 0.08).

Failure mode for both the feline bone and SFE model were similar and occurred via a diaphyseal transverse fracture initiating on the trans-cortex and propagating into a cis-cortical butterfly fragment (**Figure 1.7B**).

Material	BC (°/Nm)	AD (°)	F_M (Nm)	F_M
Bone	0.9 ± 0.4[a]	1.2 ± 0.5[b]	12.7 ± 3.2[c]	Fracture **Trans**
SFE	1.2 ± 0.1[a]	1.5 ± 0.1[b]	9.7 ± 0.1[c]	Fracture **Trans**

Table 1.3: Bending properties for cadaver bone and surrogate models
Bending properties (mean ± SD) for cadaver bone and SFE surrogate models. Tenth cycle outcome measures used for comparison of cadaveric bone to surrogate materials were bending compliance (BC), angular deformation (AD) and failure moment. Failure mode was also recorded. Cadaver bone and SFE outcome measures were not statistically different.

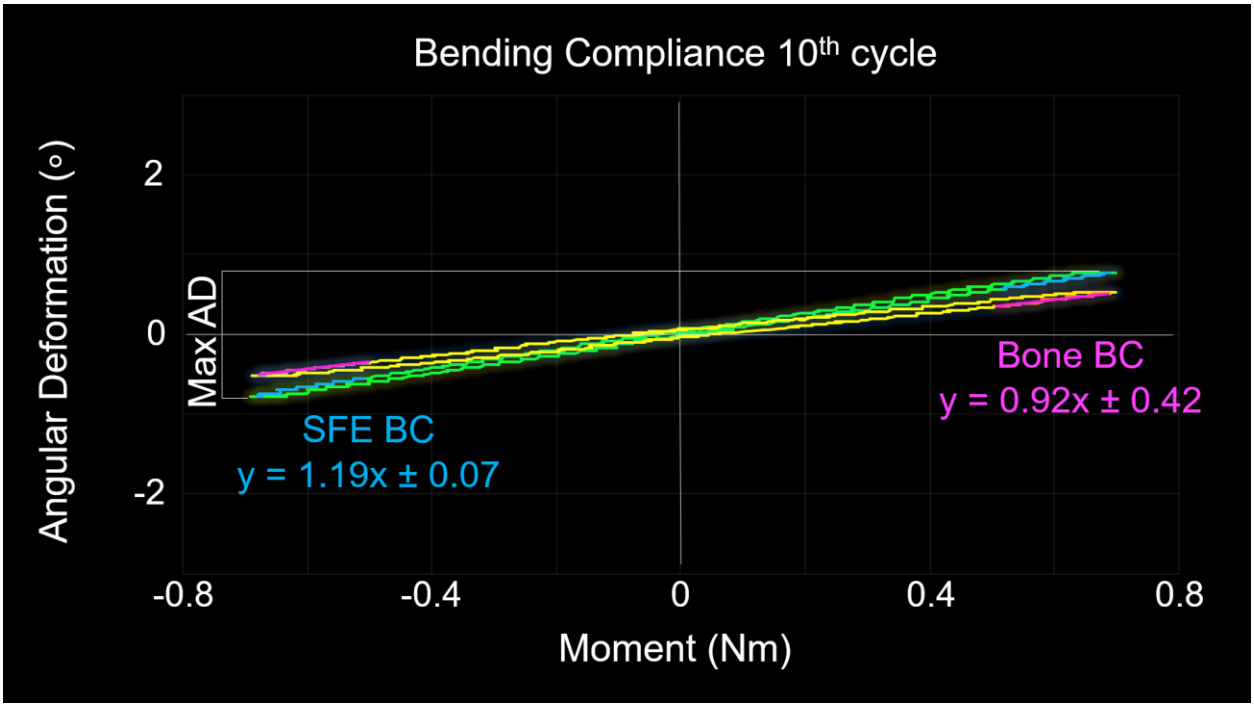

Figure 1.9: Representative mean bending compliance curve (10th cycle) of cadaveric bone and SFE model

Bending compliance (BC, mean ± SD) for the sample populations was 0.92 °/Nm ± 0.42 °/Nm (cadaver bone, yellow) and 1.19 °/Nm ± 0.07 °/Nm (SFE model, green) while maximum angular deformation (AD, mean ± SD) was 1.15° ± 0.49° and 1.56° ± 0.09°, respectively.

DISCUSSION

Although our null hypothesis was rejected, the results of this study showed that the composite SFE surrogate model that was designed had torsional and bending structural properties similar to those of native feline bone.

Historically, mechanical testing of implants has been performed using cadaveric bone. To circumvent inherent limitations associated with natural bone, various materials have been empirically used to create bone surrogates in an effort to reduce inter-specimen variability and limit the number of samples required to reach statistical significance. To date, machining of such models from solid rods has been the only available method of obtaining a realistic shape. Major disadvantages of this approach include cost, time and substantial material waste.

As an alternative to conventional machining methods, the development of 3D printing has revolutionized numerous industries including medicine.[27,28] Surgeons can now print a wide variety of objects ranging from implants, fixtures, and instruments, to biological specimens.[29] Computer based designs allow for rapid alterations to be made, which reduces the lead time associated with product development. Perhaps most importantly, 3D printing allows for complete customization of specimens which is ideal in cases of surgical planning or implant design. As an example, pilot holes for screw placement in a given model can be standardized between specimens to further reduce variability. Yet another advantage of 3D printing over machining is optimization of costs through reduction of materials, labor, and equipment.

Considering the potential benefits of 3D printing, our group aimed to use this technology to design and print a bone surrogate that would behave similarly to native bone, in hopes that it would replace hazardous and elusive biological specimens as well as cost prohibitive and time consuming conventional machining methods.

While numerous printable materials exist, to the authors' knowledge, none has been mechanically tested as a potential bone surrogate. Furthermore, while the material properties of some of these materials may be available, the evaluation of the structural properties of a printable realistic bone model had yet to be performed. Indeed, previous studies using bone models have primarily relied on published material properties of composites as a basis for their use as a bone surrogate. Six printable materials most likely to behave similarly to bone based on available material data sheets were selected. Unexpectedly, none of the materials used to create a surrogate bone model could mimic the torsional structural properties of the native feline femur. In particular, likely due to the ductility of printable materials, most models underwent marked plastic deformation without fracture at torsion angles in excess of 240°. While one model did eventually fracture (PBE), failure occurred at a significantly lower torque than that of native cadaver bone. Based on these findings, all printable materials evaluated in this study were deemed unsuitable for use in a surrogate bone model.

Additive methods such as post printing epoxy coating and carbon fiber reinforcement during printing have been devised to increase strength and / or brittleness of printable materials. While theoretically attractive, these techniques are challenging to implement and standardize. Indeed, the flare of the epi-metaphyseal sections of our model makes the application of an even coating next to impossible. This, in turn, would

jeopardize the structural properties of our model thus diminishing its clinical relevance. Similarly, while printing simple relatively flat objects using carbon fiber reinforced materials is becoming ubiquitous in many fields including the automotive industry, the printing of more complex structures, such as cylinders and cones, remains elusive.

While SFE had been previously validated as a surrogate for human bone,[30] it had not yet been assessed as a feline bone substitute. Based on the findings of this study, we believe that the current SFE machined model could be used to realistically evaluate small implants designed for the treatment of feline fractures.

Our model dimensions and shape were based on those of natural feline femora, which may provide several advantages compared to simple cylindrical models. First, the more realistic shape of our model allows for anatomic contouring of eccentrically applied implants such as bone plates. We believe that this should provide a more accurate clinical representation of construct mechanical behavior *in vivo*. Indeed, it has been suggested that a complex shape may be more appropriate to model physiologic loading when bone-implant constructs are being evaluated.[4] Second, testing of intramedullary implants utilizing bridging osteosynthesis, such as interlocking nails, using a simple tubular model would considerably limit the clinical relevance of the findings. Indeed, placement of bolts in the wider epiphyseal or metaphyseal portion of a flared model increases their working length and thereby compliance.[7,31] Conversely, testing the same implant in a simple tubular model of identical diaphyseal dimensions would artificially decrease construct compliance and thus could bias the outcome in favor of a nail compared to a plate. The more realistic shape of our model may allow for more meaningful conclusions regarding the efficacy of one implant versus another in future *in vitro* mechanical evaluations.

Finally, our results showed that failure torque, failure moment, and failure mode were similar between the SFE model and native bone. This suggests that orthopedic surgeons could more accurately predict the location and type of fracture sustained if our model were used to evaluate the effect of implant removal.

As with any study, some limitations exist. First, femoral structural properties were evaluated in this study since the femur is the most commonly fractured long bone in small animals,[32] however, various long bones may behave differently. Second, the difference in sample size between cadaver and surrogate groups presented a challenge with regard to homogeneity of variance. Since parametric tests are considered more powerful, we elected to use the randomization method. Given that the P value for each randomization (performed three times) was not significant, we felt that appropriate sampling had been conducted and our results were therefore valid.

Despite our expectations, this study demonstrated that common printable materials are unsuitable for the creation of a bone surrogate. As 3D printing technology continues to advance, one should anticipate that a suitable material will eventually become available for use in biomechanical studies. In the meantime, researchers may continue to rely on either cadaver specimens or as suggested in this study, SFE material.

Indeed, the findings of this study validate the use of a machined SFE bone model as a feline cortical bone surrogate. The similar structural properties of feline cadaver bone and the SFE model should allow for meaningful comparison of small orthopedic implants designed for the treatment of feline long bone diaphyseal fractures. Without confounding variables inherent to cadaveric bone, testing could be performed rapidly, reliably, and safely, with a low number of samples needed to reach statistical significance.

STUDY 2:

MECHANICAL COMPARISON OF TWO FELINE INTERLOCKING NAILS USING A BONE SURROGATE

INTRODUCTION

Long bone fractures from high energy trauma frequently result in varying degrees of comminution[33] which affects osteosynthesis methods. In feline patients, veterinary surgeons have historically had limited options for fracture fixation. The development of locking plates (LCP) has offered several advantages over traditional plates including better preservation of the periosteal blood supply and increased resistance to failure via screw pull-out.[34-37] While 2.0 mm and 2.7 mm LCPs have long been available, these plates may be ill fitted for feline patients.[38] Recently, an intermediate size, the 2.4 mm LCP, was made available and is often the preferred choice of many surgeons for feline fracture osteosynthesis.[34,38] From a mechanical perspective, however, a plate's eccentric location increases its susceptibility to bending, which may result in yield or fatigue failure when cortical reconstruction is not possible,[35,39] or in cases of delayed or non-union.

In contrast, as intramedullary devices, interlocking nails (ILN) have inherent advantages over bone plates, including shielding from deleterious bending moments due to their proximity to the bone neutral axis. While ILN osteosynthesis is gaining acceptance in veterinary orthopedics,[15,16,18] small implants suitable for cats have not been readily available. Therefore, despite inherent biomechanical limitations, bone plates remain the first choice of many surgeons for feline fracture fixation.

Recently, two angle-stable ILNs (AS-ILN) appropriate for cats were developed, each with a fundamentally different locking mechanism (**Figure 2.1**). The small 3 mm and 4 mm I-Loc (BioMedtrix, Whippany, NJ, USA) feature an hourglass profile with two threaded cannulations at each extremity. Similar to the larger diameter I-Loc (6, 7 and 8 mm), matching threaded bolts provide the angular stability of this locking mechanism. While numerous studies have validated the larger I-Loc design, [6.20,21,40] its smaller version has yet to be investigated.

The second recently introduced AS-ILN is the Targon (B. Braun Aesculap, Tuttlingen, Germany), which features a 2.5 mm or 3 mm intramedullary rod (IMR) eased through two cannulated bolts located at the junction between metaphyses and diaphysis. Once tightened, set screws within the bolts lock the IMR via friction, thus providing construct angular stability.[41] While early evaluation showed promising results,[41,42] a recent study demonstrated that locking mechanism slippage at the IMR/set screw interface led to torsional instability.[43] Yet another potential shortcoming of this design is its reliance on a thin IMR, which could substantially increase construct compliance. Perhaps more importantly, the specific design of the Targon nail requires that large bolts be used to accommodate the set screw of the locking interface. Should explantation of the nail be indicated, the relatively large diaphyseal bone defect of the pilot holes may jeopardize the structural integrity of the healed bone.

Given the lack of mechanical data on the small I-Loc nails, concerns about the locking mechanism of the Targon nails, and the fact that bone plates currently remain the preferred osteosynthesis method for many surgeons, the purpose of this study was to compare the mechanical behavior of these three implants using a recently developed

feline bone surrogate (FBS) model.[44] In addition, the effect of pilot hole size on the strength of the FBS was evaluated. Our null hypotheses were that regardless of the group: 1) There would be no significant difference in construct compliance (TC and BC, °/Nm) or maximum angular deformation (AD, °) between groups, 2) Pilot hole size would have no significant effect on the failure load (F_T and F_M, Nm) of the FBS for any group and 3) The failure mode would be similar between a) the intact FBS and native femurs as well as b) the explanted FBS specimens.

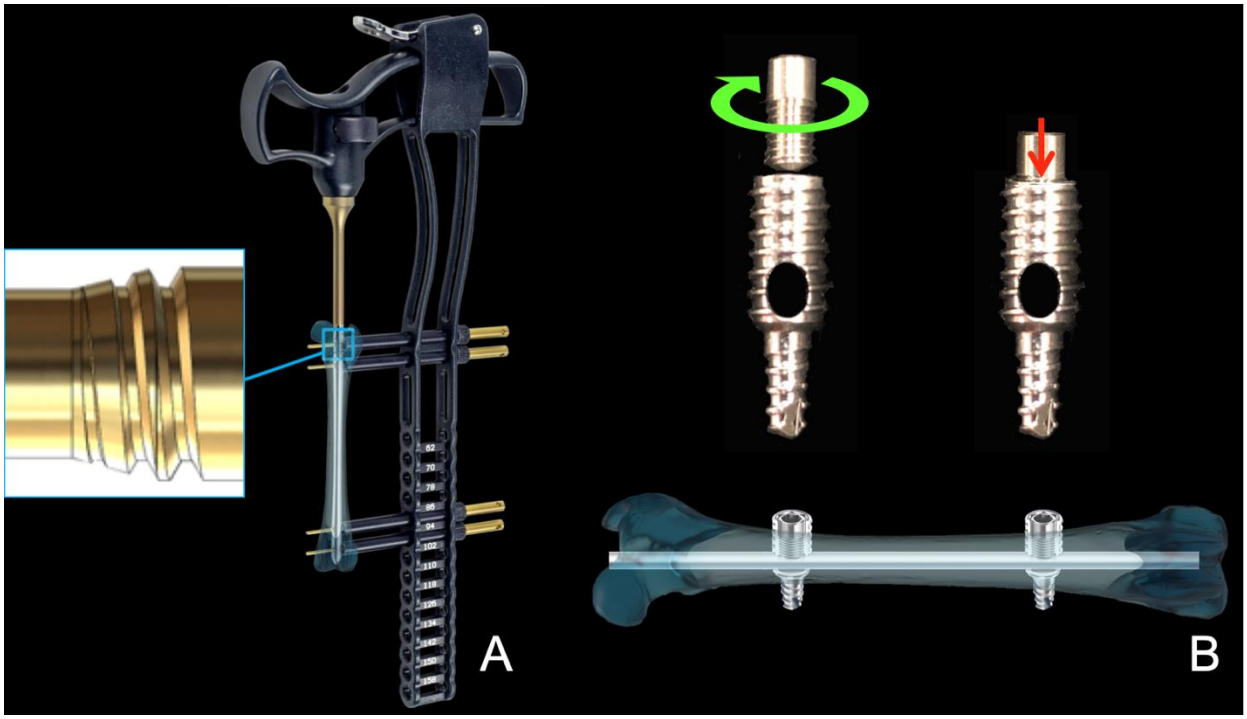

Figure 2.1: Locking mechanisms of the interlocking nails evaluated in this study
A, The I-Loc interlocking nail (ILN) features threaded cannulations for matching threaded bolts. As the bolt is tightened, interference between the bolt solid cis-section and the edge of the threaded cannulation provides rigid locking. B, Conversely, the Targon ILN features threaded bolts with smooth oblong cannulations. Set screws are tightened to generate friction against a dedicated intramedullary rod, which locks the implant.

MATERIALS AND METHODS

2.1. STUDY DESIGN

A feline bone surrogate model previously described, was used in this study.[44] This model, manufactured from a SFE bar stock (SawBones, Vashon Island, WA, USA), featured a diaphyseal section of 10 mm diameter, as well as epi-metaphyseal flares (slope 11° – end diameter 20 mm) at each extremity. Cortical thickness was 1.5 mm throughout. This study was conducted in two phases.

Phase I, a diaphyseal gap fracture model was used to evaluate the mechanical properties of constructs stabilized using one of six implants (groups 1–6, n = 4 / group). These implants included I-Loc 3 and 4, Targon 2.5 and 3 as well as LCP 2.0 and 2.4. Implant selection represented treatment options for long bone fractures in cats with a body weight of ~4–6 kg (I-Loc 3, Targon 2.5, and LCP 2.0) or ~7–10 kg (I-Loc 4, Targon 3, and LCP 2.4).[38,41,43,45] Constructs were cyclically tested in torsion and 4-point bending using a recently developed FBS.[44]

Phase II, six additional groups (A–F) consisting of intact FBS with implant specific pilot holes were evaluated (n = 4 / group). Specimens were tested in torsion and 4-point bending until failure.

2.2. 3D MODELING, PRINTING AND MACHINING

See **SOP S2**

2.3. SPECIMEN PREPARATION

Phase I, a 30 mm mid-diaphyseal gap simulating a comminuted fracture was created in the FBS (**Figure 2.2**). To simulate metaphyseal cancellous bone,[46] conical 20 pcf (pounds per cubic foot) polyurethane foam plugs (SawBones, Vashon Island, WA, USA) were press-fit and glued (Gorilla Glue, Sharonville, OH, USA) at both extremities of each model. In the ILN groups, the center of each plug was pre-drilled at a diameter matching that of the specific nail. This was done to guarantee that the ILN axis was accurately aligned with the axis of the coupling fixture during testing. All implants and specific instrumentation used for construct preparation were obtained from the original manufacturers (BioMedtrix [I-Loc], B. Braun Aesculap [Targon], and DePuy Synthes [LCP]).

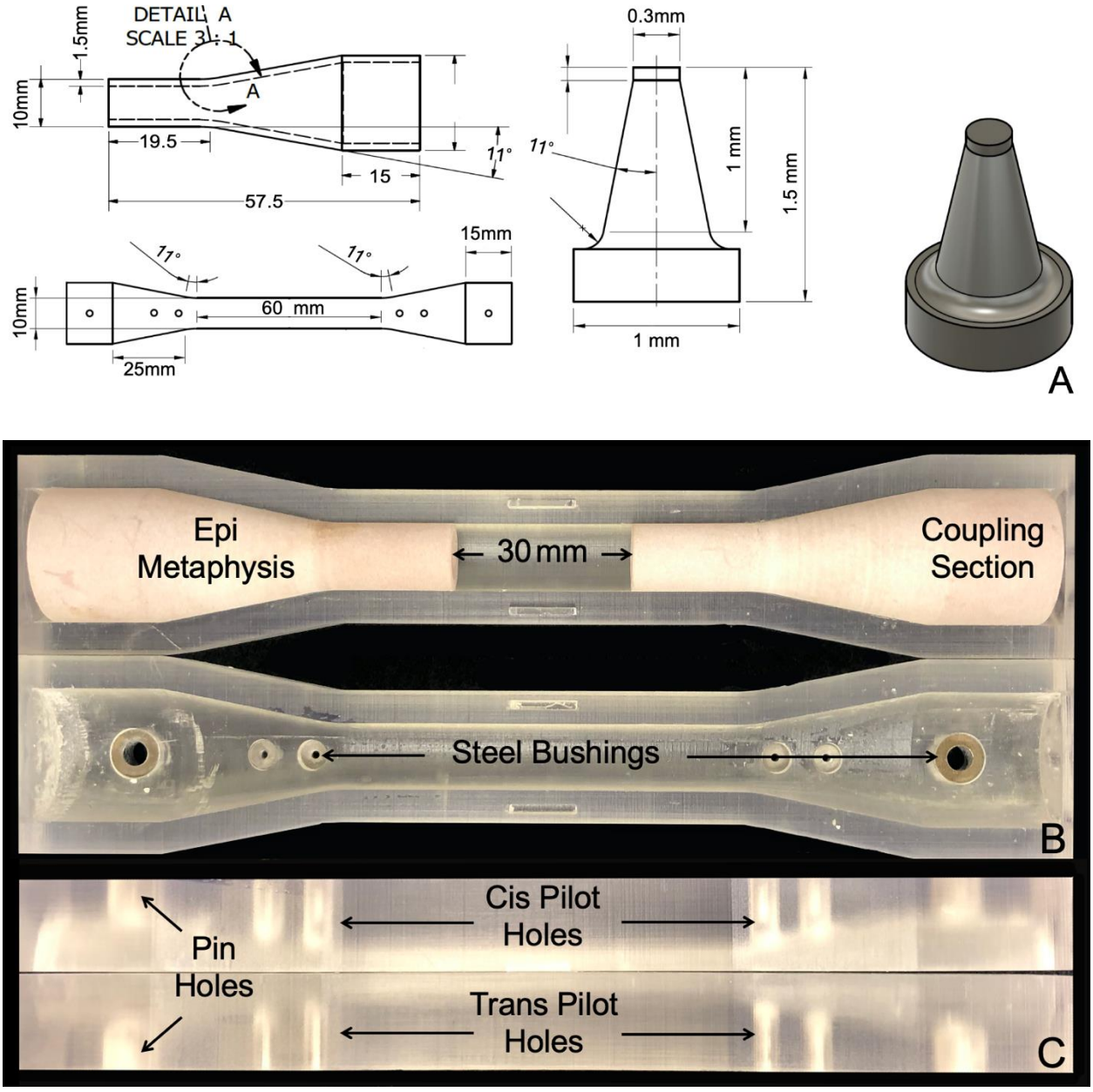

Figure 2.2: Feline bone surrogate CAD and model
A, Computer aided design (CAD) dimensions of the feline bone surrogate (FBS) gap model (left, top) and intact CAD with sample I-Loc and holding peg holes (left, bottom). Additionally, the CAD and 3D model of the cancellous bone plug are shown (right). B and C, FBS model made from short fiber epoxy, featuring a 30 mm gap inside an implant specific 3D printed drill guide. Each guide featured two symmetrical halves fitted with steel bushings that allowed accurate and reproduceable drilling of the pilot holes specific to each implant. Additional bushings at the drill guide extremities were used to create pin holes that allowed placement of the locking pins that secured the models to the testing cups.

To ensure accurate and consistent placement of all pilot holes, dedicated implant and size specific drill guides were designed using Fusion 360 CAD (Autodesk Inc, San Rafael, CA, USA) then 3D printed (Form 2, Formlabs Inc, Somerville, MA, USA). Each guide featured two hollow halves that secured the bone model during drilling. Hardened steel precision bushings (McMaster-Carr, Aurora, OH, USA) with internal diameters matching those of the locking bolts or screws were press-fit in the guide halves at locations specific to each implant (**Figure 2.2**).

All pilot holes were drilled using a table-top drill press (Ryobi 10 inch EXACTLINE Laser alignment system, Milwaukee tools, Fort Lauderdale, FL, USA) after securing the drill guides to the base (**Figure 2.3**).

Figure 2.3: Tabletop drill press used to create pilot holes in bone surrogates
Table-top drill press with I-Loc drill guide attached using C-clamps. The drill press ensured consistent drilling for each hole, for all specimens. Pin holes were drilled first, and steel rods were inserted so that models could not move within the drill guide. Subsequently, implant specific holes were drilled using appropriately sized drill bits.

2.3a. I-Loc nails: Nails were 102 mm in length and 3 mm or 4 mm in diameter (groups 1 and 2, respectively). Nails were inserted through the center of the foam plugs into the medullary canal of the model and secured using two size specific bolts at each extremity (**Figure 2.4**). The span between the innermost locking bolts was 72 mm. All bolts were secured using 0.6 Nm torque ("two-finger tight").

2.3b. Targon nails: IMR were 2.5 mm or 3.0 mm (groups 3 and 4, respectively). As per manufacturer recommendations, a diaphyseal locking bolt was inserted adjacent to each metaphysis of the FBS. The *cis* and *trans* diameters of the locking bolts were respectively 4.8 mm and 2.8 mm (Targon 2.5, group 3) and 5.6 mm and 4.0 mm (Targon 3.0, group 4). All Targon bolts were 16 mm in length. A dedicated 2.5 mm or 3.0 mm IMR (Targon, B. Braun Aesculap, Tuttlingen, Germany) cut to 110 mm was inserted through the center of the foam plugs and bolt cannulations. The span between the locking bolts was 56 mm (**Figure 2.4**). The IMR was then locked in place by tightening set screws at the recommended 1.4 Nm torque using a dedicated calibrated torque screw driver.[42]

2.3c. Locking compression plates: Plates were 14 holes 2.0 mm or 12 holes 2.4 mm (group 5 and 6, respectively). The LCP lengths were chosen so that the distance between the innermost screws of the 2.0 and 2.4 LCPs (74 mm and 69 mm, respectively) closely matched the working length of the I-Loc nails (72 mm). A custom bending press was designed to ensure accurate and consistent plate contouring over the metaphyseal flare of the bone surrogates. Plates were then secured using two size matched bicortical locking screws at each extremity (**Figure 2.4**). As per manufacturer recommendation, all

screws were secured at a 0.8 Nm torque.

Phase II, additionally, intact FBS (without a 30 mm central gap) were prepared. As described for Phase I, FBS were fitted with cancellous plugs in each extremity. Then, using the same custom drill guides, implant specific pilot holes were drilled and left empty to mimic the cortical defects that would be seen following implant removal.

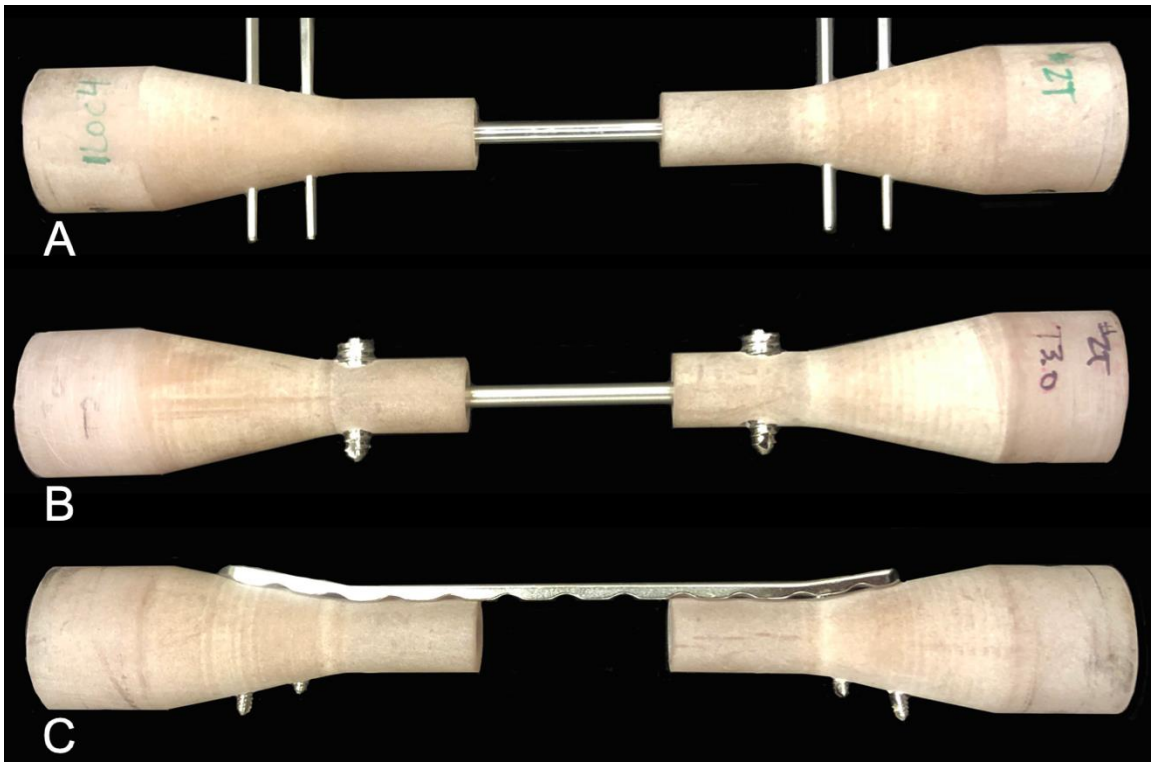

Figure 2.4: Implanted fracture gap constructs
A, I-Loc 4; B, Targon 3.0; C, LCP 2.4 mm. The working lengths of the I-Loc and LCP constructs were similar, while the diaphyseal bolted Targon ILNs had a substantially shorter working length due to manufacturer's design. The LCPs were contoured using a dedicated bending press to match the 11º flare of the feline bone surrogate.

2.4. MECHANICAL TESTING

Using custom designed loading cups (**Figure 2.5**), all specimens (Phase I and Phase II) were mounted in the frame of a servo-hydraulic testing machine (Instron model 1331, Instron Corp., Canton, MA, USA). Torsion and bending fixtures were instrumented with rotary encoders (Baumer Electric, Southington, CT, USA) to document angular deformation of the constructs. Additionally, the bending fixture featured an X-Y table to allow freedom of movement and unconstrained deformation of the specimens during testing. Tests were conducted as previously described under load control for 10 cycles at a sampling rate of 250 Hz.[44] Data recorded in the 10th cycle was used for statistical analysis.

2.4a. Torsion tests: Torsion was achieved using a rack and pinion assembly that converts the linear displacement of the Instron actuator into rotation. The torsion fixture featured a 22.6 Nm torque load cell (Model TRT-200, Transducer Technique LLC, Temecula, CA, USA) that recorded the magnitude of the applied torques. The six groups in Phase I were tested non-destructively at a torque of ± 1 Nm in alternating clockwise and counterclockwise direction simulating internal and external rotation. The six groups in Phase II were loaded to failure at a displacement rate of 1° / second. [6,43,44]

2.4b. Bending tests: The bending fixture was coupled to the testing machine via a 100 pound load cell (Model 1500ASK-100, Interface Manufacturing Inc., Scottsdale, AZ, USA). Phase I groups were non-destructively tested under load control in alternating positive and negative directions beginning from a neutral position,[20,22] using a bending

moment of ± 0.7 Nm. Following cyclic testing, a 500 pound load cell (Model 1010AF-500, Interface Manufacturing Inc., Scottsdale, AZ, USA) was coupled to the machine and the six groups in Phase II were loaded to failure at a displacement rate of 1 mm / sec in the mediolateral direction.

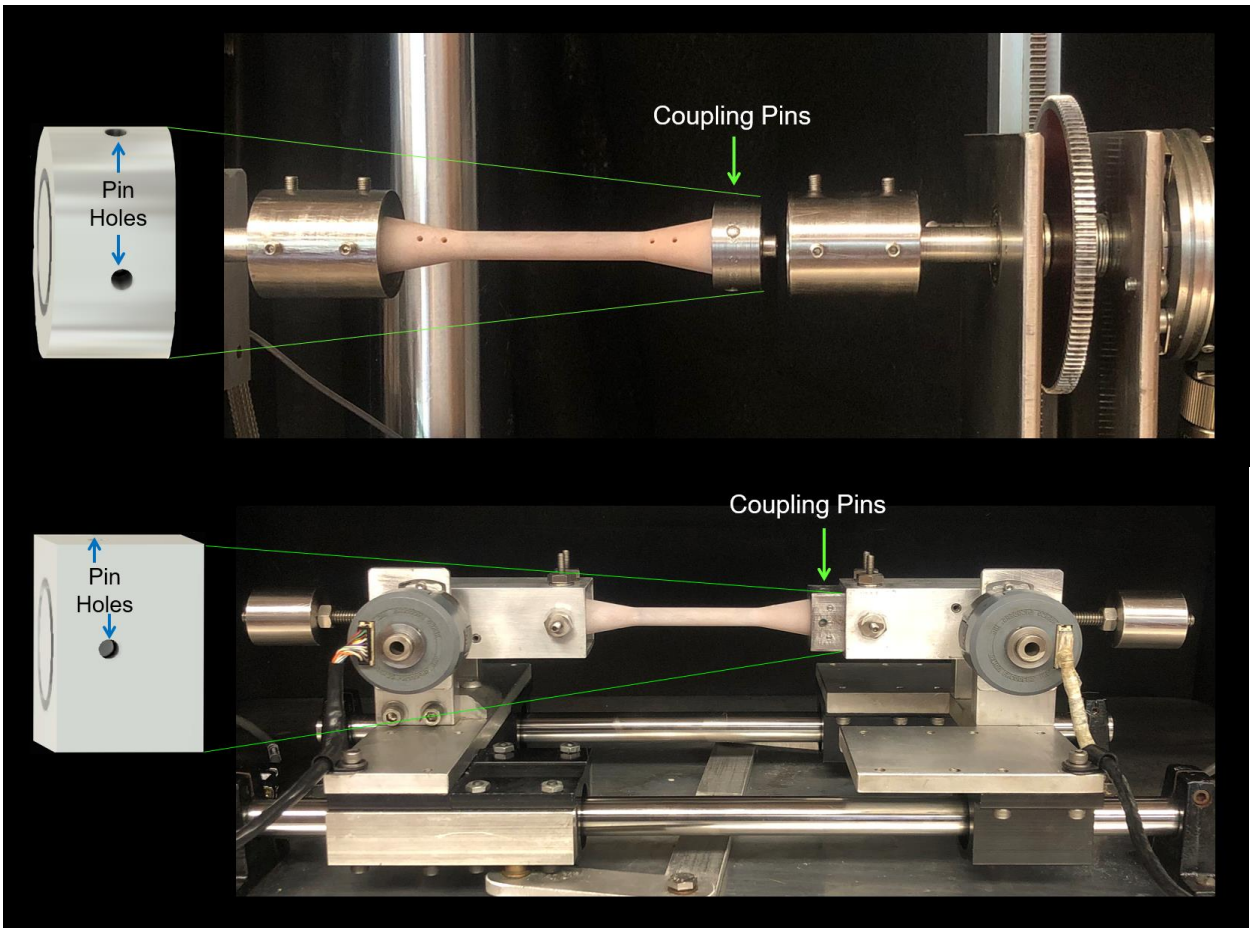

Figure 2.5: Three-dimensional CAD and machined custom loading cups with bone models, loaded in the servohydraulic testing machine
An explanted bone model specimen is mounted in a torsion (top) and bending fixture (bottom) coupled to the servohydraulic testing machine. The fixtures were instrumented with a load cell and a rotary encoder used to record torque / moment and angular deformation of the specimens, respectively. A computer-aided design (CAD) of the testing cups (left) were manufactured from stainless steel (right). Holes created in the testing cup matched pin holes drilled in each specimen. Steel pins were used to rigidly secure the specimens to the fixtures during testing.

2.5. A POSTERIORI ADDITIONAL GROUPS

Following initial Phase I and II testing, five additional groups were evaluated to assess alternative clinical scenarios and potentially provide additional clinically relevant data. The data pertaining to these *a posteriori* tests was included in the statistical comparison.

2.5a. Targon nail constructs: The set screws of the Targon 2.5 were tightened at a higher torque (2 Nm) than the recommended 1.4 Nm (group 7). The impetus for this additional test (performed in torsion only) was to improve construct stability and therefore clinical efficacy, by potentially eliminating the locking interface slippage observed during initial torsional testing of the Targon 2.5 mm nail.

Next, in order to reduce the ratio of cortical defect to bone surrogate diameter, the Targon 3.0 bolts were moved from the diaphysis to the metaphyses at a location centered between that of the I-Loc bolts (group 8, **Figure 2.6**). The wider medullary canal diameter in that position (10.5 mm vs 7 mm in the diaphysis), matched recent recommendations reported for the larger Targon bolts.[42]

Subsequently, intact Targon 3.0 bone surrogates (group G) had pilot holes drilled in the new metaphyseal location. These specimens were tested to failure and compared to the other explanted groups.

2.5b. Locking plate constructs: In both the LCP 2.0 mm and 2.4 mm groups, a third screw was added on either side of the fracture gap (groups 9 and 10, respectively). This

scenario was intended to create a less compliant construct, which may be favored by some surgeons, by shortening the working length of the LCP.

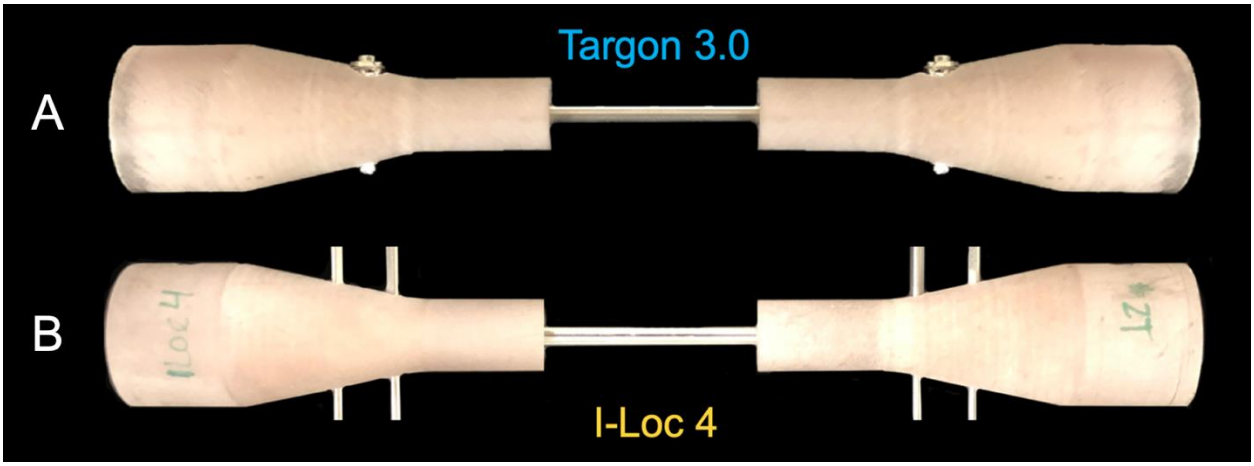

Figure 2.6: Location of the metaphyseal bolted Targon 3.0 constructs
A, Targon 3.0 with a metaphyseal bolt location. The pilot hole positions were chosen to be mid-way between the bolts of the I-Loc nails. B, I-Loc 4 construct to show comparison of more closely matched working length.

2.6. DATA ACQUISITION

The sample size (n = 4 / group) was selected based on previous studies from our laboratory.[6,20,44] Similar to previous studies, compliance rather than stiffness was computed since testing was conducted under load control.[6,20,44,47] Torsional compliance was defined as the loading slope of the angle of twist versus torque curves between ± 0.5 and ± 1 Nm during clockwise and counterclockwise torsion. Mean TC (between clockwise and counterclockwise torsion) was calculated. Total AD was calculated as the sum of the absolute value of the AD between maximum applied torques. Bending compliance was defined as the loading slope of the deformation versus applied moment between ± 0.5

and ± 0.7 Nm during positive and negative loading. Mean BC (between positive and negative loading) was calculated as previously described. Total AD was calculated as the sum of angular deformations between the maximum positive and maximum negative bending moments. Total AD was recorded as the sum of the absolute value of the AD provided by the rotary encoder between maximum applied moments.

Failure torque (i.e. torsional strength, F_T) and failure moment (i.e. bending strength, F_M) were defined as either: 1) The maximum torque or moment prior to a 10% drop in torque / moment magnitude, 2) An angle of twist greater than 25º (torsion only) or 3) Visible structural failure of the FBS. Failure modes were recorded and reported as descriptive statistics.

2.7. STATISTICAL ANALYSIS

Normality of numerical data was ascertained using Kolmogorov-Smirnov test. Data were then compared using one-way ANOVA and Tukey post-hoc test to identify significant differences between groups. Additionally, F_T, F_M, and failure mode from Phase II were compared *a posteriori* to those of intact FBS without pilot holes from Study 1 of this thesis.[44] The significance level was set at $P < 0.05$.

RESULTS

2.8. TORSION

Deformation versus load curves were monophasic in all but the Targon 2.5 constructs (**Figure 2.7**). In that group, the compliance curve had a multiphasic appearance characterized by the presence of a central slack region interrupted by a recurrent resistive torque. This pattern correlated with structural damage of the IMR and subsequent slippage of the locking interface during reversal of the torque direction (**Figure 2.8**).

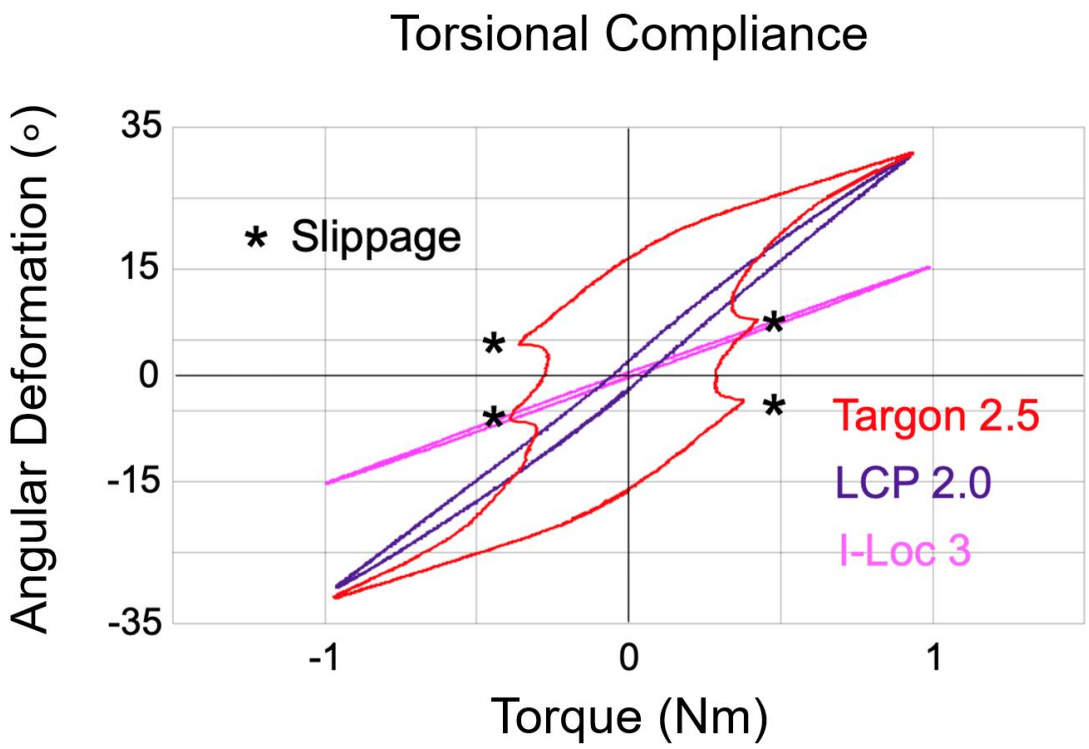

Figure 2.7: Multimodal curve of Targon 2.5 constructs
Representative torsional compliance curves of the small implants illustrating the characteristic biphasic shape of the Targon 2.5 group. Sequential locking interface slippage (asterisks) was associated with distinctive transient angular resistive spikes along the slack section of the Targon 2.5 curves. Shown for comparison are the typical monophasic curves of the I-Loc 3 and LCP 2.0 groups.

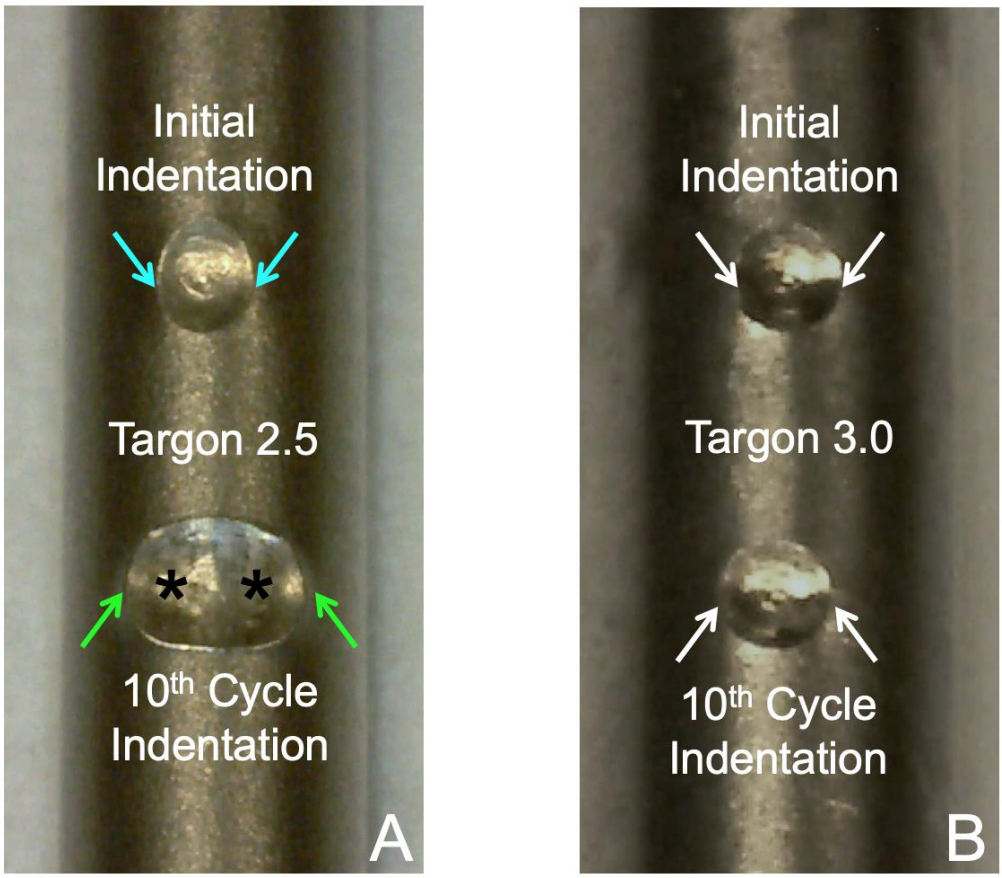

Figure 2.8: Microscopic image showing Targon 2.5 IMR structural deformity secondary to locking interface slippage

A, Microscopic image of an actual Targon 2.5 IMR specimen with the initial conical indentation (blue arrows) created by the set screw tightened at the recommended 1.4 Nm torque (top) and after 10th cycle testing (bottom). As torque was applied, the initial indentation deformed into an oblong depression (green arrows) featuring two symmetrical ridges (asterisks) matching the edges of the initial indentation. Note that the initial indentation was recreated *a posteriori* for illustration purposes because cyclic loading resulted in additional structural deformation. B, In contrast, the conical indentation in the Targon 3.0 IMR remained unchanged throughout 10 cycles of testing.

2.8a. Phase I – Torsional compliance: **Figure 2.9** – The I-Loc 4 had the lowest TC overall (5.4 ± 0.1 °/Nm), which was significantly smaller than all other groups evaluated ($P < 0.05$). The LCP 2.0 had a significantly larger TC than any other group (31.7 ± 2.7 °/Nm – [$P < 0.05$]). Construct TC was not significantly different between the LCP 2.4 and Targon 3.0 constructs ($P = 0.72$).

Compared to the original groups, *a posteriori* iterations had the following effects:

First, changing the set screw torque from 1.4 Nm to 2.0 Nm did not significantly alter TC of the Targon 2.5 constructs. However, structural damage to the set screw coupling interface precluded reaching the intended 2 Nm torque during screw tightening in 3 of 8 screws (i.e. ~40%).

Second, moving the Targon 3.0 bolts from a diaphyseal to a metaphyseal location significantly increased construct TC by 30% from 9.9 ± 0.6 °/Nm to 12.9 ± 0.9 °/Nm ($P = 0.005$).

Third, adding a 3rd screw to the LCP 2.0 constructs significantly reduced TC by 29% from 31.8 ± 2.7 °/Nm to 22.6 ± 1.7 °/Nm ($P < 0.0001$) which was no longer different from the Targon 2.5 TC (21.3 ± 0.18 °/Nm – [$P = 0.99$]). In contrast, while the addition of a 3rd screw in the LCP 2.4 constructs reduced TC from 11.2 ± 0.16 °/Nm to 8.9 ± 0.12°/Nm, this difference was not significant ($P = 0.09$). However, the TC of the LCP 2.4 constructs with 6 screws was now significantly lower than that of the Targon 3.0 with a metaphyseal bolt location (8.9 ± 0.12 °/Nm and 12.9 ± 0.9 °/Nm, respectively – $P = 0.0002$).

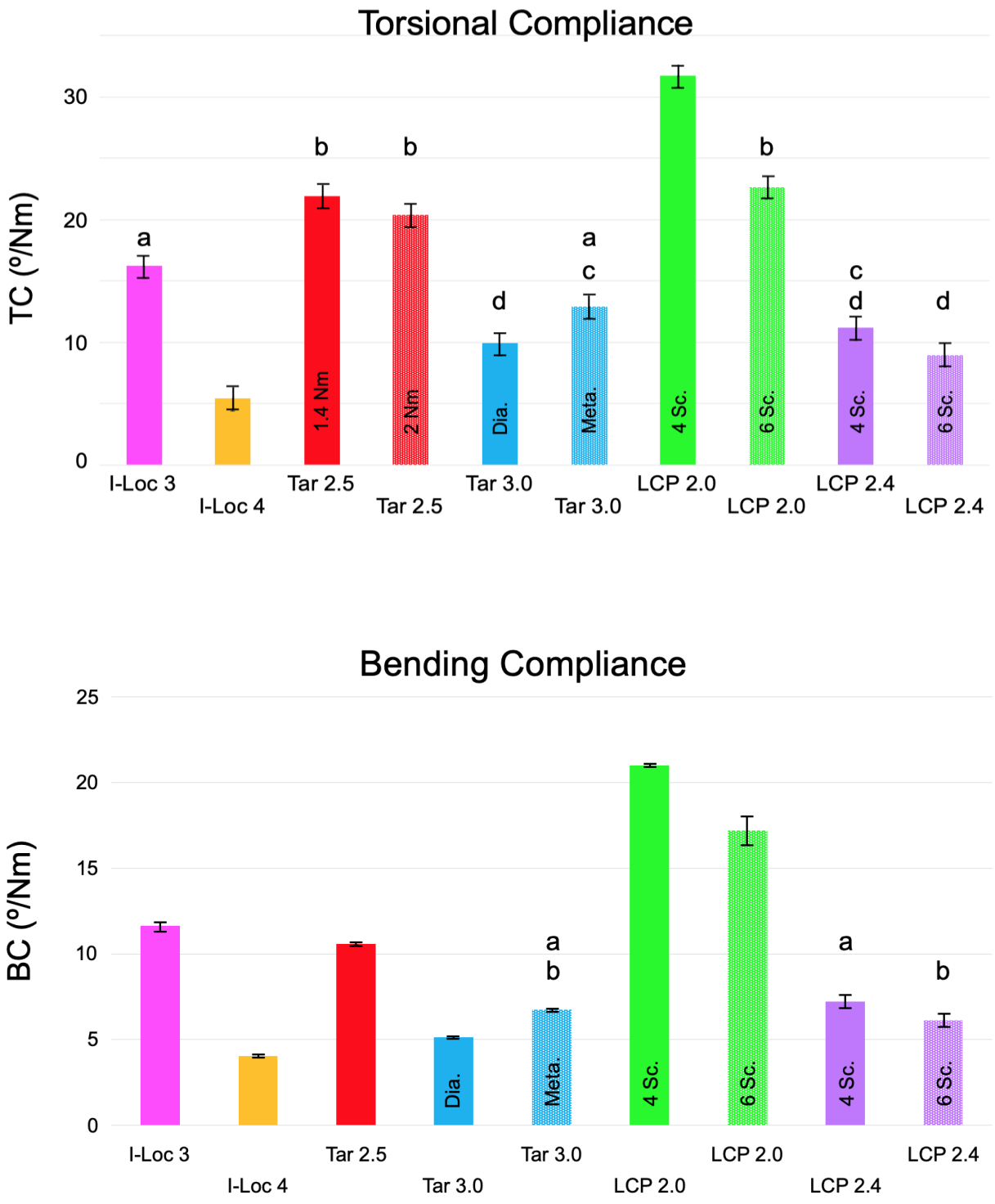

Figure 2.9: Mean torsional and bending compliances for all groups
Histogram of the mean torsional (top) and bending (bottom) compliance of all constructs. Similar letters denote groups that were not statistically different (P > 0.05) from one another. Dia, diaphyseal; LCP, locking compression plate; Meta, metaphyseal; Sc, screw; Tar, targon; TC, torsional compliance.

2.8b. Phase I – Torsional angular deformation: **Figure 2.10** – Similar to TC, the I-Loc 4 experienced the lowest AD (10.6 ± 0.3°), which was significantly smaller than all other groups ($P < 0.05$). The largest AD was seen in both the Targon 2.5 and LCP 2.0 constructs, each exhibiting approximately 59° of AD. While there was no significant difference between these groups ($P = 0.99$), sequential locking interface slippage was observed in the Targon 2.5 constructs. Slippage was associated with gross structural deformity of the IMR caused by the set screw (**Figure 2.8**). Slippage was not noted in the Targon 3.0.

As with TC, differences in construct AD were again noted in the *a posteriori* groups.

First, the higher set screw torque of 2 Nm in the Targon 2.5 constructs resulted in a significant 45% reduction in construct AD from 59.6 ± 2.4° to 32.8 ± 3.0° ($P < 0.0001$). This lower AD was no longer statistically different from the I-Loc 3 constructs (31.1 ± 1.1°, respectively – [$P = 0.051$]).

Second, moving the Targon 3.0 bolts to the metaphyses significantly increased the AD of the construct by 30% from 15.9 ± 0.6° to 20.7 ± 1.6° ($P < 0.0001$).

Third, adding a 3rd screw to the LCP constructs lowered the AD by 28% and 20% in the LCP 2.0 and 2.4, respectively. These differences were significant ($P < 0.008$).

2.8c. Phase II – Failure torque explanted specimens: **Figure 2.11** – Failure torque was significantly lower ($P < 0.0001$) in both the Targon 2.5 (4.8 ± 0.1 Nm) and 3.0 (3.5 ± 0.1 Nm) specimens when compared to the I-Loc 3 (8.9 ± 0.3 Nm) and I-Loc 4 (8.4 ± 0.4 Nm) as well as LCP groups (9.0 ± 0.2 Nm [LCP 2.0] and (7.8 ± 0.5 Nm [LCP 2.4] – $P < 0.0001$). Conversely, mean F_T was not significantly different between the I-Loc 3, I-Loc 4,

or LCP 2.0 bone surrogates. Additionally, the mean F_T was not different between the I-Loc 4 and LCP 2.4 specimens ($P = 0.19$), although the LCP 2.4 FT was significantly lower compared to the I-Loc 3 and LCP 2.0 groups ($P < 0.05$).

Interestingly, when the Targon 3.0 pilot holes were moved to the metaphyses, this resulted in a significantly higher F_T ($P < 0.0001$), which was not different from the I-Loc 4 or LCP 2.4 specimens ($P = 0.7$ and 0.9, respectively).

Finally, when the F_T of the I-Loc, LCP and metaphyseal Targon 3.0 groups were compared to that of intact surrogates without cortical defects,[44] no significant difference was noted between groups ($P > 0.05$).

Failure mode for all groups was via spiral fracture through the innermost pilot hole (**Figure 2.12**). Conversely, intact surrogates in Study 1 failed via a spiral fracture in the diaphysis.[44]

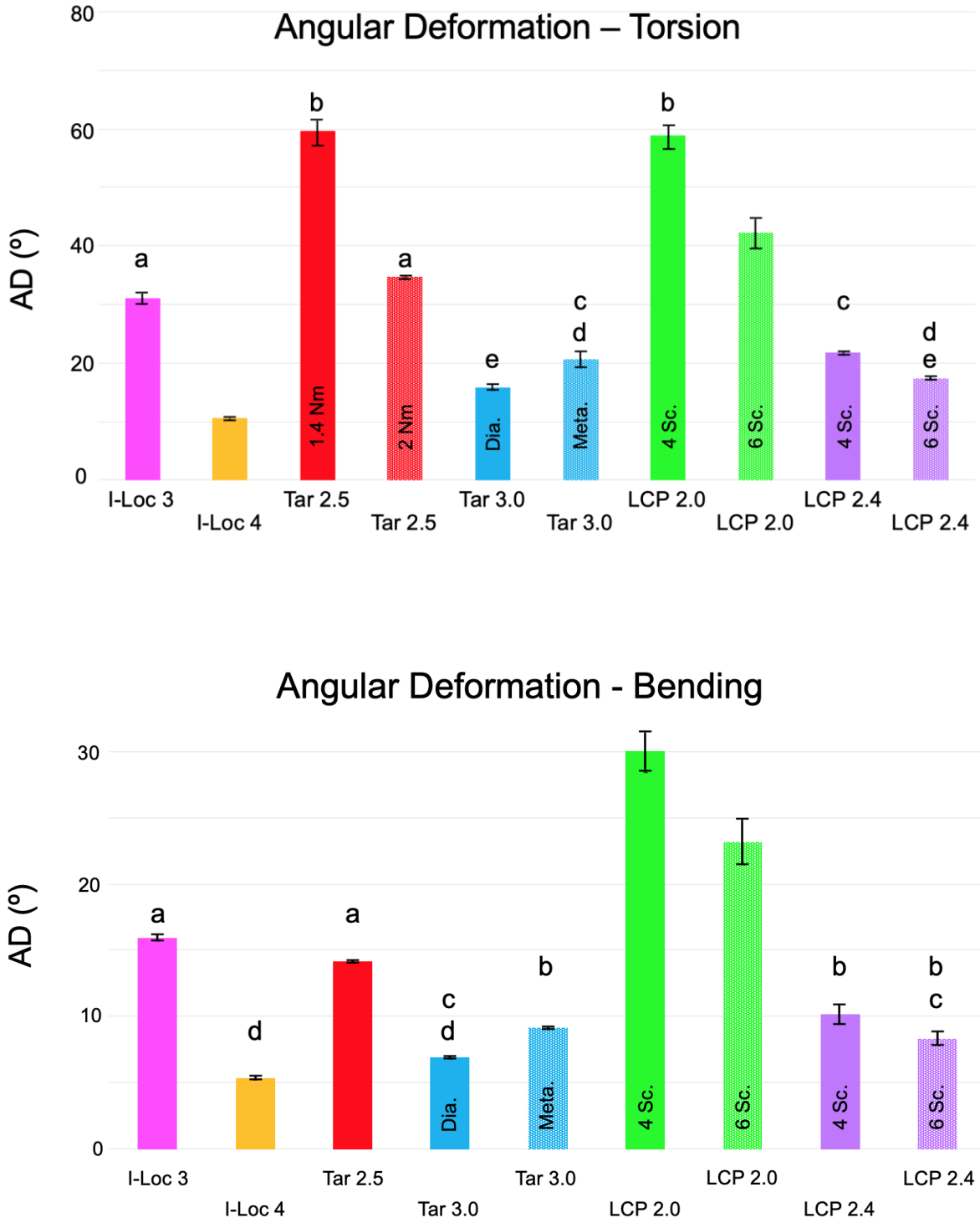

Figure 2.10: Mean torsional and bending angular deformations for all groups
Histogram of the mean torsional (top) and bending (bottom) angular deformation of all constructs. Similar letters denote groups that were not statistically different (P > 0.05) from one another. Dia, diaphyseal; LCP, locking compression plate; Meta, metaphyseal; Sc, screw; Tar, targon; TC, torsional compliance.

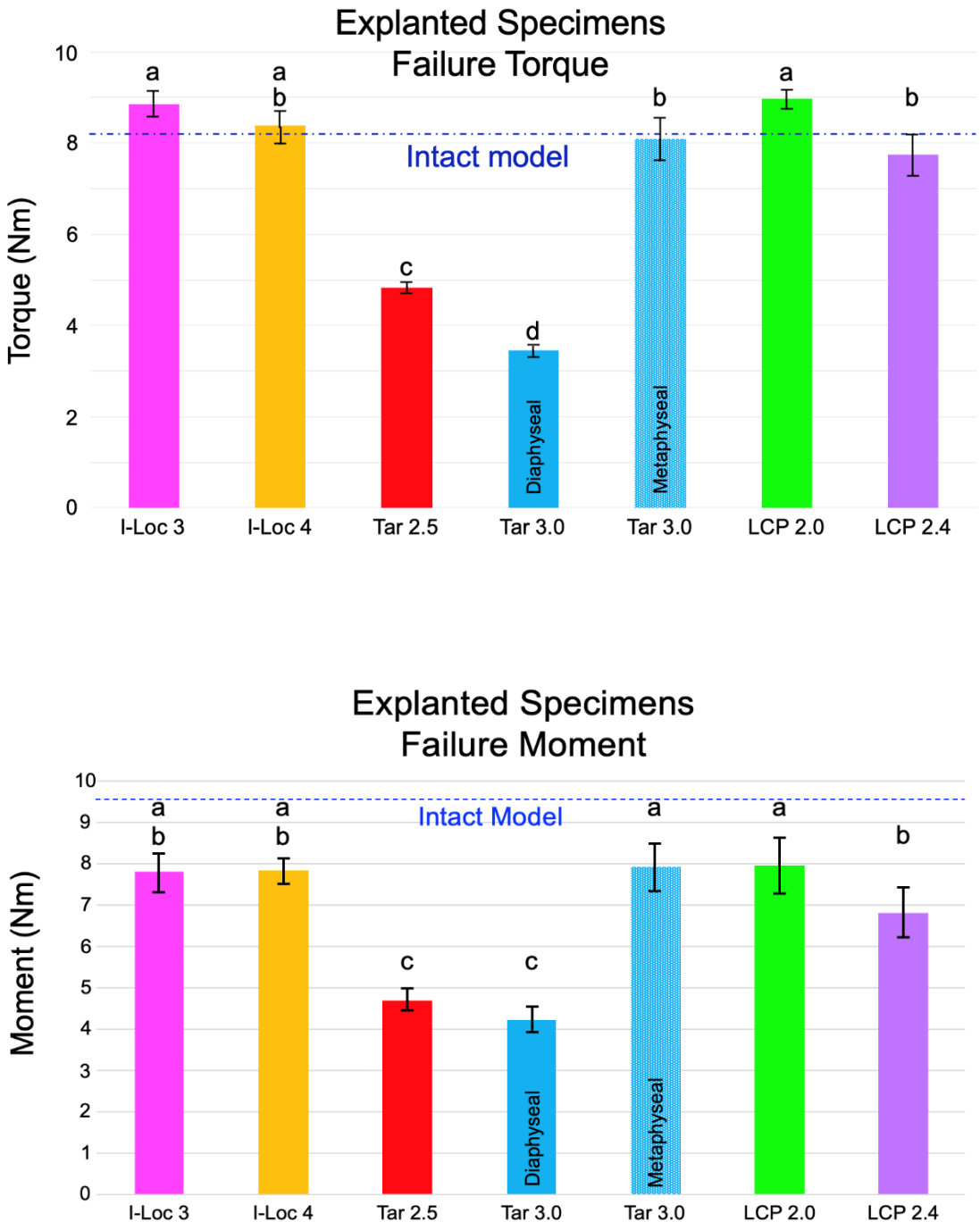

Figure 2.11: Mean explanted bone surrogate failure torque and moment
Histogram of the mean failure torque (top) and moment (bottom) of all explanted bone surrogates. Similar letters denote groups that were not statistically different (P > 0.05) from one another. The mean failure torque of the I-Loc 3 and 4, LCP 2.0 and Targon 3.0 models with metaphyseal holes were not statistically different (P > 0.05) when compared to that of the intact models without pilot holes (blue dotted line) from Study 1.[44]

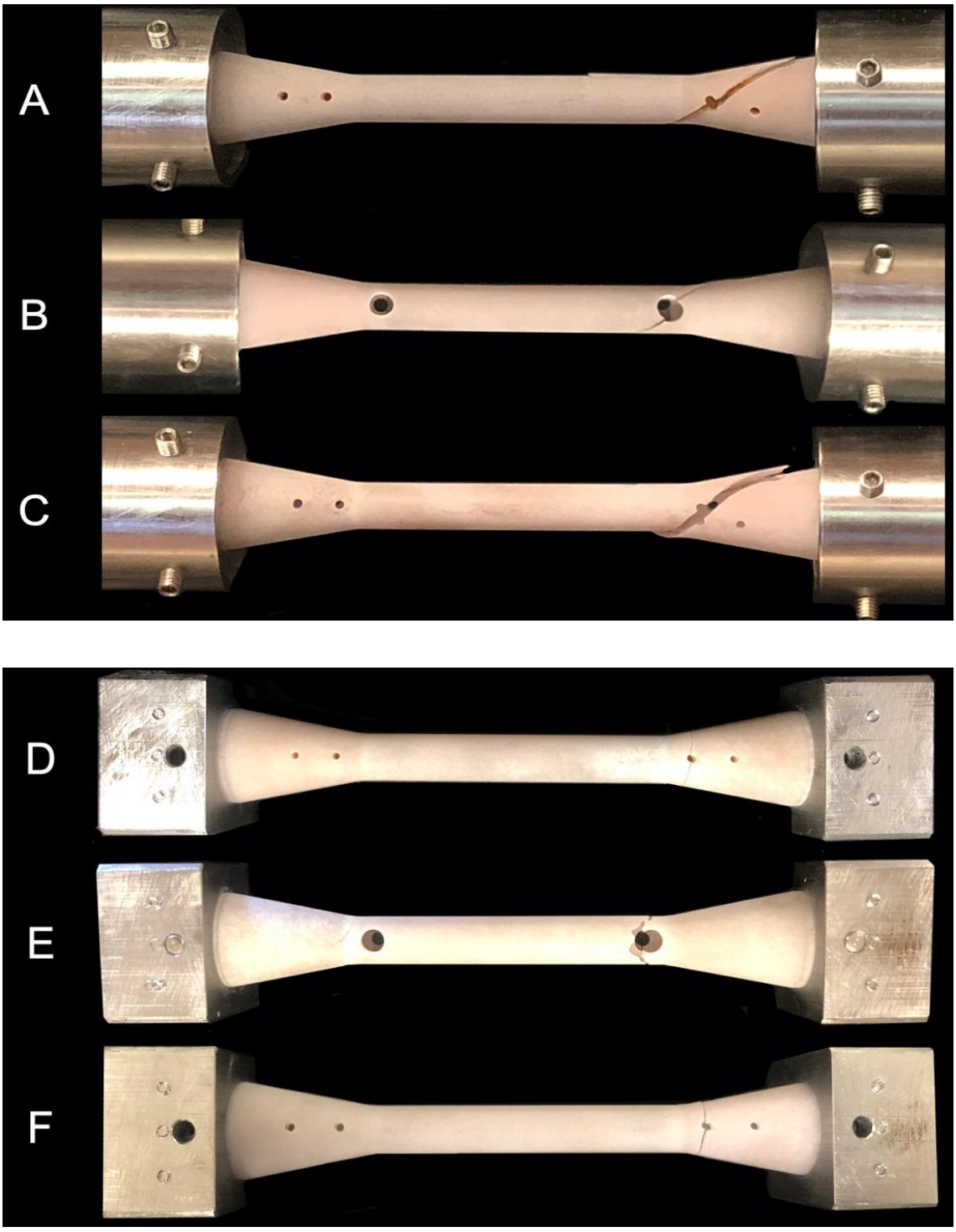

Figure 2.12: Failure mode of explanted bone surrogates in torsion and bending
Structural failure of the explanted bone surrogate models (Torsion: A, I-Loc 4; B, Targon 3.0; C, LCP 2.4; Bending: D, I-Loc 4; E, Targon 3.0; F, LCP 2.4). Regardless of the pilot hole size and mode of testing, all models failed through the innermost pilot hole where the defect to surrogate diameter ratio was the greatest.

2.9. BENDING

2.9a. Phase I – Bending compliance: **Figure 2.9** – The I-Loc 4 had the lowest BC (4.04 ± 0.1 ° / Nm) of all constructs evaluated (P < 0.001). while the LCP 2.0 with 2 screws per fragment had a larger BC (21.03 ± 0.2 °/Nm) than any other construct (P < 0.001).

A posteriori iterations had the following effects:

First, moving the Targon 3.0 bolts from the diaphysis to the metaphyses increased the BC by 22% from 5.2 ± 0.1 °/Nm to 6.8 ± 0.1 °/Nm (P < 0.001).

Second, when a 3rd screw was added to the LCP 2.0 constructs, the BC was reduced by 18% (P < 0.001) from 21 ± 0.2 °/Nm to 17.2 ± 0.9 °/Nm. Similarly, adding a 3rd screw to the LCP 2.4 constructs lowered the BC by 15% (P = 0.004) from 7.1 ± 0.3 °/Nm to 6.1 ± 0.4 °/Nm. However, BC of the LCP 2.4 constructs with 2 or 3 screws was not different from the metaphyseal bolted Targon 3.0.

2.9b. Phase I – Bending angular deformation: **Figure 2.10** – As with BC, the I-Loc 4 had the lowest AD (5.4 ± 0.2°), which was different (P < 0.001) from all constructs, except for the diaphyseal bolted Targon 3.0 (6.9 ± 0.1°). Similarly, the AD of the I-Loc 3 (15.9 ± 0.3°) and Targon 2.5 (14.2 ± 0.2°) were not different from one another. The largest AD of any group was seen with both LCP 2.0 constructs (30 ± 1.6° and 23.2 ± 1.7° [2 and 3 screws per segment, respectively]).

As with BC, differences in construct AD were again noted in the *a posteriori* groups.

First, when the Targon 3.0 bolts were moved to the metaphyses, the AD (9.2 ± 0.1°), was larger (P < 0.001) than that of the I-Loc 4. Conversely, the AD of this

metaphyseal Targon 3.0 was not different from either of the LCP 2.4 constructs with 2 or 3 screws (10.2 ± 0.7° or 8.3 ± 0.5°, respectively).

Second, adding a 3rd screw to the LCP 2.0 constructs reduced the AD by 23% from 30.1 ± 1.6° to 23.2 ± 1.7° ($P < 0.001$). Interestingly, while adding a 3rd screw to the LCP 2.4 did lower the AD by almost 19%, this reduction was not significant.

2.9c. Phase II – Failure moment explanted specimens: **Figure 2.11** – Failure moment was lower ($P < 0.0001$) in both the Targon 2.5 (4.7 ± 0.3 Nm) and Targon 3.0 (4.2 ± 0.3 Nm) surrogates when compared to all I-Loc and LCP groups. However, the F_M was not different between the Targon 2.5 and Targon 3.0 specimens. Similarly, the F_M was not different between the I-Loc 3 (7.8 ± 0.5 Nm), I-Loc 4 (7.8 ± 0.3 Nm), LCP 2.0 (7.9 ± 0.7 Nm) or LCP 2.4 (7.0 ± 0.4 Nm) surrogates.

A single *a posteriori* effect was noted. Moving the Targon 3.0 pilot holes to the metaphyses, resulted in a higher F_M (6.7 ± 0.5 Nm, $P < 0.0001$), which was not different from the LCP 2.4 specimens.

Finally, the F_M of all explanted groups was smaller than that of intact surrogate without cortical defects ($P < 0.001$).

Failure mode for all groups was via a transverse fracture through the innermost pilot hole. This is in contrast to the intact surrogates from Study 1,[44] which failed via a transverse fracture with cis-cortical butterfly fragment in the diaphysis (**Figure 2.12**).

DISCUSSION

The results of this study indicate that the I-Loc 3 and I-Loc 4 had lower TC and AD when compared to size-matched Targon nails and LCPs. In bending, the smallest overall BC and AD were seen in the I-Loc 4. Therefore, our first null hypothesis was rejected.

2.10. CONSTRUCT COMPLIANCE

Construct compliance (CC) is influenced by several factors,[48,49] including the implant area moment of inertia (AMI), a structural property related to its geometry reflecting the implant's ability to resist bending. Compliance is also affected by implant working length (WL), defined as the distance between the innermost fixation screws or bolts.

Despite the I-Loc and LCP having a longer WL than size-matched Targon nails (72 mm vs 56 mm), the I-Loc 4 constructs had a significantly lower TC and BC than all other groups. This is a somewhat counterintuitive finding that likely results from differences in implant geometry as well as implant material properties. Indeed, while the Targon 2.5 and 3.0 IMR diameters remain constant throughout their lengths, due to their hourglass profiles, those of the I-Loc nails gradually increase from a central core diameter of 2.4 mm or 3.2 mm to 3 mm and 4 mm at their extremities (I-Loc 3 and 4, respectively). Accordingly, the I-Loc 4 had the largest AMI of all implants tested (**Table 2.1**). In contrast, the AMI of LCPs vary more sharply between the plate solid sections and those with plate holes, while the AMI of Targon systems are inherently consistent throughout due to the constant nail diameters. Differences in material properties between the I-Loc and Targon

nails could also contribute to CC findings. The I-Loc nails are manufactured from 316L surgical grade stainless steel (ASTM F138). While the Targon IMR material is proprietary, one could speculate that it is relatively ductile since the locking mechanism relies on structural deformation of the IMR by a set screw. This could further explain the higher TC of the Targon constructs.

In contrast, the I-Loc nails' WL was similar to that of the 2.0 and 2.4 LCPs (72 mm versus 74 mm and 69 mm, respectively), yet, TC and BC were lower in I-Loc than size-matched LCP constructs. Since both implants are manufactured from 316L surgical grade stainless steel, discrepancies in implant geometries likely contribute to differences in construct CC. While torsional polar moment of inertia of the plates and nails cannot be directly compared due to the different behavior of rectangular and cylindrical implants, mechanical concepts can still be applied. Indeed, eccentrically located non-circular objects, such as plates, warp with applied torque. This alters the stress-strain distribution in their cross section.[50] The distribution is further distorted depending on which section of the plate is being evaluated (the solid section, locking, or non-locking hole). In contrast, a cylindrical implant such as a nail, located along the torsional axis of the construct, will behave linearly, with a uniform stress distribution.[50] Interestingly, despite a reduction in WL and CC (torsion and bending) when a 3rd screw was added to the LCP *a posteriori,* the I-Loc remained less compliant than size-matched LCP constructs. This suggests that from a clinical perspective, the lower CC of the I-Loc constructs could improve stability in cases when load sharing between the bone fragments cannot be re-established.

Targon nails had a similar WL compared to the LCP 2.0 and LCP 2.4 with 3 screws per fragment (56 mm vs 60 mm vs 61 mm, respectively). Yet, the Targon constructs had

a significantly lower BC than both LCP groups. This finding also likely results from differences in implant geometry and AMIs. Indeed, the Targon nail has an AMI which is as much as 2.1 times greater than the LCP 2.0 (**Table 2.1**). Furthermore, the Targon (and I-Loc) nails are located in the center of the FBS along its neutral axis, whereas the LCPs are applied eccentrically on the FBS surface. This eccentric location subjects plates to higher bending moments than centrally located implants such as the Targon or I-Loc, thereby likely increasing their BC.

Implant	Center	Extremity	Locking Hole	Non-Locking Hole	Between Holes
I-Loc 3	1.62	3.97	-	-	-
I-Loc 4	5.15	12.57	-	-	-
Targon 2.5	1.92	1.92	-	-	-
Targon 3.0	3.92	3.97	-	-	-
LCP 2.0	-	-	1.01	0.89	1.08
LCP 2.4	-	-	3.08	2.69	3.36

Table 2.1: Area moment of Inertia (AMI) for the implants evaluated
Area moment of inertia (AMI) for the implants evaluated. The AMI were obtained at the specified relevant locations. The I-Loc nails featured an hourglass profile resulting in a larger AMI at each extremity compared to that at the center of the nails. In contrast, the AMI of the Targon nails IMR was constant throughout the nail IMR length. The AMI of the LCPs were obtained from DePuy Synthes (personal communication). The thickness of the 2.0 and 2.4 LCPs were 1.5 mm and 2.0 mm, respectively.

In an effort to more closely match the WL and to mitigate the risk of construct failure following implant removal, the Targon 3.0 bolts were moved to the metaphyses, effectively increasing the nail WL from 56 to 79 mm. As expected, this resulted in a significantly more compliant construct. In contrast, adding a 3rd locking screw per segment in the LCP constructs reduced plate WLs by ~13%, which significantly lowered TC by ~20% and 28%, and BC by ~18% and 14% (LCP 2.0 and 2.4 mm, respectively). Regarding bending, in a mechanical study evaluating the fatigue life of plated SFE constructs using a comminuted fracture gap model, the interfragmentary displacement within the opposite cortex was increased by approximately 40% when using 2 versus 3 screws per segment.[51] The authors of that study speculated that such changes could impact the type and duration of fracture healing and should be considered when selecting a fixation method.[51] Similarly, our results suggest that using 3 screws on either side of the fracture gap could be recommended to improve construct stability.

2.11. ANGULAR DEFORMATION

As expected from TC data, torsional AD was lower in I-Loc than Targon nail constructs. While the unimodal shape of the angle of twist versus torque curve was anticipated since both nails were designed to provide angular stability, the unique multimodal shape of the Targon 2.5 curve suggested that sequential slippage at the IMR/set screw interface occurred. The Targon locking mechanism relies on the structural deformation of the IMR by the locking bolt set screw. As torque was applied however, the initial conical indentation further deformed into an oblong depression featuring two symmetrical ridges (**Figure 2.8**). Each ridge generated characteristic transient angular

resistive spikes along the slack section of the Targon 2.5 curves (**Figure 2.7**). Although slippage remained sequential during 10 cycles, one could speculate that ongoing deformation of the locking interface could lead to progressive flattening of the IMR ridges. This in turn could increase construct slack, hence instability, over time and risk of implant failure via fatigue fracture of the IMR at the level of the indentations. To reduce slippage, in an *a posteriori* experiment, the tightening torque of the Targon 2.5 set screws was increased from 1.4 Nm, as per manufacturer recommendation, to 2 Nm. As predicted, slippage was eliminated, likely as a result of increased friction at the locking interface. With elimination of the incremental slack, Targon 2.5 constructs underwent a marked 45% reduction in AD from 59° to 32.7°, which was not different from that of the I-Loc 3 (31.1°). The increase in tightening torque, however, led to structural damage to the set screw driving interface in ~40% of the screws. This precluded implementation of the desired 2 Nm and may be a limiting factor when considering application of a larger torque in clinical cases. Interestingly, slippage of the locking interface was not observed in the Targon 3.0 constructs (**Figure 2.8**). Considering that the same sized set screw is used to deform both the 2.5 mm and 3.0 mm IMR, one can assume that this relatively smaller defect in the larger IMR makes the system more resistant to slippage.

Interestingly, while the lowest torsional AD was consistently seen in the I-Loc constructs, the AD of the LCP 2.0 and Targon 2.5 constructs were similar. This suggests that, although I-Loc constructs provide greater angular stability, the small Targon and LCP implants could be used interchangeably in clinical cases. While increasing the set screw torque in the Targon 2.5 resulted in a statistically similar AD to that of the I-Loc 3, this could not be achieved reliably, which in turn limits the clinical usefulness of this

technique iteration. In contrast, the AD of the LCP 2.4 was greater than that of the Targon 3.0. However, this difference was eliminated by the addition of a 3rd screw to the LCP, thus suggesting that either construct could be selected in similar clinical cases.

While no significant differences in bending AD were noted between size-matched I-Loc 3 and Targon 2.5, or I-Loc 4 and Targon 3.0 nails, when the Targon 3.0 bolts were moved to the metaphyses differences were noted.

When bolted into the metaphysis, the Targon 3.0 WL increased to 79 mm. This resulted in torsional and bending AD between 41–49% larger than that of the I-Loc 4 and 23–25% larger than the diaphyseal bolted Targon 3.0 (both of which were significant). Additionally, the AD of the metaphyseal bolted Targon 3.0 was not significantly different from that of the LCP 2.4, regardless of whether 2 or 3 screws were used in torsion or bending. While this suggests that either a Targon or LCP construct could be chosen for a metaphyseal fracture, the current instrumentation available for the Targon system does not allow placement of metaphyseal bolts.[41] Indeed, the dedicated drill guide mandates that bolts be positioned perpendicular to the diaphyseal long axis to allow insertion of the nail IMR in the bolt cannulations. While metaphyseal bolts could be placed free-handed, this technique is more challenging and may be less reliable. From a clinical perspective, the significantly larger AD could result in delayed bone healing, should interfragmentary strain become excessive. Therefore, our results suggest that in cases where a bridging construct is necessary, such as highly comminuted fractures, the I-Loc may provide superior mechanical stability when compared to Targon or LCPs.

2.12. EXPLANTED SURROGATE FAILURE

Our results showed that the failure torques and moments of the explanted intact bone surrogates varied between groups, therefore, we rejected our second null hypothesis. Although seldom performed, implant removal following bone healing may become necessary in cases such as infection or implant associated soft tissue irritation. Indeed, nail explantation due to distal bolt exposure was required in 6% of feline fractures treated with Targon nails.[42] Following implant removal, cortical defects may act as stress risers, predisposing the bone to fracture at these sites.[52-54] A previous experimental study demonstrated that a circular defect representing 20% of the bone diameter resulted in a 34% decrease in torsional strength compared to intact bone. Increasing that defect size to 50% of the bone diameter led to a significant 62% reduction in torsional strength.[54] Based on such studies, it has been recommended that in clinical cases, the size of a screw or bolt should not exceed 20%[54] of the bone diameter. In our study, the largest cortical defect to bone diameter ratios (**Table 2.2**) in the I-Loc and LCP bone models (at the level of the innermost bolt or screw) were 17.4% (I-Loc 4) and 14.5% or 18% (LCP 2.4 with 4 and 6 screws, respectively). From a clinical perspective, such ratios suggest that I-Loc or LCP implant removal following clinical union is safe and unlikely to result in iatrogenic refracture. Indeed, the torsional strength of the bone surrogates with I-Loc and LCP pilot holes was not different from that of intact bone models in a previous study.[44] Conversely, the largest cortical defects left by the Targon 2.5 and Targon 3.0 pilot holes represented 48% and 56% of the bone surrogate diameter, respectively. This resulted in a F_T that was 59% and 42% that of intact bone surrogates[44] Similarly, in bending, Targon defects resulted in a significant 41% (Targon 2.5) and 47% (Targon 3) reduction in F_M.

These findings suggest that Targon nail explantation could increase the risk of iatrogenic fracture. Interestingly, a retrospective clinical study suggested that the Targon 2.5 could be placed in a bone with a diameter of 6.4 mm at the level of the locking bolt.[42] If explanted, that cortical defect would represent approximately 75% of the bone diameter. Based on a previous study by Edgerton,[54] one may extrapolate that the torsional strength of that explanted bone would be less than 25% that of the intact bone (**Figure 2.13**).

Implant	Innermost Cis Hole ∅ (mm)	Innermost Hole Surrogate ∅ (mm)	Innermost Hole Cortical Defect %
I-Loc 3	1.6	11.48	13.9
I-Loc 4	2.0	11.48	17.4
Targon 2.5	4.8	10	48
Targon 3.0	5.6	10	56
Targon 3.0 Meta	5.6	13.35	41.9
LCP 2.0 (4 screws)	1.5	12.54	12
LCP 2.0 (6 screws)	1.5	10	15
LCP 2.4 (4 screws)	1.8	12.40	14.5
LCP 2.4 (6 screws)	1.8	10	18

Table 2.2: *Cis* pilot hole diameter for each implant and corresponding ratio to bone diameter (% cortical defect) at the innermost hole
Cis pilot hole diameter for each implant relative to the FBS outer diameter at that location are listed in columns 2 and 3. The ratio (cortical defect %) at the innermost hole, closest to the diaphysis, is shown in column 4. All implants except the Targon 2.5 and Targon 3.0 had ratios that remained less than the recommended 20% of bone diameter.

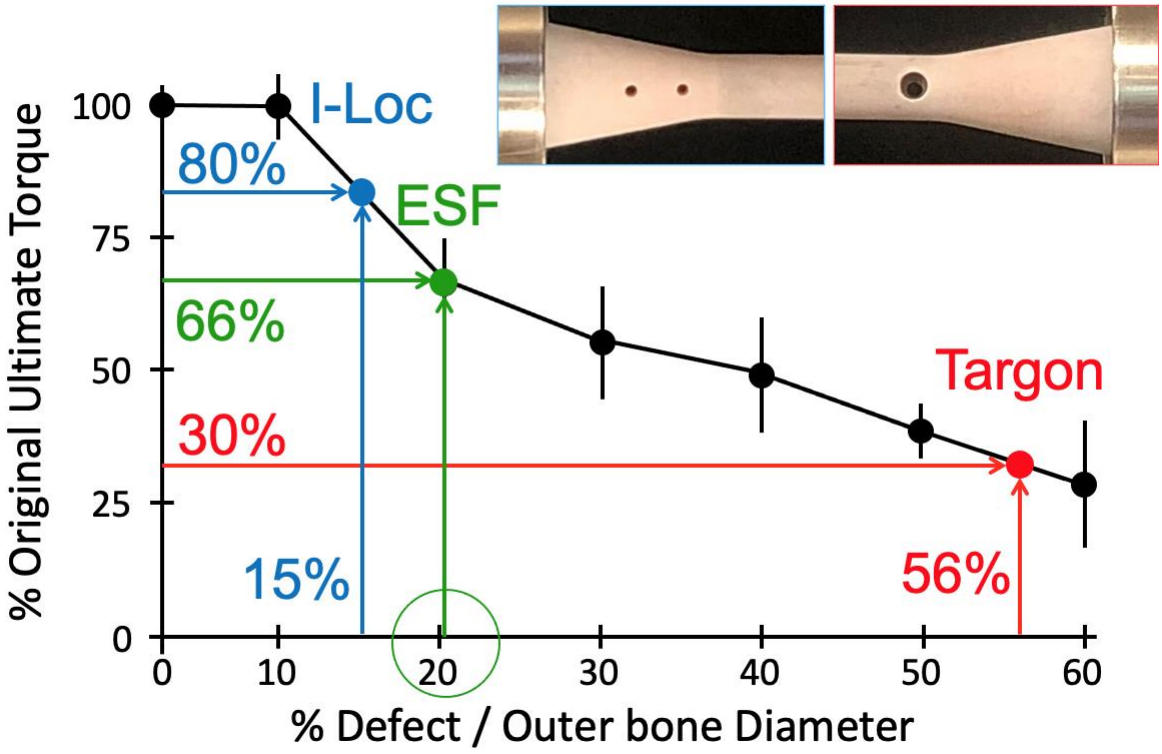

Figure 2.13: Graph showing reduction in torsional bone strength at corresponding pilot hole diameters

Original ultimate torque versus bone / surrogate defect diameter (%), adapted from Edgerton et al 1990. A pilot hole that comprises ~20% of the bone diameter, results in bone torsional strength which is only 66% of the original.[54] In this thesis, the I-Loc nail pilot holes were ~15% of the diameter of the bone surrogate at that location, resulting in a bone surrogate with 80% of the original torsional strength. Conversely, Targon nails created pilot holes that were a maximum of 56% of the bone surrogate diameter. Subsequently, a torsional strength only 30% of the original bone surrogate was identified.

When the metaphyseal pilot hole location was evaluated *a posteriori* in the Targon 3.0 group, the F_T increased and was not statistically different when compared to that of the I-Loc 4 and LCP 2.4 groups. Conversely, although moving the bolts to the metaphyses did result in a significant 63% increase in bending strength, it remained significantly lower (15%) than that of the I-Loc and LCP bone models. While this suggests that the risk for iatrogenic fracture following Targon explantation may be mitigated by moving the bolts to the metaphyses, the previously outlined limitations of this alternate position should be considered.

Interestingly, all explanted models failed at a significantly lower moment than the intact FBS. However, as torsion is the main loading mode of long bones,[10,55,56] one could argue that, while bending data should not be discounted, torsional data may be more relevant during clinical decision making.[51]

Lastly, we accepted our third null hypothesis that all groups would exhibit similar failure modes, both in torsion and 4-point bending. Indeed, all bone surrogates failed in torsion via a spiral fracture through the pilot hole, and in bending via a transverse fracture through the pilot hole, regardless of its size. Additionally, all fractures in our study involved the *innermost* pilot holes where the defect to bone surrogate diameter was the greatest. This finding was expected based on the results of previous experimental studies evaluating the effect of diaphyseal circular defect diameters on the torsional strength of human and lapine long bones,[52-54,57] Indeed, these studies demonstrated that torsional strength significantly decreased with increasing defect size and shape (**Figure 2.13**).[52-54] Similarly, as bending moments are applied, fractures propagate from the tension side of the bone to the compression surface transversely.[1] As expected, the fractures began at

the innermost pilot holes on the tension side, where stress concentration is the highest[58] and then progressed to the compression side. Accordingly, our results suggest that the risk of post explantation refracture should be considered when devising patient recovery plans.

As with any mechanical study, some limitations may be identified. While synthetic bone models likely behave differently than cadaveric specimens, these have several advantages including ethical considerations, ease of procurement, limited inter-specimen variations as well as reduced biohazard risks. Nonetheless, this model was previously validated as a suitable feline bone model surrogate.[44,59]

Our primary rationale for this study was to compare novel AS-ILNs devised for feline patients. While the implants, as well as fixation methods, chosen in control groups represent a subset of available implants and osteosynthesis techniques, these have commonly been used in clinical and experimental studies.[38,60,61] As in our study, the 2.0 mm and 2.4 mm LCPs were the most commonly used locking plates in a recent retrospective study of 64 feline fractures.[38] Although other fixation methods, such as orthogonal plating and plate rod combination were not assessed in this study, alternative plate screw distributions were evaluated and showed that, should an increase in construct stability be desired, the addition of one screw per segment could be considered as a potentially less invasive alternative.

All implants evaluated in this study were applied in a bridging mode over a large 30 mm gap fracture model. In the absence of cortical continuity, implants are subjected to high torques and bending moments, and subsequently larger angular deformations. As suggested in a previous study,[40] had a contact or small gap fracture model been used,

potential interference between implants and model could have yielded different results. Our goal, however, was to simulate a comminuted mid-diaphyseal fracture pattern commonly encountered in small animal traumatology.[38,42,62]

In summary, this study suggests that the I-Loc 3 and I-Loc 4 nails provide greater overall stability than Targon nails and small LCPs. Although the previously documented slippage of the Targon 2.5 locking interface was confirmed in our study, instability was not identified in the Targon 3.0 nail, which suggests that the larger Targon should selected whenever possible. However, the diaphyseal defects created by the Targon bolts significantly reduced the torsional and bending strength of bone model surrogates. Conversely, the small pilot holes of the I-Loc and LCP implants had no effect on the torsional strength of the bone models, which is the primary loading mode *in vivo*. This suggests that the risk of fracture following I-Loc and LCP implant removal may be clinically irrelevant. Furthermore, while both I-Loc and Targon implants were mechanically superior to size-matched bone plates, addition of a 3rd screw per segment may be used to improve the stability of plated constructs. Given our results, I-Loc nails may represent effective alternatives to other available feline osteosynthesis options.

STUDY 3:

CLINICAL APPLICATION OF THE SMALL I-LOC INTERLOCKING NAIL IN 30 FELINE FRACTURES: A PROSPECTIVE STUDY

INTRODUCTION

Despite innovations in implant development such as locking plates (LCP), and a shift towards minimally invasive plate osteosynthesis (MIPO), complications following feline fracture repair remain a challenge for orthopedic surgeons.[63,64] Recognized complications include, but are not limited to, implant yield or fatigue (7-13%),[38,63] pin migration (3-19%),[16,38] and non-union (NU).[62,64] Perhaps the most challenging of these is NU,[62,64]which has been reported in as many as 4-8% of cases with internal fixation.[62,64] Regardless of the cause, complications can severely affect prognosis. While orthogonal plating has been proposed to reduce complication rates,[63,65,66] this approach represents a departure from the current paradigm shift toward more biological techniques.[67-70] Alternatively, the use of interlocking nails (ILN) may offer a method of improving outcomes while still adhering to biological osteosynthesis principles.[15,18,21,71] As intramedullary (IM) devices, ILNs provide several advantages over other modes of fixation. First, ILNs preserve the periosteal blood supply, which is crucial to fracture healing. Second, ILNs are shielded against deleterious bending moments due to their location along the bone neutral axis and better resist bending due to their relatively larger AMI compared to size-matched bone plates. Third, ILNs utilize bridging osteosynthesis, which has been shown to enhance bone healing via preservation of the fracture hematoma and decreases

disruption of the fracture environment.[72] Bridging osteosynthesis also provides sufficient stability to allow callus formation while limiting stress-shielding, which may result in delayed union compared to traditional techniques.[73]

Drawbacks to original ILN designs included persistent torsional and bending instability known as slack,[47] which may impair bone healing, as well as fatigue failure in nails with continuous hole distribution.[17] Off site screw placement ("missed screw") rates of 4-12% have been also reported.[15,17] Early ILN designs were only indicated for fixation of diaphyseal fractures, likely as a result of unrecognized slack and a subsequent angular limb deformity.[74] To circumvent these limitations the I-Loc, a novel AS-ILN, was devised.[6] The large I-Loc nails (6, 7 or 8 mm in diameter) have been evaluated experimentally[6,20,22] in which mechanical superiority to plates was demonstrated. Additionally, excellent clinical results were reported a subsequent prospective study of 100 trauma cases, including challenging epi-metaphyseeal fractures.[18]

Recently, a smaller I-Loc system (3, 4 and 5 mm nails) suitable for feline use became available. Evaluation of the smaller I-Loc nails (3 and 4 mm) was the object of Study 2 of this thesis work, and results showed mechanical superiority to Targon nails and LCPs.[75] However, these smaller nails have yet to be evaluated clinically. Therefore, the purposes of this study were to 1) prospectively describe patient outcomes following use of the small I-Loc in cats and 2) report clinically relevant recommendations for I-Loc use in feline traumatology. Our hypotheses were that 1) interlocking nailing in cats using the small I-Loc is achievable, even in cases of epi-metaphyseal fractures and 2) healing times and complication rates would be improved from previous reports on either ILN or traditional fixation for feline long bone osteosynthesis.

MATERIALS AND METHODS

3.1. IMPLANT DESCRIPTION

The I-Loc 3-4-5 mm instrumentation and nail design are similar to the larger 6-7-8 mm system (**Figure 3.1**), yet some specific differences exist between the two nail families. Briefly, the smaller nails retain the hourglass profile with a bullet nose distal tip to aid in nail insertion and fracture reduction. Threaded bolts engage threaded cannulations in the nail. In contrast to the tapered threaded design of the I-Loc 6-7-8, the top thread of the I-Loc 3-4-5 is plastically deformed during tightening, effectively locking the implant and creating a rigid, angle-stable construct. Dedicated instrumentation includes an insertion handle coupled to a nail extension and an alignment guide. Additional instrumentation is comprised of an awl and trial nail, drill sleeves and bits, temporary threaded fixation posts, depth gauge, bolt cutters and screwdriver which are used to complete fixation (**Figure 3.1**). A dedicated hammer pin can be used to impact the nail in the distal metaphysis. The I-Loc 3-4-5 mm nails are available in lengths ranging from 60 mm–160 mm, with 8 mm increments between sizes. The *cis* hole is drilled at 1.6 mm, 2.0 mm or 2.6 mm (I-Loc 3, I-Loc 4, I-Loc 5, respectively); the *trans* hole is drilled at 1.2 mm, 1.6 mm, or 2.0 mm (I-Loc 3, I-Loc 4, I-Loc 5, respectively).

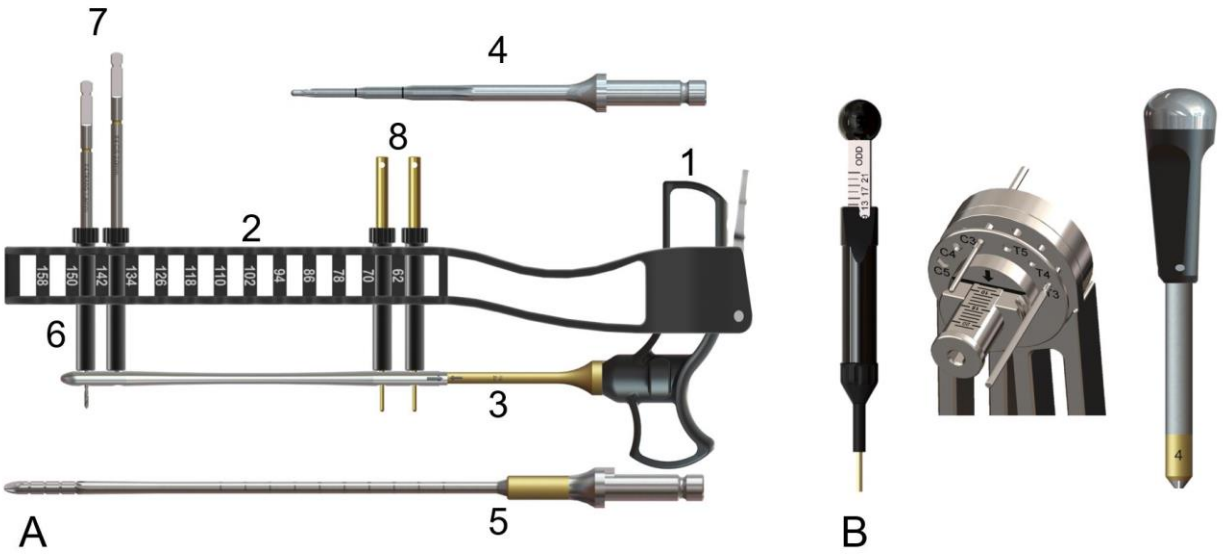

Figure 3.1: Instrumentation for the I-Loc 3-4-5 mm interlocking nail system
A – Dedicated instrumentation includes an insertion handle (1) coupled to an alignment guide (2) and a nail extension (3). Additional instrumentation is comprised of an awl (4), trial nail (5), drill sleeves (6) and bits (7) as well as temporary fixation posts (8). B – Depth gauge, bolt shearers and screwdriver (left to right, respectively) are used to complete fixation.

3.2. POPULATION AND PRE-OPERATIVE ASSESSMENT

Consecutive, client owned cats presenting to the College of Veterinary Medicine at Michigan State University with fractures of the femur, tibia and humerus were prospectively enrolled in the study. Exclusion criteria were limited to cases in which the senior surgeon (Loïc M. Déjardin) was not directly involved in pre-operative planning and/or the surgical procedure. While various osteosynthesis options were both discussed with each cat owner and considered during pre-operative planning, the final decision regarding surgical treatment was left to the discretion of the surgeon managing the case. As interlocking nailing has been the standard of care at our institution for more than a decade, and since direct comparison between osteosynthesis techniques was not the purpose of this prospective study, neither institutional approval nor client consent to a specific surgical technique were required. Nonetheless, client consent to perform surgical repair was obtained as part of the admission process in all cases.

Patient signalment and fracture etiology were recorded. Concurrent injuries in cases of polytrauma were classified as orthopedic, soft tissue or neurologic. Orthogonal radiographs of both the affected and contralateral bone were obtained as part of the pre-operative planning. Linear and/or spherical magnification markers were incorporated in all radiographic views. When fractures involved the epi-metaphyses, a computed tomography (CT) scan was performed to further characterize the fracture pattern[32] and aid with surgical planning. Radiographs were uploaded into surgical planning software (OrthoView VET, Hampshire, UK) and templated for selection of a suitably sized I-Loc. When the appropriate nail length was determined to be between two sizes, the longer nail

was chosen and the distal tip was shortened (**Figure 3.2**) to allow maximal bolt purchase in the distal metaphyseal/epiphyseal cancellous bone.

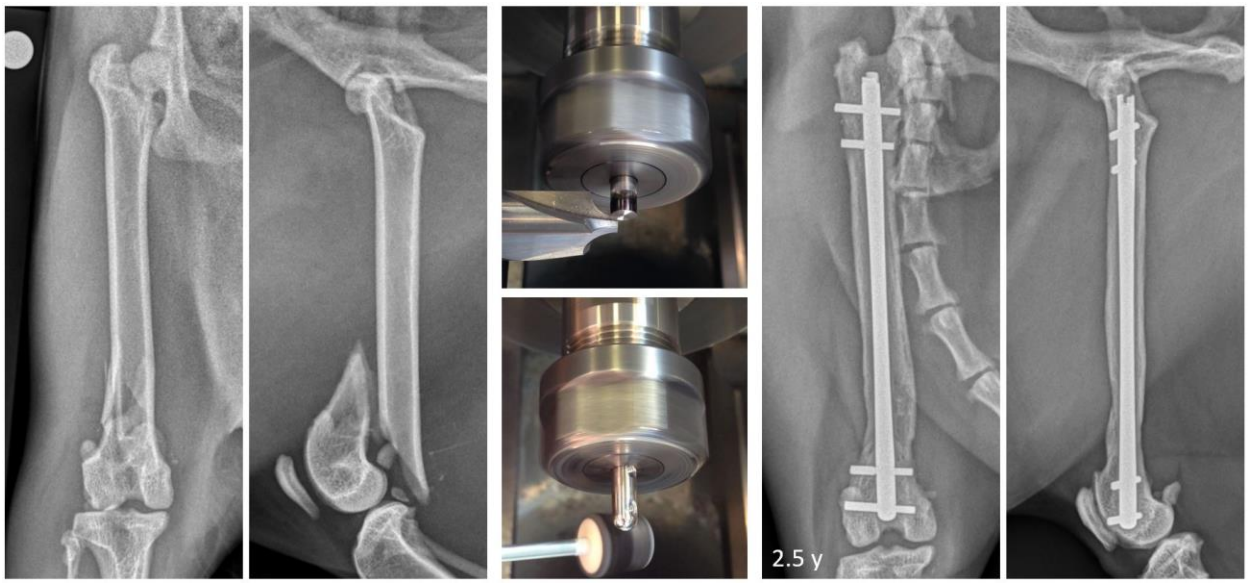

Figure 3.2: Feline femoral fracture repair using a modified I-Loc nail
A computer numerical control lathe is used to shorten and polish the distal tip of an I-Loc 4 (middle panel). The modified nail was used to repair a comminuted supratrochlear femoral fracture (left panel). Shortening of the distal tip allows deep seating of the nail immediately proximal to the Blumensaat's line, thus optimizing bolt fixation in the strong cancellous bone of the distal epi-metaphysis (right panel).

3.3. SURGICAL PROCEDURE

Anesthesia, aseptic preparation for surgery, peri-operative antibiosis and post-operative pain management were conducted according to standard protocols at our institution. All surgeries were performed by one or two board-certified surgeons. The surgical approach (open reduction internal fixation [ORIF] or minimally invasive nail osteosynthesis [MINO])[76] as well as use of ancillary fixation were left to the surgeon's discretion and recorded for each patient. Following bone specific approaches, the proximal epi-metaphysis was opened by inserting Kirschner wires or Steinman pins of increasing diameter followed by a dedicated awl. Next, the distal metaphysis was prepared using a trial nail that corresponded to the I-Loc size selected for each patient. The nail was attached to the insertion handle via a nail extension and introduced normograde until it was deeply seated into the distal metaphysis. According to I-Loc specific surgical guidelines previously established by the inventor of the system (Loïc M. Déjardin), cis then trans cortical pilot holes were drilled sequentially through the dedicated alignment guide starting with the most proximal nail cannulation. Threaded posts were then inserted in the proximal nail cannulation(s), thereby temporarily securing the nail in place (**Figure 3.3A**). After ensuring rotational alignment, the distal cannulation(s) were drilled either using the alignment guide or a free-hand technique (**Figure 3.3B**). Appropriately sized cut-to-length bolts were then inserted in sequential order from proximal to distal. Nail orientation, customization and variations from the standard 2:2 bolt distribution, i.e. 1:1, 2:1 or 1:2 were documented. Finally, the occurrence and location of off-site drilling and/or bolt insertion (missed nail cannulations) were recorded. Routine closure in layers using appropriately sized suture concluded each procedure.

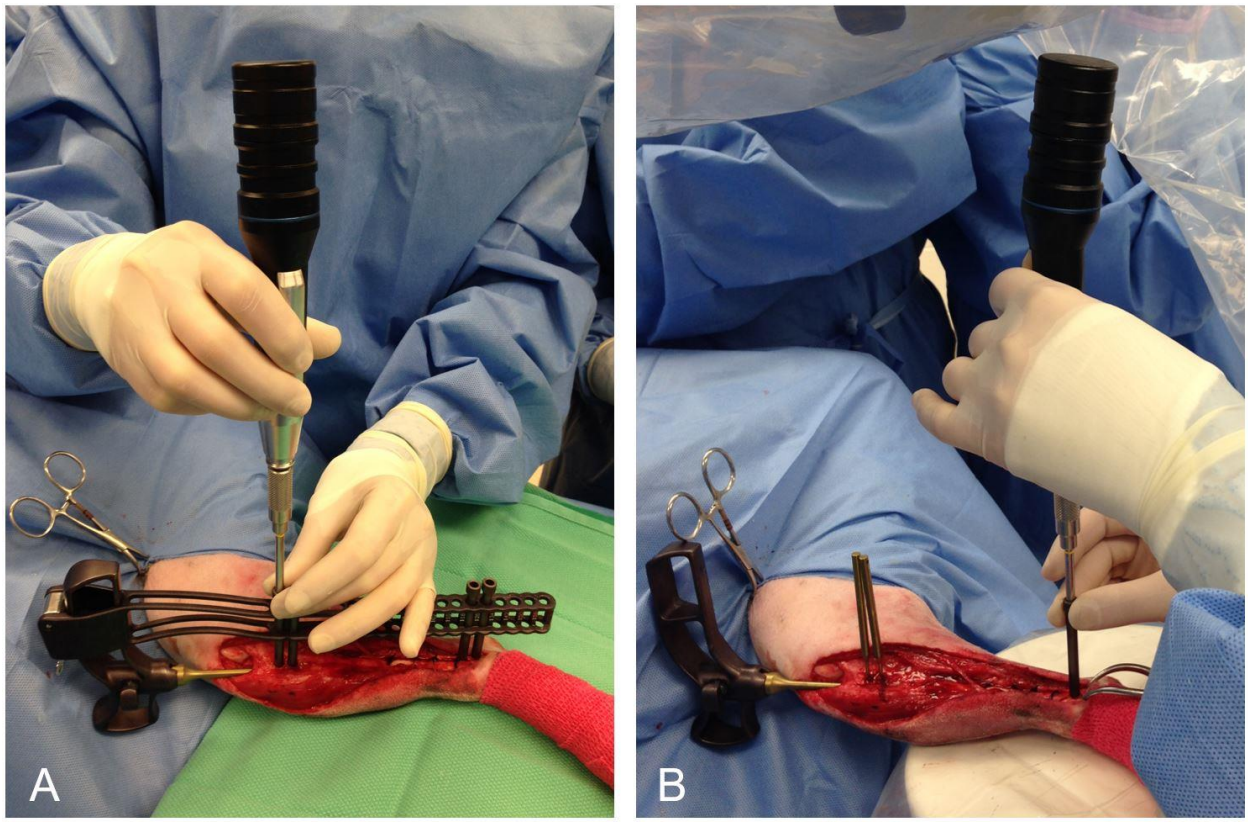

Figure 3.3: Image of a small lightweight drill used for clinical cases
Using a small lightweight, battery-powered drill facilitates proper alignment with I-Loc cannulations. Proximal cannulations are routinely drilled using the alignment guide (A), while distal cannulations in the tibia and humerus may be drilled free-hand while holding the drill sleeve parallel to the insertion handle (B).

3.4. POST-OPERATIVE RADIOGRAPHIC ASSESSMENT

Orthogonal radiographs of the operated limb were taken immediately post-operatively. Subsequent radiographic rechecks were recommended at 3, 6 and 9 weeks PO, or until documentation of clinical union[77] was achieved.

Alignment in the transverse plane (valgus and varus) was evaluated on craniocaudal radiographic projections as previously described.[67,78,79] Alignment in the sagittal plane (pro and recurvatum) was subjectively assessed on mediolateral views, except for tibial fractures where the tibial plateau angle (TPA) was measured as described by Warzee et al.[80] These angles were compared to those of contralateral intact bones and reported as differences from normal. Rotational alignment was subjectively evaluated in comparison to the contralateral bone in the sagittal (femur and tibia) or transverse (humerus) planes. Femoral neck version was described as anatomical, anteverted or retroverted based on the location of the femoral head in relation to the proximal cranial femoral cortex. Tibial and humeral torsion were described as anatomical, external or internal based on the relationship between the caudal edges of the tibial plateaus or the humeral head location in relation to the bone mechanical axis, respectively).

Fragment apposition or adjacency was recorded as good, adequate or unacceptable as previously described.[67]

Nail size in relation to cat's body weight and bone type were documented. In order to determine the percentage of the medullary canal (MC) filled by the nail (nail width to MC width ratio), the MC diameter was measured at the bone isthmus and compared to the nail diameter at that location.

3.5. POST-OPERATIVE PATIENT ASSESSMENT

Cats were subjectively assessed daily for limb use while hospitalized, then at each revisit. If a recheck examination was missed, an owner telephone interview was conducted to assess patient progress. Limb function was subjectively evaluated by one of two board certified surgeons at each revisit as well as at the time of CU. Limb function was noted as either ”normal” or ”residual lameness”. Complications were classified as major or minor and were recorded until the time of clinical union (CU). Major complications were defined as those requiring revision surgery under general anesthesia. Minor complications were defined as those that could be treated locally or with oral medications, or those not requiring treatment of any kind.

3.6. DATA ANALYSIS

Descriptive statistics were recorded and compared to published historical data for cats when available. Outcome measures included 1) patient signalment and fracture etiology, 2) bone distribution and fracture pattern, 3) surgical technique (including approach (ORIF or MINO) and ancillary fixation, primary vs revision surgery, nail modification as well as bolt distribution and off-site insertion, 4) postoperative assessment (including alignment, nail size relative to body weight, nail to MC ratio) and 5) limb function and time to CU as well as complication rate and type (major and minor).

RESULTS

3.7. POPULATION AND PRE-OPERATIVE ASSESSMENT

3.7a. Signalment and fracture etiology: A total of 29 cats (25 DSH, 1 DMH, 1 Snowshoe, 1 Savannah Cat, 1 Siamese) with 30 long bone fractures were included. There were 24 males and 5 females. The mean age was 5.2 ± 5.1 years (range 6 weeks – 19 years) and the mean body weight was 4.7 ± 1.8 kg (range 1.1 – 8.37 kg). Fracture etiology included unwitnessed trauma (n = 16), trauma from jumping (n = 2), fall from a cat tree or counter (n = 3), gunshot wound (n = 3), road traffic accident (n = 1), iatrogenic from bone marrow biopsy (n = 1), dog bite (n = 1) and revision surgery (n = 2, **Figure 3.4**).

Concurrent injuries occurred in 8 cats and consisted of soft tissue lesions (proximal urethral tear, small open wounds and infected tail injury) in 5/8 cats (62.5%) and/or were multiple orthopedic injuries in 4/8 cats (50%). These included: pubic fractures and an ipsilateral sacroiliac luxation in one cat; an ipsilateral tibial fracture in the cat with a proximal urethral tear; a contralateral tibial fracture; and a contralateral femoral fracture non-union. No concurrent neurological abnormalities were noted in any patient.

3.7b. Bone distribution and fracture pattern: There were 16 femoral fractures (53.3%), 9 tibial fractures (30%) and 5 humeral fractures (16.7%). Diaphyseal fractures were observed in 80% of cases. Of these, 46% were comminuted and 54% were considered simple. Epi-metaphyseal fractures (**Figures 5 and 6**) represented 20% of the cases, with an equal distribution between proximal and distal locations. Overall,

comminuted fractures were observed in 20/30 (67%) cases. Four fractures were classified as open (13%) including gunshot wounds in two humeri and one femur as well as one comminuted tibial fracture.

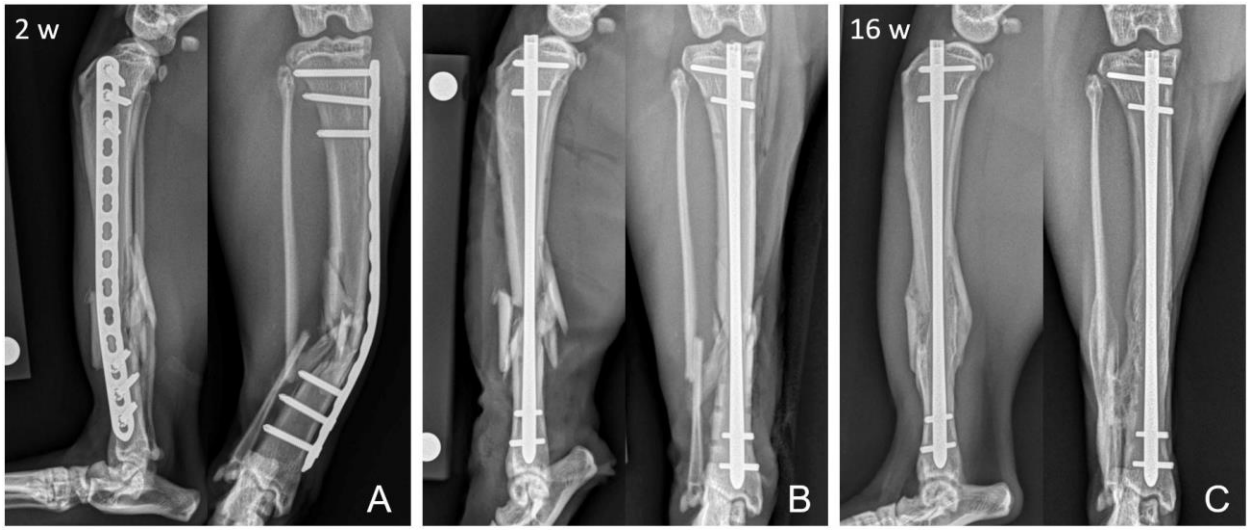

Figure 3.4: Radiographic images of plate yield failure and subsequent revision using an I-Loc nail
This comminuted tibial fracture was initially repaired using a 2.4 mm locking compression plate (LCP). Due to the comminuted nature of the fracture, the trans cortex was not reconstructable. At two weeks postoperatively, the LCP underwent yield failure (A). Following plate removal, the fracture was successfully revised using an I-Loc 4. To avoid previous plate screw holes, the bolts were oriented at approximately 45° to the sagittal plane (B). This technique illustrates the versatility of interlocking nailing compared to plate osteosynthesis. Bone remodeling is seen at 16 weeks after revision surgery (C).

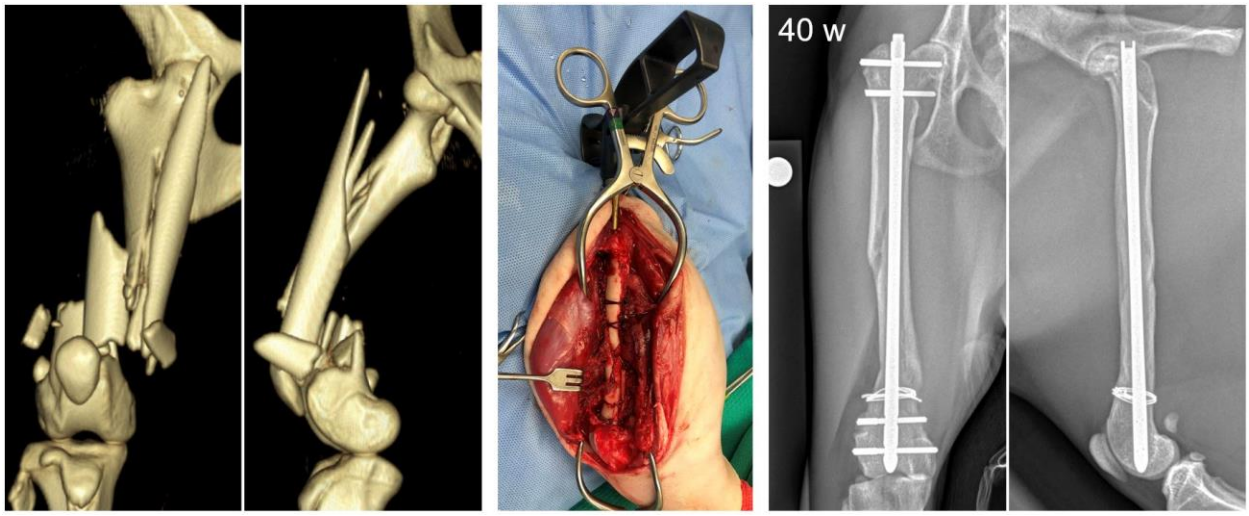

Figure 3.5: Example of an epi-metaphyseal fracture repair
Epi-metaphyseal fractures occurred in 20% of the cases seen in this study and were equally distributed between proximal and distal extremities (left). The diaphysis was reconstructed using proximal PDS “lassos” and one double loop cerclage wire distally to improve load sharing (middle). Over-reduction of the distal femoral fragment was performed in order to more deeply seat the I-Loc in the robust distal cancellous bone shelf and allow placement of two condylar bolts (right).

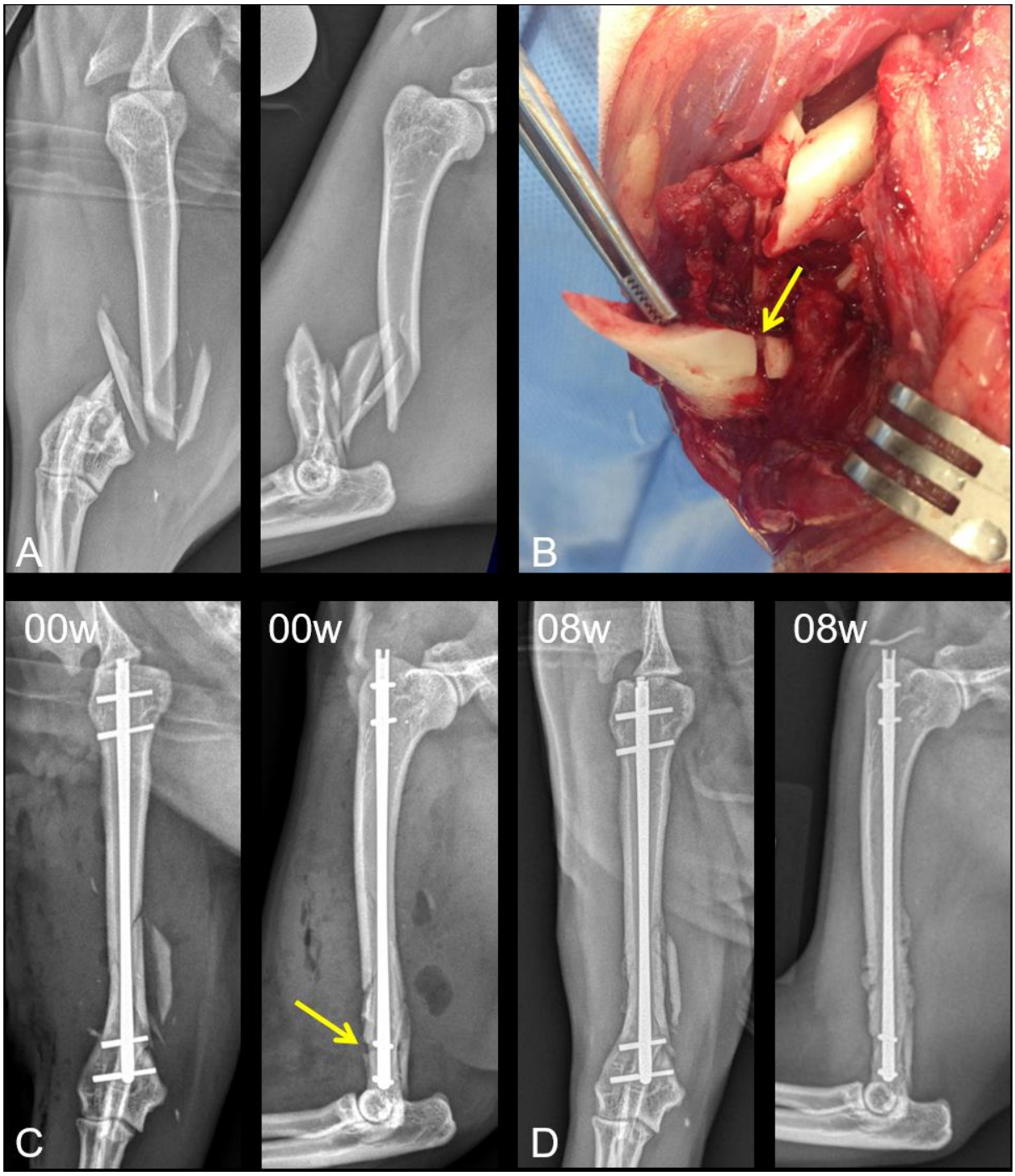

Figure 3.6: Fixation of a comminuted supracondylar fracture extending into the epi-metaphysis past the supracondylar foramen

A, Supracondylar fracture. B and C, An ostectomy of the supracondylar foraminal osseous bridge was performed (yellow arrows) to free the median nerve and brachial artery. C, An I-Loc 3 was modified to allow placement of two bolts in the short distal fragment. This technique is beneficial to avoid iatrogenic damage to this neurovascular bundle during fragment manipulation and reduction as well as drilling of the bolt pilot holes D, Bone healing is shown at 8 weeks.

3.8. SURGICAL PROCEDURE

An ORIF approach was taken for 22 fractures (73%) while the other 8 (27%) were repaired using MINO techniques.

In 28/30 cases (93.3%) primary fracture repair was performed while revision surgeries comprised 6.7%.

Ancillary fixation was employed in 5 cases (17%) and included double loop cerclage, lag screws, or Kirshner-wires as well as temporary external skeletal fixation.

In 5 cases (3 femora, 1 humerus, 1 tibia), the nail was shortened using a lathe in order to achieve deep seating in the distal metaphysis (**Figures 3.2 and 3.6**). One nail was placed in a cranio-caudal orientation in order to avoid fissures.

A 2:2 bolt distribution was used in the majority of fractures (77%). Alternative distributions, used in the remaining 23% of cases, were 2:1 (13%), 1:2 (7%) and 1:1 (3%, **Figure 3.7**).

Four out of 120 (3.3%) possible cannulations were missed intraoperatively, 100% of which were distal. All were retrieved immediately in surgery.

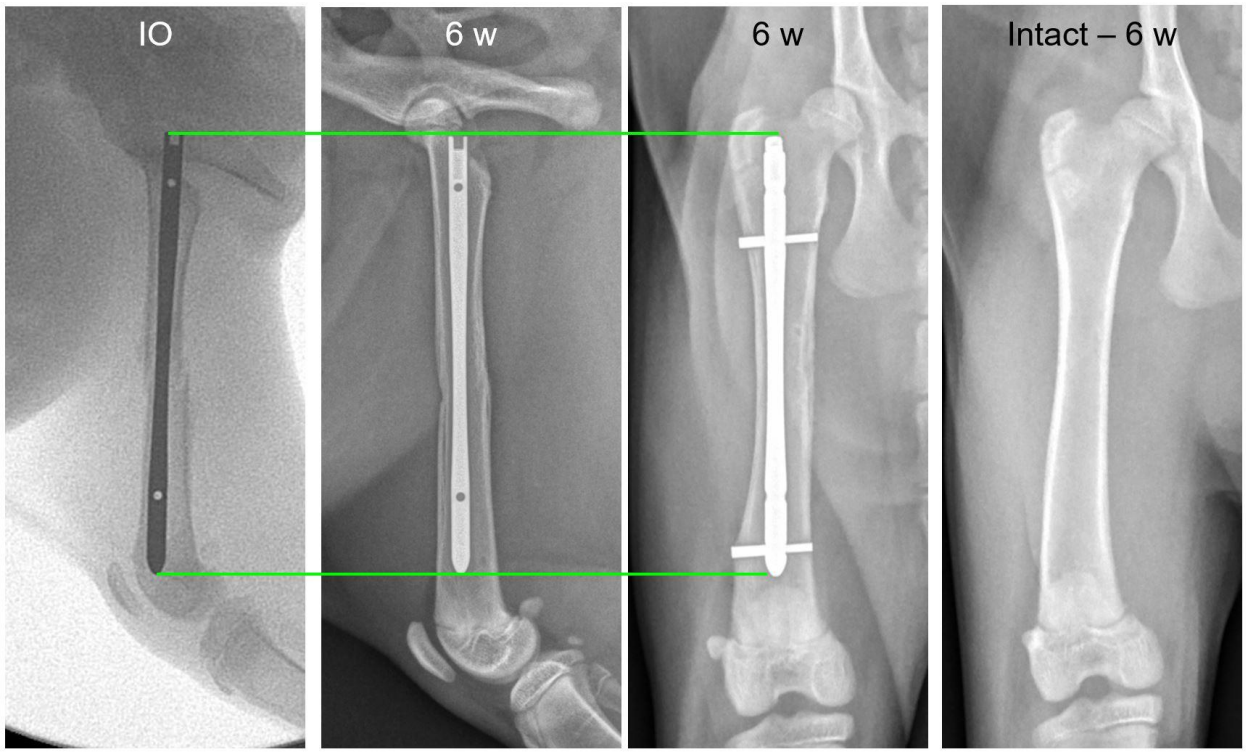

Figure 3.7: Intraoperative illustration of one of the alternate bolt distributions (1:1) Intraoperative (IO) illustration of one of the alternate bolt distributions (1:1) used in this study (left). At 6 weeks of age, this was the youngest patient enrolled in this study (center). Axial growth and hip conformation were not altered following nail osteosynthesis (green lines show identical radiographic magnification). No evidence of angular deformity was noted, as demonstrated by comparison to the normal contralateral limb at 6 weeks postoperative (right).

3.9. POST-OPERATIVE ASSESSMENT

Alignment in the transverse (femur, tibia, humerus) and sagittal (TPA) planes was within 2 degrees of the intact contralateral bone in all cases. There was no overt, appreciable difference in pro or recurvatum between post-operative and contralateral intact bones in any case. Rotational alignment was consistently assessed as anatomical or near anatomical. Femoral neck anteversion or retroversion were documented in 2/16 and 3/16 cases, respectively. In one of the latter, unacceptable post-operative retroversion following MINO was immediately corrected to normal using minimally invasive techniques. Mild external torsion was observed in one of the 8 tibial cases. No rotational malalignment was appreciable in any humeral fracture. Overall, alignment was evaluated as anatomical (25/30 – 83%) or near anatomical (5/30 – 17%) in all cases. Good post-operative fragment apposition or adjacency[67] was observed in all cases.

The I-Loc 3 was placed in a total of 16 fractures (5 femora, 6 tibiae, 5 humeri), and the I-Loc 4 was utilized in a total of 14 fractures (11 femora, 3 tibiae). No cat was large enough for an I-Loc 5. The mean body weight (± standard deviation) of cats receiving the I-Loc 3 was 4.4 ± 2.2 kg (range 1.1 – 8.4 kg); it was 5.2 ± 1.2 kg (range 3.2 – 6.3 kg) for the I-Loc 4.

The mean percentage of the medullary canal occupied by either the 3 mm or 4 mm nail was 48 ± 0.3% (range 38% – 67%). All cats began partially weight bearing within 2 days of surgery.

3.10. FOLLOW-UP

Complete follow-up with radiographic documentation of CU or bony union (BU) was available for 26 cases (90%). The median time to the first revisit appointment was 4 weeks with mean CU documented at 7.2 weeks (range 3 weeks – 18 weeks). All cases made a complete functional recovery. Three patients (10%) were unavailable for comprehensive radiographic follow-up. For these cases, phone interviews were conducted and all owners reported an excellent outcome with no appreciable lameness.

None of the cats in this study experienced major complications. There were, however, two cases with minor complications (6.6%). In the first case, fracture of both distal bolts in an I-Loc 3 at the nail interface was incidentally noted at the 8 weeks recheck (**Figure 3.8**). The cat was ambulating normally and evidence of callus formation was present radiographically, so revision surgery was not pursued. In the second case, fracture of an I-Loc 3 proximal bolt was noted at the 3 weeks recheck. This cat was also ambulating normally with only a mild radiographic alteration of limb alignment, therefore revision was not attempted. No case required ILN or bolt removal at any time point.

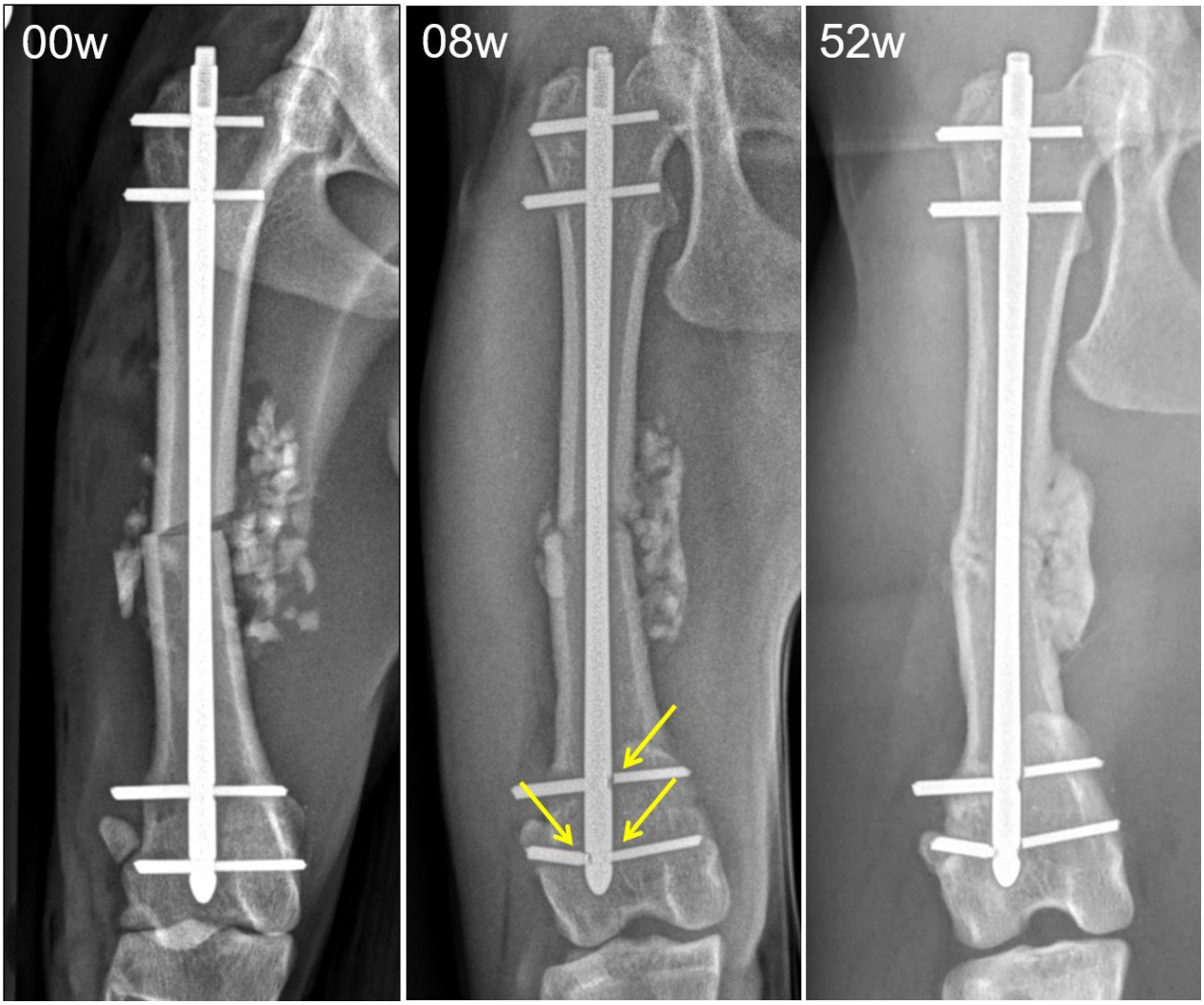

Figure 3.8: Fracture of the I-Loc 3 distal bolts in the case of an ostectomized chronic fracture

Fracture of an I-Loc 3 distal bolts (green arrows) was noted on routine 8 weeks postoperative radiographs of a mid-diaphyseal femoral fracture. Since this incidental finding had had no effect on limb alignment or function, revision was not considered. Bone union was documented on postoperative radiographs at 52 weeks. This patient had chronic (~3 weeks) unstable transverse fractures of the right femur and contralateral tibia at the time of nail osteosynthesis. A mid diaphyseal 1 cm ostectomy was performed on both bones to allow reduction. The diaphyseal segments were morselized and used as autogenous cortical grafts. Due to the inherently smaller area moment of inertia of the I-Loc 3 bolts, a 2:2 bolt distribution is recommended to improve construct stability and reduce the risk of bolt fatigue failure.

DISCUSSION

The results of this study showed that, using the I-Loc 3 and I-Loc 4 mm interlocking nails, excellent patient outcomes and functional recovery were achieved in a wide variety of fracture configurations, including epi-metaphyseal fractures. Therefore, the first hypothesis was confirmed. As with other published studies,[15,17,42,62,81] ours had a large percentage of cats with comminuted fractures (64%). Historically, these have been associated with higher complication rates, often related to implant failure, and poorer outcomes. [38,63,64,81-83] In an effort to reduce implant related complication rates, particularly in tibial fractures, orthogonal plating has been recommended.[66] While this technique resulted in a lower complication rate (12.5%) than previously reported, the time to CU was substantially longer than in our study with only 37.5% achieving CU by 14 weeks post-operatively[66] In contrast, in our study, the mean time to CU was 7.2 weeks with some achieving CU in as little as 3 weeks. Interestingly, the longest times to reach CU were seen in the 2 cats who experienced bolt fractures. Longer CU times could presumably have resulted from decreased stability. These cases increased the mean time to CU by 1.2 weeks. One of the most challenging complications reported in feline traumatology has been NU. In one study, 61% of NUs affected the feline tibia,[64] presumably due to minimal soft tissue coverage and poor blood supply to the region. In contrast, none of the cats in our study experienced a NU. Accordingly, the I-Loc may offer an advantage in terms of reducing delayed and NU rates.

Currently, there is a paucity of data on the use of ILNs in cats.[15,17,42,62] While ILNs have inherent biomechanical advantages compared to bone plates, major complication

rates ranging from 8-18% have been documented in both standard (Innovative Animal Product, Rochester, MN) and angle-stable (Targon) designs. [15,42,62] In one retrospective study evaluating both cats and dogs, ILN removal was performed in 27% of cases,[15] while in another, 41% of cases required partial or complete explantation.[42] Importantly, while these earlier ILN studies have described high complication rates, none of our cats experienced major complications. Therefore, the second hypothesis was also confirmed.

It is noteworthy that both minor complications in our study were I-Loc 3 bolt fractures. One of these cats had a comminuted proximal epi-metaphyseal tibial fracture and weighed 8.1 kg (body condition 8/9). Although the I-Loc 3 was appropriately sized relative to the medullary canal width, the cat's excessive body condition may have contributed to early bolt fatigue. Indeed, due to the fracture configuration and fissure expansion, the bolt was not well supported in the metaphyseal cancellous bone shelf, which has been shown to protect ILN bolts from both axial fatigue and torsional failure.[31] Based on this observation, and considering the relative weakness of the I-Loc 3 bolt inherent to its small size, we recommend that only a 2:2 bolt distribution be used in I-Loc 3 nails. Interestingly, intraoperative I-Loc 3 bolt fracture also occurred in two other cases during routine bolt tightening. Both bolts were retrieved intraoperatively and replaced. However, to avoid iatrogenic bolt fracture, the authors recommend careful "2-finger-torque" (i.e. ~0.6 Nm) application during I-Loc 3 bolt tightening.[75]

Fractures expanding into the metaphyses or epiphyses are relatively common in veterinary medicine, particularly since the majority of fractures are comminuted.[15,42,62] Indeed, 20% of our fractures were epi-metaphyseal. Previously, these fractures were considered contraindications for interlocking nailing with standard ILN because of the

torsional and bending instability (or slack) inherent to their locking mechanism.[40,47,84,85] The angular stability of the I-Loc design, however, has allowed surgeons to repair these challenging fractures successfully.[18,40] We surmise that the rationale for this is four-fold. *First*, the metaphyseal bolt location provides strong cancellous support,[31] for fixation of very proximal or distal fractures (**Figures 3.5 and 3.6**). *Second*, the bolt distribution (1:1, 2:1, 1:2) can be safely altered if a fracture extends proximally or distally beyond the location of bolts #2 or #3, respectively. *Third*, as with any current veterinary nail, the I-Loc cannulations can be oriented anywhere from the transverse to sagittal planes to optimize bone purchase. *Finally*, the nail can be shortened to allow deeper seating in very distal fractures (**Figures 3.2 and 3.6**). The importance of angular stability in newer implants has become well recognized. Recently a second AS-ILN (Targon, Aesculap-Braun, Bethlehem, PA, USA) was introduced and reported to have a good outcome in 49 cats.[42] However, two independent mechanical studies identified torsional instability secondary to locking mechanism slippage.[43,75] Additionally, as per manufacturer recommendation, the Targon nail is contraindicated for epi-metaphyseal fractures because the nail design dictates that the locking bolts can only be placed in the diaphysis.[41,42] Using traditional fixation such as bone plates to repair epi-metaphyseal fractures, may also represent a substantial challenge. First, the limited bone stock available for fixation may force a surgeon to use non-locking screws in order to aim away from the fracture or joint. Additionally, placement of only 1 or 2 screws in the smaller fragment may result in a relatively unstable repair. Though it may be possible to augment the plate with an IM rod, the risk for repair failure via screw pullout due to motion at the fracture site remains. This risk would likely be accentuated in juveniles because of the soft material properties of

immature bone.[86] However, the risk of screw pullout is eliminated when using an entirely IM device, such as an ILN. As such, given the positive clinical results reported here and challenges associated with alternative stabilization options, the I-Loc 3 and 4 nails may be advantageous in management of epi-metaphyseal fractures in cats.

The second purpose of this study was to report clinically relevant recommendations for I-Loc use in cats. During pre-operative planning, one of the criteria used to select an appropriately sized ILN is the width of the MC. In our study, the nail encompassed an average of ≤50% of the MC diameter, regardless of the bone involved. Conversely, the selection of standard ILNs filling 100% of the canal at its isthmus has been previously recommended.[17,62] Due to their large AMI, however, standard ILNs are relatively stiffer than size-matched bone plates.[20,85] One could speculate that the combination of stress protection and reaming could be a predisposing factor to the high rate of NU reported in the literature.[62,87] Nonetheless, reaming of the medullary cavity to insert large nails has been recommended. This technique, however, results in substantial destruction of the IM blood supply.[87] In contrast to standard ILNs, the I-Loc design features an hourglass profile. The impetus behind this unique design was two-fold. First, through an increase in implant compliance one could theoretically limit the deleterious effect of stress protection. Second, by eliminating the need for reaming, the endosteal blood supply could be better preserved and revascularization of the medullary cavity facilitated. Accordingly, the I-Loc may promote faster healing and thus, return to function when compared to standard ILNs. Conversely, while the Targon nails' thin 2.5 mm to 3.0 mm rods would not likely interfere with restoration of the IM blood supply, this nail has been shown to be significantly more compliant than size-matched I-Loc nails, as

demonstrated in Study 2.[75] This increased compliance could induce excessive motion at the fracture site and result in delayed bone healing.

Based on the patient population in this prospective study, the I-Loc 4 would be recommended for the majority of feline femora. Indeed, the feline femur is a relatively straight bone with a wide MC, which easily accepts a 4 mm nail. In small cats, surgeons may safely choose the I-Loc 3, which was placed in approximately 33% of our femoral fractures. Interestingly, the smallest and youngest patient in our study weighed 1.1 kg and was 6 weeks old at the time of surgery. Despite the reported risks of placing a femoral IM implant[88] in an animal this young, the cat did not experience any alteration in growth or limb alignment (**Figure 3.7**). This suggests that the I-Loc can also be placed in juveniles when careful tissue handling and meticulous surgical technique are used. Considering the biomechanical challenges of operating on immature bone, the I-Loc may be an effective fixation option for these young patients.

In contrast to the femur, the feline tibia is a sigmoid bone with a narrow MC. Additionally, anatomical differences between cats and dogs should be considered when planning for surgery. One such difference in cats is that the most robust source of vascularization is the IM blood supply.[89] Although revascularization may occur within several weeks following disruption of this blood supply,[90] preserving it as much as possible during surgery is critical for bone healing. For these reasons, the majority of tibiae in our study (75%) received the I-Loc 3.

Similar to the tibia, the feline humerus has important anatomical differences that affect implant selection. Specifically, cats have a supracondylar foramen which reduces the width of the MC distally, which limits the diameter of an IM implant that can be used.[91]

This suggests that the I-Loc 3 will likely be the most appropriate size for nearly all domestic feline humeri.

A procedural challenge reported in the ILN literature is missed cannulations during drilling. Indeed, post-operative off site placement of the distal-most locking device has been reported in 4% to 12% of cases.[15,17] This technical mistake is possible for any nail system when using an alignment guide. Indeed, small deviations in the distal portion of the guide can occur secondary to the length of the guide and the small size of the nail couplings which inherently affect the angular rigidity of the nail/insertion coupling. Therefore, in order to prevent this complication, meticulous care must be taken intra-operatively to avoid movement of the guide during drilling. To mitigate the risk of missing the distal bolts, the I-Loc instrumentation includes temporary locking posts designed to reduce motion of the alignment guide while drilling through the distal cannulations. Furthermore, sharp drill bits should always be used to prevent slippage of the drill bit over the *cis* cortex. In the current study, while the alignment guide was used to locate the position of the distal cannulations along the nail axis, free-hand drilling was routinely performed in tibial and humeral fractures. While often perceived as more challenging, free-hand drilling allows the surgeon to account for multiple factors. *First*, the drill bit tends to slip off the edge of the distal tibia and humerus secondary to the cortical curvature at these sites. Without the alignment guide in place, the drill bit can be oriented perpendicularly to the cis cortex then slowly reoriented until it is parallel to the straight surface of the insertion handle or to the proximal temporary posts. *Second*, a lighter, smaller drill such as the “Hornet” (Rita Leibinger Medical, Tuttlingen, Germany), or “VetKiss” (IMEX Veterinary Inc, Longview, TX, USA) microdrills or the “Hall MicroFree”

drill (CONMED, Utica, NY, USA) can be used to better control potential drill bit slippage on the cis cortex (**Figure 3.3**).

As with any study, some limitations exist. We reported descriptive statistics with all surgeries performed by one or both senior surgeons familiar with the I-Loc system. Results from multiple institutions where surgeons may be less acquainted with this system could vary. When compared to the available literature, our case numbers may initially appear small. Yet, all previous reports (ILN or more conventional fixation) have been retrospective in nature. Our prospective design virtually eliminated confounding factors and resulted in regular patient follow-up, allowing us to make meaningful conclusions regarding healing and outcome. Lastly, we compared the results of this prospective study to those of several retrospective reports. However, since cat populations, fracture patterns and distributions as well as percentage of open fractures were similar between ours and previous studies,[16,42,62,66] we believe that such comparisons are acceptable.

In conclusion, cats in this study had faster healing times than those previously reported and underwent complete functional recovery. Additionally, challenging epi-metaphyseal fractures were successfully repaired using the I-Loc. Notably, none of the cats experienced non-union or other major complication. Whilst the I-Loc 3 is likely the most appropriate size for most feline tibiae and all humeri, the I-Loc 4 can be placed in the majority of femora. It is unlikely that any domestic cat would be large enough for an I-Loc 5. Considering the excellent patient outcomes and low complication rate in this study, our results suggest that the I-Loc 3 and I-Loc 4 are safe and effective alternatives to other feline fracture osteosynthesis options.

STANDARD OPERATING PROCEDURES

SOP S1 – CAT FEMUR SURROGATE

4.1. BONE POTTING PROCEDURE

A custom designed fixture (**Figure 1.2**) was used to ensure centralization within the loading cups as well as a consistent distance between loading cups for all specimens. Prior to placement in the fixture, a working length of 85 mm was measured using the digital calipers and was marked on each femur with a marking pen. Additionally, to ensure consistent orientation during testing, the cranial and medial cortices were marked on the proximal metaphysis of all specimens. With the femurs properly aligned in the fixture, potting of the epiphyses was achieved as follows:

1) Potting cups were sprayed with lubricant (LPS 2, Grainger Inc, Lake Forest, IL)

2) 15 grams of acrylic powder was placed (Technovit J0061PA, Jorgenson Laboratories, Loveland, CO) into a mixing cup

3) 6 milliliters of liquid hardener was added to the powder (methyl methacrylate monomer, Technovit® Jorgenson Laboratories, Loveland, CO)

4) The mixture was stirred using a tongue depressor until no clumps remained

5) The mixture was carefully poured into the potting cup until the cup was filled to 1 millimeter below the top

6) Set screws were inserted until flush with the outside of the cup, then the cup was placed under the bone until the potting mixture reached the previously made mark

7) The cup was secured using the fixture bar

8) The mixture was allowed to harden for 5 minutes, then the fixture was turned 180° to pot the second side as outlined above

9) Prepared samples were wrapped in saline soaked gauze sponges until testing was completed, within 24 hours

4.2. BONE SURROGATE DESIGN AND POTTING

4.2a. Design: Fusion 360 software (Fusion 360™, Autodesk Incorporated, San Rafael, CA, USA) was used to design all components of this study (**Figure 4.1**).

1) From the origin, a line was drawn to the right, measuring 77.5 mm

2) From the end of this line, a vertical line was drawn, measuring 10 mm

3) From the end of this line, a line was drawn 90° to the left, measuring 20 mm

4) From the end of this line, a 24.04 mm line was drawn with an angle of 168.9° toward the origin

5) From the end of this line, a line to the left was drawn, measuring 30.06 mm

6) The fillet tool was used to create an 11.1° smooth curve

7) Finally, a line measuring 5 mm was drawn at 90° to the end of this line, connecting it to the origin point

8) The ‘front’ plane was selected and the revolve tool was used to create a mirror image sketch, making one half of the model

9) The shell tool was used to create a uniform 1.5 mm wall thickness

10) The mirror tool was used to create a symmetrical second half of the model

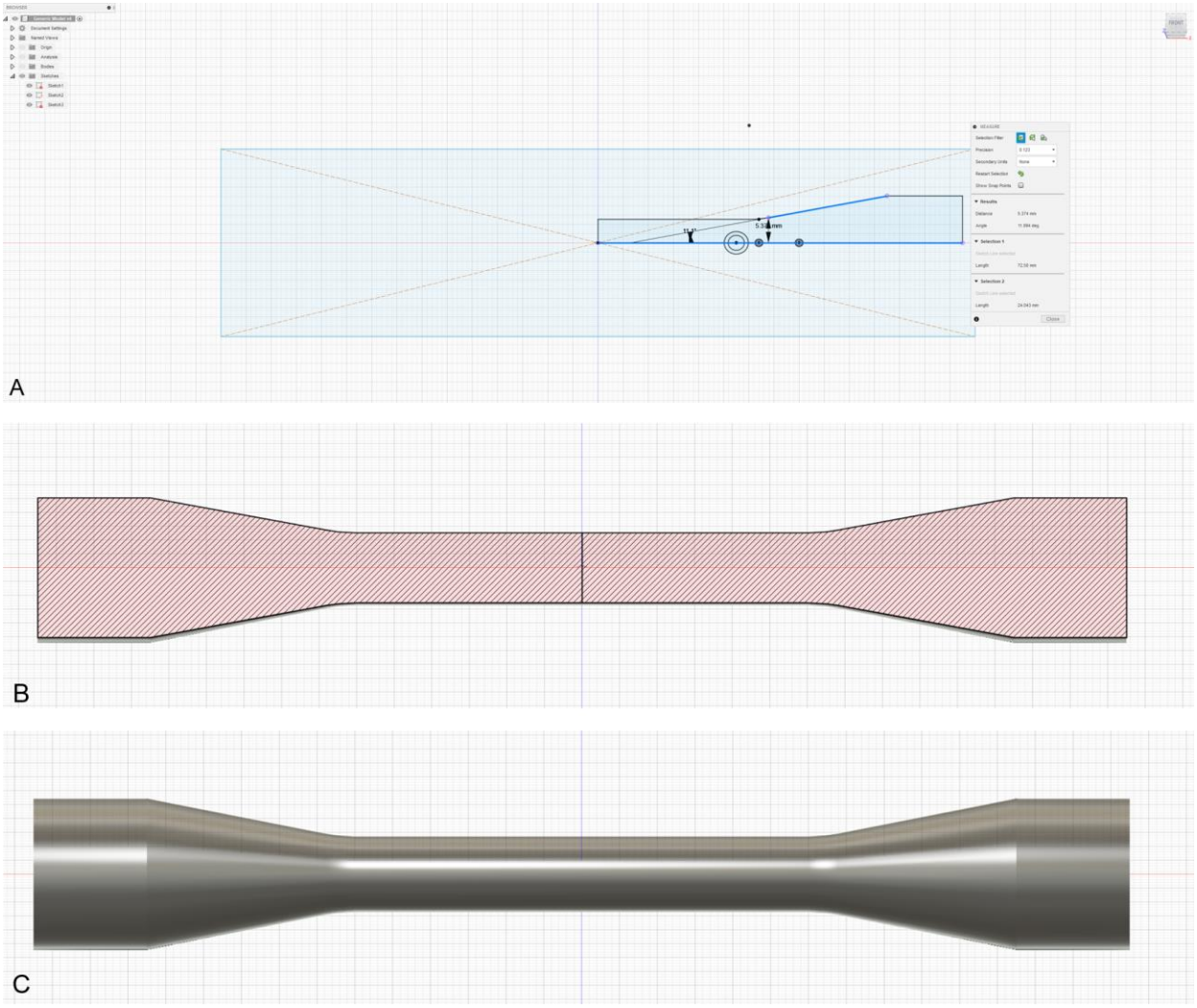

Figure 4.1: Fusion 360 sketch of surrogate bone model
Initial sketch with measurements showing the bone surrogate drawing (A). Sectioned complete 3D body sketch (B), and full rendering of surrogate model (C).

4.2b. Potting: Models were potted using the same protocol described for the cadaveric bone samples (for both torsion and bending) with the following differences:

1) Prior to mixing the acrylic potting material, a 1.5 mm intramedullary pin was drilled into the coupling section of each model extremity

2) The ends of the pins were cut so that 1.5 mm was exposed on either side of the model – this pin was used to prevent slippage of the model in the potting material during testing

3) After pin placement, the models were mounted in the potting fixture as described for the cadaveric femurs

SOP S2 – 3D MODELING, PRINTING, AND MACHINING

Fusion 360 software (Fusion 360™, Autodesk Incorporated, San Rafael, CA, USA) was used to design all components of this study.

4.3. DRILL GUIDES

The 3D bone model design from the first study was imported into a new design window and a drill block with the same shape was created around it. The boolean operation “cut” was selected which resulted in a “negative” impression of the model on the inside of the drill block. The block was digitally sectioned in half longitudinally resulting in two lids that could be placed around each bone model to secure it in position (**Figure 2.2**). Next, 2 mm diameter holes were created at either extremity (from here on called peg holes), 65 mm from the center. These peg holes ensured stability of the model once pilot hole drilling for each implant began, which allowed for homogeneity among samples. Following creation of peg holes, implant specific holes were created (**Figure 4.2**):

1) I-Loc 3 and 4 – the innermost pilot holes were 36 mm from the center of the model, while outermost pilot holes were 44 mm from the center

2) Targon 2.5 and 3.0 – pilot holes were located 28 mm from the center

3) LCP 2.0 – the innermost pilot holes were located 37.3 mm from the center along a plane while the outermost holes were located 44.3 mm from the center along the same plane. Pilot holes were perpendicular to the 11.1° flare.

4) LCP 2.4 – the innermost pilot holes were 34.8 mm from the center along the plane perpendicular to the flare, while the outermost holes were 42.8 mm from the center. Additionally, for the LCP drill guides, the *trans* side of the block had a

rectangular section measuring 106 mm long x 4 mm wide removed, to allow the drill bit to easily pass regardless of drill bit orientation (due to plate bend).

Following 3D printing (GPL04 resin, Form 2, Formlabs, Somerville, MA, USA) of the above guides, each hole was press-fit with its corresponding hardened steel bushing (McMaster-Carr, Aurora, OH, USA), with inner diameters matching those of the specific drill bit used for that implant (**Figure 2.2**) and outer diameters measuring 4 mm. *Cis* and *trans* inner diameter bushing sizes were as follows:

1) I-Loc 3: 1.6 mm and 1.2 mm, respectively

2) I-Loc 4: 2.0 mm and 1.6 mm, respectively

3) Targon 2.5: 4.0 mm and 2.5 mm, respectively

4) Targon 3.0: 4.8 mm and 3.0 mm, respectively

5) LCP 2.0: *Cis* only at 1.5 mm

6) LCP 2.4: *Cis* only at 1.8 mm

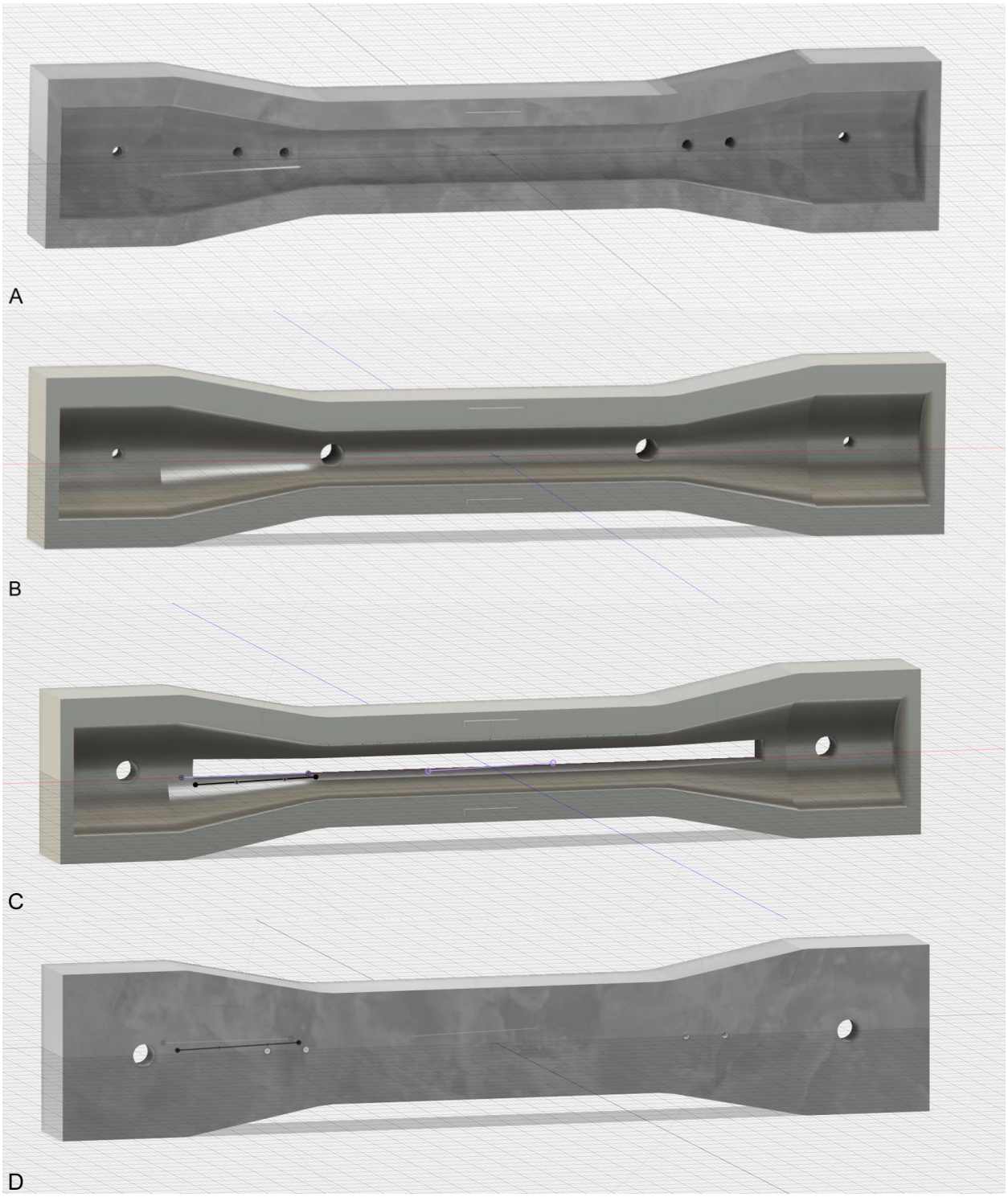

Figure 4.2: CAD rendering of I-Loc, Targon, and LCP drill guides
Drill guides designed in Fusion 360 for the I-Loc (A), Targon (B), and LCP (C and D) groups. The *trans* side of the LCP guide (C) featured an open section for the drill bit to pass easily though, while the *cis* side (D) featured pilot holes in the desired locations.

4.4. TESTING CUPS

4.4a. Torsion testing cups: To match the inner diameter of the testing cups on the torsion testing machine, linkage cups were designed (**Figure 4.3**) with an overall outer diameter of 31.62 mm, inner diameter of 20.2 mm (to match the outer diameter of the model with a tolerance of 0.2 mm) and a height of 16.7 mm (the height of the testing cups). Inside of this, a second cylinder was created with an outer diameter of 16.9 mm (the inner diameter of the model at the linkage portion with a 0.2 mm tolerance). The depth of the inner cylinder was 15 mm, matching the length of the linkage portion of the model. Next, a hole was created 7.5 mm from the top of the cup, that traversed the diameter of the entire cup. This was the corresponding peg hole to match that of the drill guide, and served to prevent any motion of the model inside of the testing cup, thereby eliminating slack.

4.4b. Bending testing cups: To match the inner diameter of the square testing cups on the bending machine, linkage cups were designed (**Figure 4.3**). The overall outer diameter was 31.56 mm while the diameter of the inner circle was 20.2 mm. Identical to the torsion cups, the innermost diameter of the portion that accepted the model was 16.9 mm. Overall height of the cup was 21 mm and height of the inner circle was 15 mm. A hole was created 7.5 mm from the top of the cup which traversed the entire diameter, corresponding to the peg hole (similar to the torsion cup).

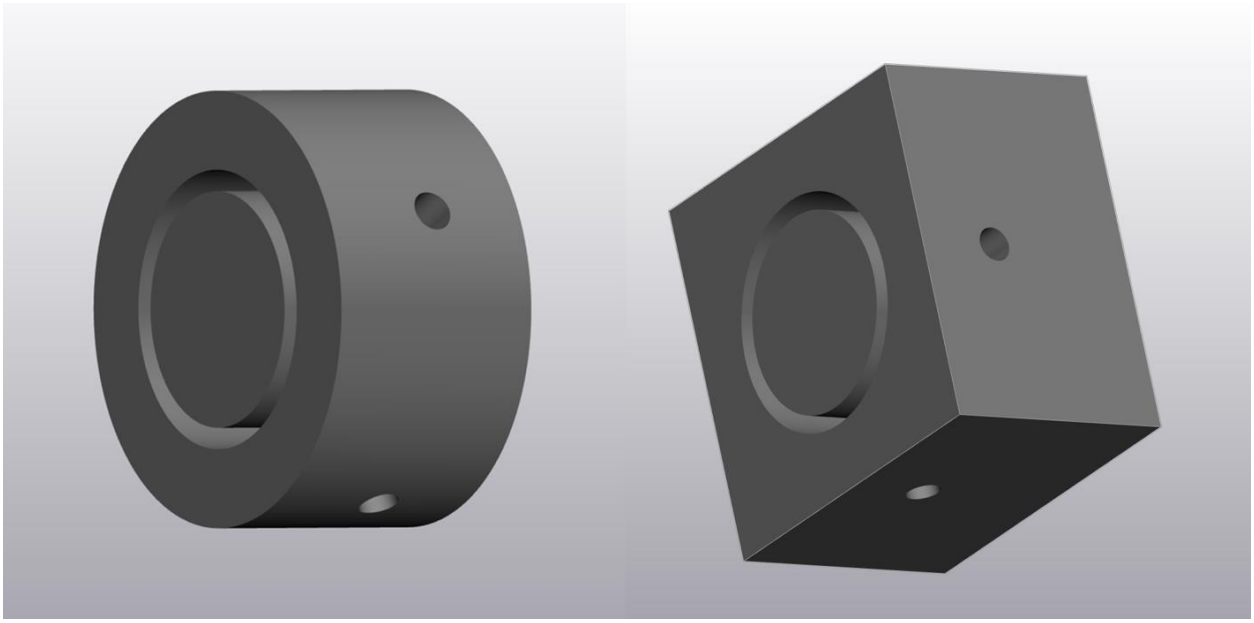

Figure 4.3: Torsion and bending cup CAD renderings
Torsion (left) and bending (right) cup CAD renderings used in Study 2. From these designs, torsion and bending cups were machined from stainless steel. Peg holes were designed in orthogonal planes to ensure each specimen was rigidly fixed during testing.

4.5. CANCELLOUS FOAM PLUGS

1) From the origin point, a vertical line was made measuring 35.5 mm as well as a horizontal line (moving to the right of the origin point) measuring 12.5 mm

2) From the end of the horizontal line, a vertical line measuring 8 mm was created

3) Next, a horizontal line measuring 3.5 mm was created, extending from the original vertical line, followed by a line extending 2 mm from the end of the 3.5 mm line

4) Finally, a diagonal line closing the shape was created, and measured 23.3 mm

5) The fillet feature was then used to curve the edge with a radius of 3.3 mm

6) Next, the revolve feature was applied to create the second, symmetrical half of the plug as a 3D object

7) Plugs were then machined from a solid 20 pcf foam block, using a CNC lathe (model Quick Turn Start 350m; Yamazaki Mazak, Binh Duong Provence, Vietnam)

4.6. FOAM PLUG HOLDING BLOCK

1) Using the cancellous plug model previously described in a new sketch window, a rectangular sketch was created (**Figure 4.4)**

2) The end of one side of the rectangle was started at the origin point of the plug fillet

3) The length of the rectangle measured 44.11 mm and the height was 29.41 mm

4) The extrude tool was used to create one half of the holding block, extruded a length of 20 mm (away from the plug edge)

5) Next, the combine tool was used to create a boolean ‘cut’ operation, removing the plug contour from the block

6) The mirror tool was used to create a symmetrical second holding block half

7) Finally, the split tool was used to create two separate halves

8) Using the Form 2 printer and Draft resin (Formlabs, Somerville, MA, USA), the holding block was printed in two halves

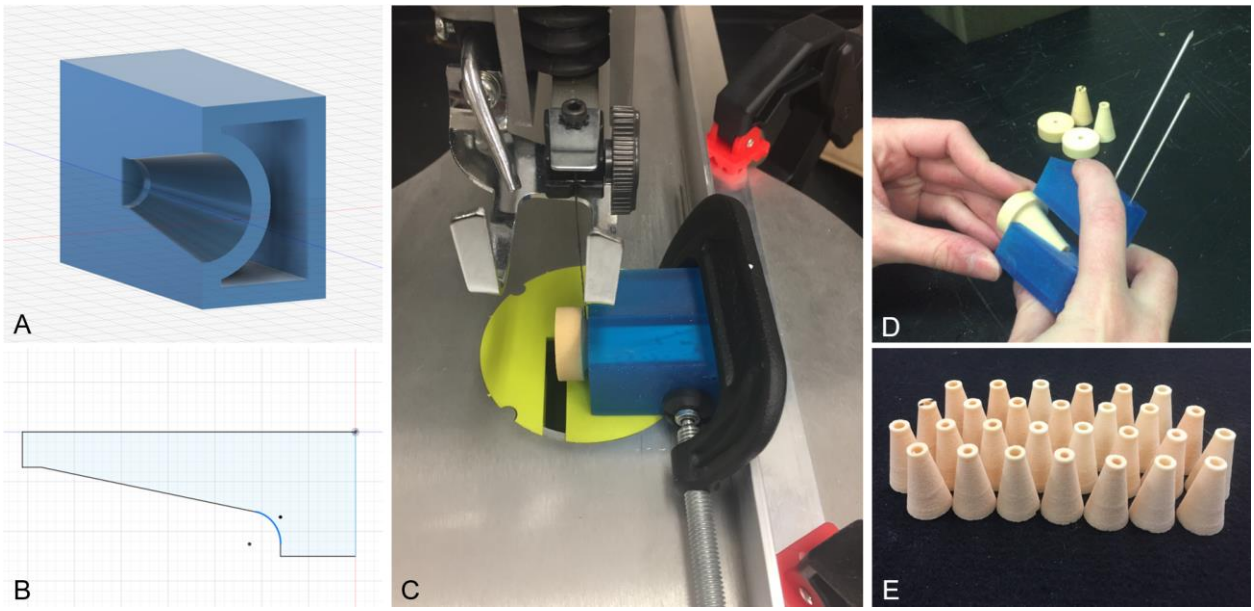

Figure 4.4: Foam plug holding block images
CAD drawing and sketch (A and B) of the foam plug holding block. A “shell” was created to reduce resin volume. The holding block was secured to a table-top sagittal saw (C) so that the ends could be removed, to allow insertion into bone surrogate ends. Each plug was secured into the holding block using metal pins (D). Finished plugs (E) were press-fit into each end of the bone surrogate specimens.

4.7. BENDING PRESS

The bending press was created in three separate parts:

4.7a. Plate holders (2.0 mm and 2.4 mm):

1) A rectangle was created from the origin measuring 60 mm x 15 mm

2) The extrude tool was used to create a 15 mm thick rectangle

3) A second rectangle was created from the origin measuring 60 mm x 5.55 mm and 60 mm x 6.55 mm for the 2.0 and 2.4 mm plates, respectively

4) This rectangle was extruded to a thickness of 4mm, in the same direction as the first rectangle

5) A Boolean ‘cut’ operation was performed to remove the second rectangle from the first one

4.7b. Top press:

1) In a new plane, free sketch was selected and a line was created measuring 69.89 mm

2) From the right edge, a line was made at 90° measuring 14.34 mm

3) The fillet tool was used to create a 35 mm line which was located 19.61 mm below the 1st

4) A line was then started from the left fillet edge, measuring 45.46 mm

5) A second fillet line was created, matching the first, to connect the first line with the last one

6) Finally, a line 14.34 mm long was created to connect the fillet edge to the first line

7) The extrude tool was used to create a component 15 mm thick

4.7c. Base:

1) In a new plane, a free sketch was created beginning with a line measuring 44.65 mm

2) A line was made at a 90° to the first, measuring 16.75 mm long

3) A fillet line 4.23 mm was created with a 4 mm diameter

4) From the left fillet edge, a 11.42 mm line was created (12.54 mm below and at an angle of 148.80° to the first line)

5) From the edge of this line, a 9 mm line was made at 90°

6) A 31.70 mm line was created at 90° to the previous one

7) Finally, to connect the last line to the first, a 3.29 mm line was created

8) The extrude tool was used to create a component 15 mm thick

9) The mirror tool was used to create a symmetrical half, completing the part

When a component was 3D printed, this process was completed by uploading the stereolithography (STL) file into a Form-2 stereolithography printer (Formlabs Inc., Somerville, MA, USA). Once uploaded, the program (PreForm, Formlabs Inc., Somerville, MA, USA) automatically attached supports. The button labelled “send to printer” was clicked and the printing process was started.

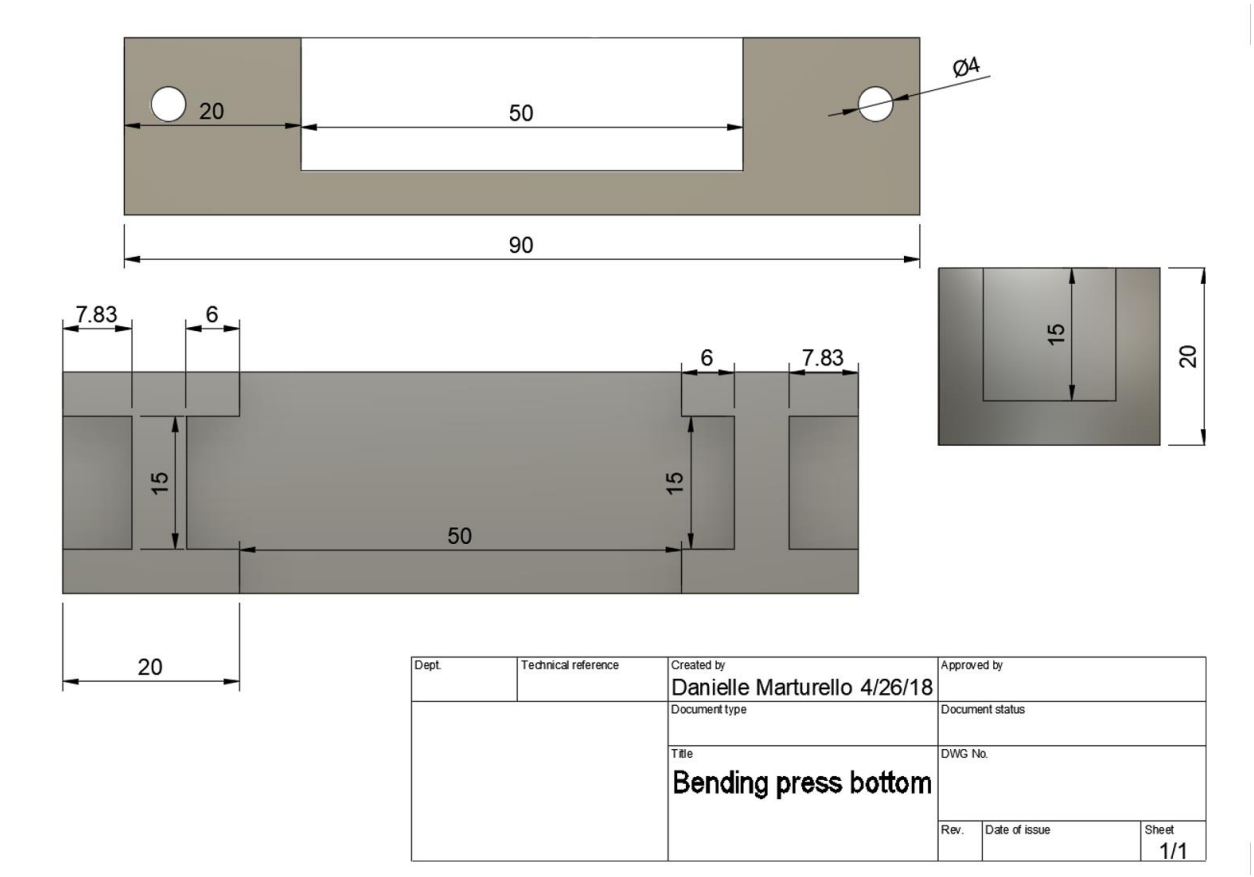

Figure 4.5: Bending press drawing, CAD rendering, and 3D printed press
Bending press base design(top) with measurements. CAD rendering (bottom left) and 3D printed (bottom right) bending press with 2.4 mm LCP loaded. Holes in both the plate holder and press ensured plate security.

4.8. GAP BONE MODEL

1) From the origin, a line was drawn to the right, measuring 19.50 mm

2) From the left end of this line, a vertical line was drawn, measuring 5 mm

3) From the end of this line, a line was drawn 90° to the right, measuring 57.50 mm

4) From the end of this line, a 10 mm line was drawn at an angle of 90° from the previous line

5) From the end of this line, a line to the left was drawn, measuring 25 mm, at an angle of 168.90° toward the origin

6) The fillet tool was used to create an 11°smooth curve

8) The ‘front’ plane was selected and the revolve tool was used to create a mirror image sketch, making one half of the gap model

9) The shell tool was used to create a uniform 1.5 mm wall thickness

The gap model was manufactured by the same CNC lathing process (Trevor Ruckle, model Quick Turn Start 350m; Yamazaki Mazak, Binh Duong Provence, Vietnam) used for the first study. When two halves were coupled to the implants to create the construct, there was a 30 mm central gap which mimicked a comminuted diaphyseal fracture.

REFERENCES

1. An YH, Barfield WR, Drauhgn RA. Basic concepts of mechanical property measurements and bone biomechanics. In: An YH, Drauhgn RA, eds. *Mechanical testing of bone and the bone implant interface.* New York: CRC Press, 2000; 23–39.

2. Gibson TW, Moens NMM, Runciman RJ, Holmberg DL, Monteith GM. The biomechanical properties of the feline femur. *Vet Comp Orthop* Traumatol 2008; 21: 312-317.

3. Acker ML, Torrance B, Kowaleski MP, Boudrieau RJ. Structural properties of synthetic bone models compared to native canine bone. In ECVS Proceedings 2010: 150-151.

4. Szivek JA. Synthetic materials and structures used as models for bone. In: An YH, Draughn RA, eds. *Mechanical testing of bone and then bone-implant interface*. Boca Raton, Fla: CRC Press LLC, 2000; 159-171.

5. Cabassu JB, Kowaleski MP, Shorinko JK, Blake CA, Gaudette GR, Boudrieau RJ. Single cycle to failure in torsion of three standard and five locking plate constructs. *Vet Comp Orthop Traumatol* 2011; 24: 418-425.

6. Déjardin LM, Lansdowne JL, Sinnott MT, Sidebotham CG, Haut RC. In vitro mechanical evaluation of torsional loading in simulated canine tibiae for a novel hourglass-shaped interlocking nail with a self-tapping tapered locking design. *Am J Vet Res* 2006; 67: 678-685.

7. Aper RL, Litsky AS, Roe SC, Johnson KA. Effect of bone diameter and eccentric loading on fatigue life of cortical screws used with interlocking nails. *Am J Vet Res* 2003; 64(5): 569-573.

8. Hammel SP, Pluhar EG, Novo RE, Bourgeault CA, Wallace LJ. Fatigue analysis of plates used for fracture stabilization in small dogs and cats. *Vet Surg* 2006; 35(6): 573-578.

9. Gibson TW, Moens NM, Runciman RJ, Holmberg DL. Evaluation of a short glass fibre-reinforced tube as a model for cat femur for biomechanical testing of orthopaedic implants. *Vet Comp Orthop Traumatol* 2008; 21: 195-201.

10. Gautier E, Perren SM, Cordey J: Strain distribution in plated and unplated sheep tibia: an in vivo experiment. *Injury* 2000; 31: C37–C44.

11. Gautier E and Sommer C: Guidelines for the clinical application of the LCP. *Injury* 2003; 34: B63–B76.

12. Smith GK. Chapter 12: Biomechanics pertinent to fracture etiology, reduction, and fixation. In: Newton CD, Nunamaker DM, eds. *Textbook of Small Animal Orthopedics*. Philadelphia, PA: J.B. Lippincott & Co, 1985.

13. Vahey JW, Lewis JL: Elastic moduli, yield stress, and ultimate stress of cancellous bone in the canine proximal femur. *J Biomech* 1987; 20: 29-33.

14. Pressel T, Bouguecha A, Vogt U, et al: Mechanical properties of femoral trabecular bone in dogs. *J Biomed Eng* 2005; 4: 1-6.

15. Duhautois B. Use of veterinary interlocking nails for diaphyseal fractures in dogs and cats: 121 cases. *Vet Surg* 2003;32(1):8-20.

16. Reems MR, Pluhar GE, Wheeler DL. Ex vivo comparison of one versus two distal screws in 8 mm model 11 interlocking nails used to stabilize canine distal femoral fractures. *Vet Surg* 2006;35(2):161-7.

17. Diaz-Bertrana MC, Durall I, Puchol JL, Sanchez A, Franch J. Interlocking nail treatment of long-bone fractures in cats: 33 cases (1995–2004). *Vet Comp Orthop Traumatol* 2005;18(3):119-126.

18. Fauron AH, Déjardin LM, Phillips R, Gazzola KM, Perry KL. Clinical Application of the I-LOC Angle-Stable Interlocking Nail in 100 Traumatic Fractures of the Humerus, Femur and Tibia. *Vet Comp Orthop Traumatol* 2018;31(S02):A3642.

19. Johnson KA, Piermattei DL. *Piermattei's atlas of surgical approaches to the bones and joints of the dog and cat.* 5th ed. St. Louis, MO: Elsevier/Saunders; 2014. Section 7, 372-373.

20. Lansdowne JL, Sinnott MT, Dejardin LM, Ting D, Haut RC. In vitro mechanical comparison of screwed, bolted, and novel interlocking nail systems to buttress plate fixation in torsion and mediolateral bending. *Vet Surg* 2007; 36: 368-377.

21. Déjardin LM, Cabassu JB, Guillou RP, Villwock M, Guiot LP, Haut RC. In vivo biomechanical evaluation of a novel angle-stable interlocking nail design in a canine tibial fracture model. *Vet Surg*. 2014;43(3):271-281.

22. Déjardin LM, Guillou RP, Ting D, Sinnott MT, Meyer E, Haut RC. Effect of bending direction on the mechanical behavior of interlocking nail systems. *Vet Comp Orthop Traumatol* 2009; 22: 264-269.

23. Rutherford S, Demianiuk RM, Benamou J, Beckett C; Ness MG, Déjardin LM: Effect of intramedullary rod diameter on a SOP-Rod construct in mediolateral bending; an in vitro mechanical study. *Vet Surg*, 2015; 44(1):737-743.

24. Trostle SS, Wilson DG, Dueland R, Markel MD. In vitro biomechanical comparison of solid and tubular interlocking nails in neonatal bovine femurs. *Vet Surg* 1995; 24(3): 235-43.

25. Mewhort DJ, Kelly M, Johns BT. Randomization tests and the unequal-N/unequal-variance problem. *Behav Res Methods* 2009;41(3): 664-667.

26. Zimmerman DW. A note on homogeneity of variance of scores and ranks. *J Exp Educ* 1996; 64(4): 351-362.

27. Anderson JR, Thompson WL, Alkattan AK, Diaz O, Klucznik R, Zhang YJ, Britz GW, et al. Three-dimensional printing of anatomically accurate, patient specific intracranial aneurysm models*. J Neurointerv Surg* 2016; 8: 517-520.

28. Crosse KR, Worth AJ. Computer-assisted surgical correction of an antebrachial deformity in a dog. *Vet Comp Orthop Traumatol* 2010; 23(5): 354-61.

29. Chia HN, Wu BM. Recent advances in 3D printing of biomaterials. *J Biol Eng* 2015; 9(1): 4.

30. Gardner MP, Chong AC, Pollock AG, Wooley PH. Mechanical evaluation of large-size fourth-generation composite femur and tibia models. *Ann Biomed Eng* 2010; 38(3): 613-620

31. Burns CG, Litsky AS, Allen MJ, Johnson KA. Influence of locking bolt location on the mechanical properties of an interlocking nail in the canine femur. *Vet Surg* 2011; 40(5): 522-530.

32. Unger M, Montavon PM, Heim UF: Classification of fractures of the long bones in the dog and cat: introduction and clinical application, *Vet Comp Orthop Traumatol* 1990; 3: 41-50.

33. Braden TD, Eicker SW, Abdinoor D, Prieur WD. Characteristics of 1000 femur fractures in the dog and cat. Vet Comp Orthop Traumatol 1995;8:203–209.

34. Voss K, Kull MA, Haessig M, Montavon PM. Repair of long-bone fractures in cats and small dogs with the Unilock mandible locking plate system. Vet Comp Orthop Traumatol 2009;22(05):398-405.

35. Perren SM. Evolution of the internal fixation of long bone fractures: the scientific basis of biological internal fixation: choosing a new balance between stability and biology. J Bone Joint Surg 2002;84:1093-1110.

36. Gautier E, Sommer C. Guidelines for clinical application of LCP. Injury 2003;34 (Suppl. 2):B63-B76.

37. Garofolo S, Pozzi A. Effect of plating technique on periosteal vasculature of the radius in dogs: a cadaveric study. Vet Surg 2013;42:255-261.

38. Vallefuoco R, Le Pommellet H, Savin A, et al. Complications of appendicular fracture repair in cats and small dogs using locking compression plates. *Vet Comp Orthop Traumatol 2016;29(1):46-52.*

39. Pohler OEM, Straumann F. Mechanical properties of the material. In: Brinker WO, Hohn RB, Prieur WD, eds. Manual of internal fixation in small animals. Berlin: Springer-Verlag 1984;91–92.

40. Ting D, Cabassu JB, Guillou RP et al. In vitro evaluation of the effect of fracture configuration on the mechanical properties of standard and novel interlocking nail systems in bending. *Vet Surg* 2009;38(7):881-887.

41. Brückner M, Unger M, Spies M. In vitro biomechanical comparison of a newly designed interlocking nail system to a standard DCP. Testing of cat femora in an osteotomy gap model. *Tierarztl Prax Ausg K Kleintiere Heimtiere* 2014;42(2):79-87.

42. Brückner M, Unger M, Spies M. Early Clinical Experience with a Newly Designed Interlocking Nail System-Targon(®) Vet. *Vet Surg* 2016;45(6):754-763.

43. Macedo AS, Moens NM, Runciman J. Ex vivo torsional properties of a 2.5 mm veterinary interlocking nail system in canine femurs. Comparison with a 2.4 mm limited contact bone plate. *Vet Comp Orthop Traumatol* 2017;30(2):118-124.

44. Marturello DM, Wei F, Déjardin LM. Characterization of the torsional properties of feline femurs and surrogate models for mechanical testing of orthopedic implants. *Vet Surg* 2019;48(2):229-236.

45. Baroncelli AB, Baroni G, Oliveri M, Piga P, Peirone B. Applicazione clinica della Placca LCP Synthes nel trattamento delle fratture dello scheletro appendicolare del cane. *Veterinaria* 2011;25(4):13-21.

46. Silbernagel JT, Kennedy SC, Johnson AL, Pijanowski GJ, Ehrhart N, Schaeffer D. Validation of canine cancellous and cortical polyurethane foam bone models. *Vet Comp Orthop Traumatol* 2002;15(4):200-204.

47. von Pfeil DJF, Déjardin LM, DeCamp CE, et al. In vitro biomechanical comparison of a plate-rod combination–construct and an interlocking nail–construct for experimentally induced gap fractures in canine tibiae. *Am J Vet Res* 2005;66(9):1536-1543.

48. Goodno BJ and Gere JM. Chapter 9: Deflection of Beams. In: Goodno BJ and Gere JM, eds. Mechanics of Materials 9th ed Boston, MA: Cengage Learning; 2018:849.

49. Stoffel K, Dieter U, Stachowiak G, Gächter A, Kuster MS. Biomechanical testing of the LCP--how can stability in locked internal fixators be controlled? Injury 2003;34: B11-B19.

50. Goodno BJ and Gere JM. Chapter 3: Torsion. In: Goodno BJ and Gere JM, eds. Mechanics of Materials 9th ed Boston, MA: Cengage Learning; 2018:327.

51. Palierne S, Froidefond B, Swider P, Autefage A. Biomechanical Comparison of Two Locking Plate Constructs Under Cyclic Loading in Four-Point Bending in a Fracture Gap Model: Two Screws versus Three Screws Per Fragment. Vet Comp Orthop Traumatol 2019;32(01):059-66.

52. Leggon RE, Lindsey RW, Panjabi MM. Strength reduction and the effects of treatment of long bones with diaphyseal defects involving 50% of the cortex. *J Orthop Res* 1988;6(4):540-546.

53. Clark CR, Morgan C, Sonstegard DA. The effect of biopsy-hole shape and size on bone strength. *J Bone Joint Surg Am* 1977;59(2):213-217.

54. Edgerton BC, An KN, Morrey BF. Torsional strength reduction due to cortical defects in bone. *J Orthop Res* 1990;8(6):851-855.

55. Main RP and Biewener AA: Skeletal strain patterns and growth in the emu hindlimb during ontogeny. *J Exp Biol* 2007;210(15):2676-2690.

56. Yang PF, Sanno M, Ganse B, et al: Torsion and antero-posterior bending in the in vivo human tibia loading regimes during walking and running. *PLoS One* 2014;9(4): e94525.

57. Massie AM, Kapatkin AS, Garcia TC, Guzman DS, Chou PY, Stover SM. Effects of Hole Diameter on Torsional Mechanical Properties of the Rabbit Femur. *Vet Comp Orthop Traumatol* 2019;32(1):51-58.

58. Ahmad M, Nanda R, Bajwa AS, Candal-Couto J, Green S, Hui AC. Biomechanical testing of the locking compression plate: when does the distance between bone and implant significantly reduce construct stability? Injury 2007;38(3):358-64.

59. Marturello DM, von Pfeil DJ, Déjardin LM. Evaluation of a Feline Bone Surrogate and In Vitro Mechanical Comparison of Small Interlocking Nail Systems in Mediolateral Bending. *Vet Comp Orthop Traumatol* 2021; 34(4): 223-233.

60. Schmierer PA, Smolders LA, Zderic I, Gueorguiev B, Pozzi A, Knell SC. Biomechanical properties of plate constructs for feline ilial fracture gap stabilization. *Vet Surg* 2019;48(1):88-95.

61. Gibert S, Ragetly GR, Boudrieau RJ. Locking compression plate stabilization of 20 distal radial and ulnar fractures in toy and miniature breed dogs. *Vet Comp Orthop Traumatol* 2015;28(06):441-447.

62. Larin A, Eich CS, Parker RB, Stubbs WP. Repair of diaphyseal femoral fractures in cats using interlocking intramedullary nails: 12 cases (1996–2000). *J Am Vet Med Assoc*. 2001;219(8):1098-104.

63. Morris AP, Anderson AA, Barnes DM, et al Plate failure by bending following tibial fracture stabilisation in 10 cats. *J Sm Anim Pract*. 2016;57(9):472-8.

64. Nolte DM, Fusco JV, Peterson ME. Incidence of and predisposing factors for nonunion of fractures involving the appendicular skeleton in cats: 18 cases (1998–2002). *J Am Vet Med Assoc*. 2005;226(1):77-82.

65. Glyde M, Day R, and Deane B. Biomechanical comparison of plate, plate- rod and orthogonal locking plate constructs in an ex-vivo canine tibial fracture gap model. Abstract, *Proceedings ECVS 20th Annual Scientific Meeting*. 2011 Ghent, Belgium. p 88.

66. Craig A, Witte PG, Moody T, Harris K, Scott HW. Management of feline tibial diaphyseal fractures using orthogonal plates performed via minimally invasive plate osteosynthesis. *J Feline Med Surg*.2018;20(1):6-14.

67. Guiot LP and Déjardin LM. Prospective evaluation of minimally invasive plate osteosynthesis in 36 nonarticular tibial fractures in dogs and cats. *Vet Surg*. 2011; 40(2):171-82.

68. Peirone B, Rovesti GL, Baroncelli AB, Piras L. Minimally invasive plate osteosynthesis fracture reduction techniques in small animals. *Vet Clin North Am Small Anim*. 2012;42(5):873-95.

69. Horstman CL, Beale BS, Conzemius MG, Evans R. Biological osteosynthesis versus traditional anatomic reconstruction of 20 long-bone fractures using an interlocking nail: 1994–2001. *Vet Surg*. 2004;33(3):232-7.

70. Aron DN, Johnson AL, Palmer RH. Biologic strategies and a balanced concept for repair of highly comminuted long bone fractures. *Compend Contin Educ Vet*.1995.

71. Endo K, Nakamura K, Maeda H, Matsushita T. Interlocking intramedullary nail method for the treatment of femoral and tibial fractures in cats and small dogs. *J Vet Med Sci*. 1998;60(1):119-22.

72. Heitemeyer U, Kemper F, Hierholzer G, Haines J. Severely comminuted femoral shaft fractures: treatment by bridging-plate osteosynthesis. *Arch Orthop Trauma Surg*. 1987;106(5):327-30.

73. Karnezis IA. Biomechanical considerations in ‘biological’ femoral osteosynthesis: an experimental study of the ‘bridging’and ‘wave’ plating techniques. *Arch Orthop Trauma Surg*. 2000;120(5-6):272-5.

74. Lang GJ, Cohen BE, Bosse MJ, et al: Proximal third tibial shaft fractures. Should they be nailed? *Clin Orthop Relat Res* 1995; 315:64–74.

75. Marturello DM, von Pfeil DJF, Déjardin LM: Mechanical comparison of small interlocking nail systems in torsion using a feline bone model surrogate. *Vet Surg*. 2020; 49(2): 380-389.

76. Johnson KA. Piermattei's Atlas of Surgical Approaches to the Bones and Joints of the Dog and Cat. Elsevier Health Sciences; 2013.

77. González YH, Martín AD, Sánchez FJ, Erasun CR. Early results with the new internal fixator systems LCP and LISS: a prospective study. *Acta orthopaedica belgica*. 2007;73(1):60-69.

78. Tomlinson J, Fox D, Cook JL, Keller GG. Measurement of femoral angles in four dog breeds. *Vet Surg*. 2007;36(6):593-8.

79. Wood MC, Fox DB, Tomlinson JL. Determination of the mechanical axis and joint orientation lines in the canine humerus: a radiographic cadaveric study. *Vet Surg*. 2014;43(4):414-7.

80. Warzee CC, Dejardin LM, Arnoczky SP, Perry RL. Effect of tibial plateau leveling on cranial and caudal tibial thrusts in canine cranial cruciate–deficient stifles: An in vitro experimental study. *Vet Surg*. 2001;30(3):278-86.

81. Perry KL, Bruce M. Impact of fixation method on postoperative complication rates following surgical stabilization of diaphyseal tibial fractures in cats. *Vet Comp Orthop Traumatol*. 2015;28(02):109-15.

82. Teeny S, Wiss DA, Hathaway R, Sarmiento A. Tibial plafond fractures: errors, complications, and pitfalls in operative treatment. *J Orthop Trauma*. 1990;4(2):215.

83. Vedrine B, Gérard F. Veterinary Cuttable Plate in a Plate-Rod Construct for Repair of Diaphyseal Femoral Fractures in the Cat. *Vet Comp Orthop Traumatol*. 2018;31(06):479-487.

84. Dueland RT, Johnson KA, Roe SC, Engen MH, Lesser AS. Interlocking nail treatment of diaphyseal long-bone fractures in dogs. *J Am Vet Med Assoc*. 1999;214(1):59-66.

85. Wheeler JL, Cross RA, Stubbs WP, Guerin RS, Lewis DD. Intramedullary interlocking nail fixation in dogs and cats: biomechanics and instrumentation. *Compendium*. 2004 July.

86. Latte Y, Drape J. Traitement chirurgical des fractures diaphysaires du femur du jeune chien ~~385~~ par plaque d'osteosynthese semi-rigide. *P M C A C* 1991; 26 (3): 187-201.

87. Klein MP, Rahn BA, Frigg R, Kessler S, Perren SM. Reaming versus non-reaming in medullary nailing: interference with cortical circulation of the canine tibia. *Arch Orthop Trauma Surg*. 1990;109(6):314-6.

88. Black AP, Withrow SJ. Changes in the proximal femur and coxofemoral joint following intramedullary pinning of diaphyseal fractures in young dogs. *Vet Surg*. 1979;8(1):19-24.

89. Dugat D, Rochat M, Ritchey J, Payton M. Quantitative analysis of the intramedullary arterial supply of the feline tibia. *Vet Comp Orthop Traumatol*. 2011;24(05):313-9.

90. Rhinelander FW, Baragry R. Microangiography in bone healing. I. Undisplaced closed fractures. *J Bone Joint Surg Am*. 1962;44:1273-98.

91. Langley-Hobbs SJ, Straw M. The feline humerus. An anatomical study with relevance to external skeletal fixator and intramedullary pin placement *Vet Comp Orthop Traumatol*. 2005;18(01):01-6.

Figure 5.1: Image of investigators working in the lab on Study 2